

DEVELOPMENT OF HIGH DUCTILITY ALUMINUM ALLOYS FOR DIE CASTING

by

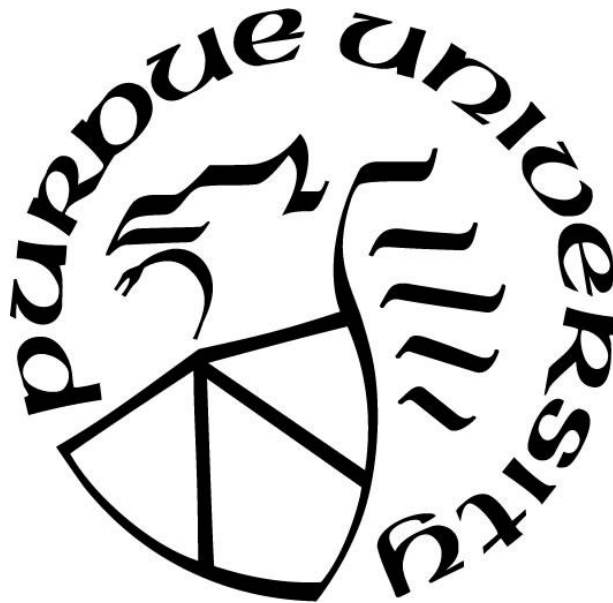
Mohamad Rusydi Mohamad Yasin

A Dissertation

Submitted to the Faculty of Purdue University

In Partial Fulfillment of the Requirements for the degree of

Doctor of Philosophy



School of Engineering Technology

West Lafayette, Indiana

August 2019

**THE PURDUE UNIVERSITY GRADUATE SCHOOL
STATEMENT OF COMMITTEE APPROVAL**

Dr. Xiaoming Wang, Chair

School of Engineering Technology

Dr. David Johnson

School of Material Engineering

Dr. Sarah E. Leach

School of Engineering Technology

Dr. Milan Rakita

School of Engineering Technology

Approved by:

Dr. Kathryne A. Newton

Head of the Graduate Program

To the love of my life,

Fahimah

Aidan

Imran

For being my rock that I could lean on, in good times and in bad.

ACKNOWLEDGMENTS

I would like to express my highest gratitude to Dr Qingyou Han for all the guidance and knowledge wisdom he has given me throughout my study, for which I will forever be grateful. Special thanks to Dr Xiaoming Wang for the advice, support and motivation throughout my study. I would also like to thank Dr David Johnson, Dr. Milan Rakita and Dr. Sarah E Leach for being on my committee and helping me get through graduate school with their advice and assistance.

I would like to thank Purdue University for providing excellent research facilities and educational support to me. I would also like to thank my sponsors, Ministry of Education (MoE) Malaysia and Universiti Malaysia Pahang (UMP) for the funding throughout the four years of my study at Purdue University.

Special appreciation to Chrysler Kokomo Casting Plant for the support in terms of facilities and expertise throughout the research. I would also like to thank my research group fellows, especially to Dongke Sun, Jianyue Zhang and Xuzhe Zhao for their assistance and guide during my projects.

I want to thank both my parents, Mohamad Yasin Jamaludin and Rozita Jamal for the care and support given. Lastly, a very special thanks to my wife, Nur Fahimah Johari and my kids, Aidan and Imran. Their support and love have been nothing but outstanding throughout this journey.

TABLE OF CONTENTS

LIST OF TABLES	8
LIST OF FIGURES	10
GLOSSARY	12
LIST OF ABBREVIATIONS.....	14
ABSTRACT.....	15
CHAPTER 1. INTRODUCTION	17
1.1 Background.....	17
1.2 Statement of Purpose	18
1.3 Significance.....	20
1.4 Research Question	21
1.5 Assumptions.....	21
1.6 Limitations	22
1.7 Delimitations.....	22
1.8 Chapter 1 Summary	22
CHAPTER 2. REVIEW OF LITERATURE	24
2.1 Aluminum Alloys.....	24
2.2 The Effect of Alloying Element on β phase	25
2.2.1 Silicon (Si).....	25
2.2.2 Iron (Fe).....	25
2.2.3 Manganese (Mn).....	26
2.2.4 Copper (Cu).....	27
2.2.5 Magnesium (Mg).....	27
2.2.6 Zinc (Zn).....	28
2.2.7 Chromium (Cr)	28
2.2.8 Beryllium (Be).....	29
2.2.9 Strontium (Sr).....	29
2.2.10 The summary of effect of alloying element	31
2.3 α and β Intermetallic Phases	32
2.4 The Justification of β Phase Research	34

2.5	The Nucleation and Growth of β Phase	37
2.6	Cooling Rate	38
2.7	Heat Treatment.....	39
2.8	Sludge Factor and Soldering Factor Limit.....	41
2.9	Chapter 2 Summary	43
CHAPTER 3. RESEARCH METHODOLOGY.....		45
3.1	Introduction to Research Methodology	45
3.2	Research Type.....	46
3.3	Thermodynamics Simulation	46
3.4	Material Design.....	48
3.5	Heat Treatment.....	51
3.6	Mechanical Properties Analysis.....	52
3.7	Microstructure Analysis.....	52
3.8	Chapter 3 Summary	55
CHAPTER 4. THERMODYNAMIC SIMULATION.....		56
4.1	Introduction of Thermodynamic Simulation	56
4.2	The Effect of Single Element to Phase Formation Sequence	56
4.2.1	Silicon (Si).....	57
4.2.2	Iron (Fe).....	59
4.2.3	Manganese (Mn).....	61
4.3	The Solidification Path of Die Casting Alloys	63
4.4	Solidification Path for Common Commercial Die Casting Alloys.....	69
4.5	Proposed Alloy Composition based on Thermodynamic Analysis	71
4.6	Chapter 4 Summary	77
CHAPTER 5. EXPERIMENTAL RESULTS.....		79
5.1	Introduction of Experimental Results	79
5.2	Mechanical Testing for Alloys at Different Compositions.....	79
5.3	Microstructure Analysis of Alloys of Different Compositions.....	84
5.3.1	Microstructure of Alloy #1	87
5.3.2	Microstructure of Alloy #2	89
5.3.3	Microstructure of Alloy #3	92

5.3.4	Microstructure of Alloy #4	95
5.3.5	Microstructure of Alloy #5	98
5.3.6	Effect of β -AlFeSi length to the Elongation	102
5.4	Mechanical Testing for Alloys at Different Heat Treatments	103
5.4.1	Modified T4 heat treatment on Alloy #1	104
5.4.2	Modified T4 heat treatment on Alloy #2	106
5.4.3	Modified T4 heat treatment on Alloy #3	108
5.4.4	Modified T4 heat treatment on Alloy #4	110
5.4.5	Modified T4 heat treatment on Alloy #5	112
5.4.6	Microscopic Observation on Effect of Heat Treatment.....	114
5.5	Chapter 5 Summary	121
CHAPTER 6. CONCLUSIONS.....		122
APPENDIX A: SOLIDIFICATION PATH OF A360.....		124
APPENDIX B: SOLIDIFICATION PATH OF B360.....		128
LIST OF REFERENCES		132
VITA.....		137

LIST OF TABLES

Table 1: The advantage and disadvantage of the alloying element	31
Table 2: Identified Fe-containing phases in aluminum alloys	33
Table 3: Physical properties of Al matrix and β phase	35
Table 4: The variation range of principal elements of A380 alloy	48
Table 5: Designed composition of alloys for mechanical characterization	49
Table 6: Composition of A380 alloy	49
Table 7: Specification of Dimensions for standard tensile bar for ASTM E 8M – 04	50
Table 8: Solidus Temperature and Solution Temperature for heat treatment.....	51
Table 9: Nucleation sequence of A380 alloy-xSi	58
Table 10: Nucleation sequence of A380 alloy-xFe.....	60
Table 11: Nucleation sequence of A380 alloy-xMn.....	62
Table 12: Composition of A360 and B360	65
Table 13: Reaction during solidification of A360 alloy	66
Table 14: Reaction during solidification of B360 alloy.....	68
Table 15: Compositions of commercial die casting alloys	69
Table 16: Proposed composition of the alloys.....	72
Table 17: Summary of elongation, UTS and Quality Index results with the nominal values of Fe, Mn and Si composition.....	81
Table 18: Intermetallic phase measurement from Alloy #1.....	88
Table 19: Intermetallic phase measurement from Alloy #2.....	91
Table 20: Intermetallic phase measurement from Alloy #3.....	94
Table 21: Intermetallic phase measurement from Alloy #4.....	97
Table 22: Intermetallic phase measurement from Alloy #5.....	100
Table 23: Solidus Temperature and Solution Temperature	104
Table 24: Summary of mechanical properties of Alloy #1 at different solution time	105
Table 25: Summary of mechanical properties of Alloy #2 at different solution time	107
Table 26: Summary of mechanical properties of Alloy #3 at different solution time	109
Table 27: Summary of mechanical properties of Alloy #4 at different solution time	111
Table 28: Summary of mechanical properties of Alloy #5 at different solution time	113

Table 29: β -AlFeSi length of Alloy #5 samples with different heat treatment time	114
Table 30: Granular eutectic silicon diameter at different solution time	118

LIST OF FIGURES

Figure 1: Possible nucleation hierarchy in AlSiMg alloys containing Fe and Mn contents (Reproduced from Cao and Campbell (2004))	38
Figure 2: Morphology of the AlFeSi phases at 525°C for (a) 0.5 h; (b) 1 hour; (c) 2 hour; (d) 4 hour (Reproduced from Wang, Xu and Han (2016))	40
Figure 3: Sludge factor and soldering factor for composition of Fe to Mn at different Sr content.....	43
Figure 4: Specification of standard tensile bar for ASTM E 8M – 04.....	50
Figure 5: Intermetallic phases observed in the designed alloy under optical microscope	54
Figure 6: Binary phase diagram of A380 alloy-xSi	58
Figure 7: Binary phase diagram of A380 alloy-xFe	60
Figure 8: Binary phase diagram of A380 alloy-xMn.....	62
Figure 9: Al-Fe-Si liquidus projection.....	63
Figure 10: Backerud’s Liquidus Projection	64
Figure 11: The solidification path of A360 alloy.....	66
Figure 12: The solidification path of B360 alloy.....	68
Figure 13: Solidification Path of DC Alloys by Thermodynamic Simulation.....	70
Figure 14: Quality Index by β -AlFeSi phase fraction.....	71
Figure 15: Solidification Path of Alloy #1	73
Figure 16: Solidification Path of Alloy #2.....	74
Figure 17: Solidification Path of Alloy #3.....	75
Figure 18: Solidification path of Alloy #4	76
Figure 19: Solidification path of Alloy #5	77
Figure 20: Elongation for five designed alloys.....	80
Figure 21: UTS and Quality Index for designed die casting alloys	81
Figure 22: Microscopic image with α -AlFeMnSi and β -AlFeSi intermetallic phases.	86
Figure 23: Microstructure of the as-cast Alloy #1 at 500X	87
Figure 24: Fracture surface of Alloy #1 at 2000X magnification.....	89
Figure 25: Microstructure of the as-cast Alloy #2 at 500X	90
Figure 26: Fracture surface of Alloy #2 at 2000X magnification.....	92

Figure 27: Microstructure of the as-cast Alloy #3 at 500X	93
Figure 28: Fracture surface of Alloy #3 at 2000X magnification.....	95
Figure 29: Microstructure of the as-cast Alloy #4 at 500X	96
Figure 30: Fracture surface of Alloy #4 at 2000X magnification.....	98
Figure 31: Microstructure of the as-cast Alloy #5 at 500X	99
Figure 32: Fracture surface of Alloy #5 at 2000X magnification.....	101
Figure 33: Effect of β -AlFeSi length to the elongation	102
Figure 34: Effect of solution time to elongation of Alloy #1	105
Figure 35: Effect of solution time to elongation of Alloy #2	107
Figure 36: Effect of solution time to elongation of Alloy #3	109
Figure 37: Effect of solution time to elongation of Alloy #4	111
Figure 38: Effect of solution time to elongation of Alloy #5	113
Figure 39: Optical sample of Alloy #5 at 1 hour solution time (500X).....	115
Figure 40: Optical sample of Alloy #5 at 2 hour solution time (500X).....	115
Figure 41: Optical sample of Alloy #5 at 4 hour solution time (500X).....	116
Figure 42: Optical sample of Alloy #5 at 8 hour solution time (500X).....	116
Figure 43: Optical sample of Alloy #5 at 16 hour solution time (500X).....	117
Figure 44: Optical sample of Alloy #5 at 32 hour solution time (500X).....	117
Figure 45: The lamellar eutectic silicon for as cast sample (20000X)	119
Figure 46: The granulated eutectic silicon at 1 hour solution time (20000X)	119
Figure 47: The granulated eutectic silicon at 8 hour solution time (20000X)	120
Figure 48: The granulated eutectic silicon at 16 hour solution time (20000X)	120

GLOSSARY

Die casting – “a versatile process for producing engineered metal parts by forcing molten metal under high pressure into reusable steel molds” (Doehler, 1951).

Hardness – “measurement of how resistant solid matter is to various kinds of permanent shape change when a force is applied” (Anderson, 1970).

Heat treatment – “a group of industrial and metalworking processes used to alter the physical, and sometimes chemical, properties of a material related to high temperature process” (Groover, 2010).

Intermetallic compounds – “solid phases containing two or more metallic elements, with optionally one or more non-metallic elements, whose crystal structure differs from that of the other constituents” (Schulze, 1967).

Mechanical Properties – “the material properties that are associated with deformation, either elastically and inelastically, or properties that involve the relationship in between the stress and strain of a material when force is applied” (Kaufman & Rooy, 2004).

Solution heat treatment – “a process in which an alloy or metal is heated to a suitable temperature, is held at that temperature long enough to allow a certain constituent to enter into solid solution, and is then cooled rapidly to hold that constituent in solution” (Cambell, 1991).

Ultimate Tensile Strength – “the maximum stress that a material can withstand while being stretched or pulled before failing or breaking” (DeGarmo, 2003).

LIST OF ABBREVIATIONS

α – Alpha

β - Beta

Al – Aluminum

Cr – Chromium

Cu – Copper

Fe – Iron

HPDC – High Pressure Die Casting

Mg – Magnesium

Mn – Manganese

QI – Quality Index

Si – Silicon

Sr – Strontium

UTS – Ultimate Tensile Strength

Zn – Zinc

ABSTRACT

Author: Mohamad Yasin, Mohamad Rusydi. PhD
Institution: Purdue University
Degree Received: August 2019
Title: Development of High Ductility Aluminum Alloys for Die Casting
Committee Chair: Xiaoming Wang

Aluminum-Silicon (Al-Si) alloys are often preferred in the die casting industry due to excellent castability, high strength, corrosion resistance and low cost. Commonly, iron (Fe) is alloyed with the alloys to prevent die soldering. However, the addition of Fe in most of Al-Si alloys leads to formation of the intermetallic β -AlFeSi. The β -AlFeSi is harmful to the alloy structural integrity due to its needle-like morphology that creates stress concentration at the microscopic level. The phase presence is unfavorable to the mechanical properties and significantly reduces the elongation of the alloys. This research attempted to find viable way to control the morphology and formation of the β -AlFeSi phase.

Thermodynamic simulations were done to investigate the sequence of intermetallic formation and other phases at different alloy compositions. The analysis of solidification paths of different alloys provided the correlation between the phase formation sequence and the fraction of the β -AlFeSi phase. The analysis also identified the feasible region of alloy design for minimizing the β -AlFeSi formation. Based on the thermodynamics simulation analysis, five alloys of different compositions were designed to validate the finding of the simulation.

The tensile test results of the alloys indicated that lowering the Fe content increases the elongation of the alloy. The results also showed that elongation was reduced with the increase of Si level due to the formation of eutectic Silicon. The change of both Fe and Mn did not significantly affect the mechanical property of the alloy when the ratio of Fe to Mn was constant. Microscopic analysis showed that lowering the Fe level had effectively altered the morphology of the β -AlFeSi needle like structure. The β -AlFeSi was found to be smaller in terms of size when Fe is lower, subsequently reducing the probability of β -AlFeSi phase to be stress riser and crack initiation.

The influence of heat treatment to the mechanical property of the alloys was also studied. The mechanical result on the heat-treated samples indicated that heat treatment is a viable method to improve the elongation property of the alloy. Microscopic observations showed that the β -AlFeSi phase was broken into shorter structures over the solution heat treatment process, resulting in better elongation.

CHAPTER 1. INTRODUCTION

1.1 Background

Aluminum is a remarkable element that can be found abundantly in the automotive, packaging and other manufacturing fields. In terms of metal casting industry, Aluminum-Silicon (Al-Si) alloys are commonly preferred for making casting parts. The examples of Al-Si alloys include A380, Silafont 36 and A356 alloy. The common usage of these alloys is attributed to their excellent castability while maintaining the high strength, good corrosion resistance, and low manufacturing cost. However, aluminum alloy ingots that are used in the metal casting industry usually contain high percentages of intermetallic impurity. The most common intermetallic impurities found in the aluminum alloy are α -AlFeSi, β -AlFeSi and Al₃Fe.

Iron (Fe) in particular is the most harmful element in aluminum alloys, mainly because it causes the formation of the impurities (Green, 2007). The mechanical properties of the alloy will be negatively impaired by the high Fe content, and the ductility will severely decrease once the Fe content is over a critical percent (Khalifa, Samuel & Gruzleski, 2003). Fe regularly forms AlFe or AlFeSi intermetallics in the aluminum alloys due to the low solubility limit of Fe in Al (<0.05%) (Verma, Sundaram, Grant & O'Reilly, 2013). These intermetallic phases are not favorable to the mechanical properties, especially the elongation of Aluminum-Silicon die-casting alloys.

Many researchers have been studying methods to reduce the undesirable effect of the β -AlFeSi presence. Removing Fe element from the alloy is very costly and difficult if

the content of Fe decreases to certain threshold percent. The Al-Si alloy that is purely free from the element of iron is rare to be found (Crepeau, 1995). Minimizing the formation and altering the morphology of the β -AlFeSi phase therefore is viable method to improve the elongation of Al-Si alloys.

1.2 Statement of Purpose

In recent years, the metal casting industry has become increasingly interested not only on the macroscopic simulation of the heat transfer and mold filling during casting, but also on the ability to predict the microstructures of the component. With advances made in phase diagram calculations, the phase formation sequence during the solidification can be forecasted by thermodynamic simulation using commercial software. The simulation can therefore be used in the alloy development to reduce the brittle and undesirable β -AlFeSi intermetallics formation by designing the optimal solidification path of the alloy.

Four methods have been introduced by die casting researchers to minimize the harmful effect of the intermetallic phases. The first method is altering the composition of the alloy. The objective of this method is to reduce the formation of intermetallic phase by reducing the elements that contributes to its formation. Significant number of researchers agree that Iron is the main element that contributes to the intermetallic formation. In practice, few alloys with low Fe content have been developed, such as Silafont-36 and Mercalloy and are gaining favorability in die casting industry (Hartlieb, 2013).

The second method is element alloying. The objective of element alloying is to change the nucleation sequence or morphology of the intermetallic microstructure by introducing some elements, therefore minimizing the detrimental effect of the intermetallic phases. Effective alloying elements such as Manganese, Chromium, Beryllium, Cadmium, Strontium can be alloyed with Al-Si alloys to alter the nucleation sequence of β -AlFeSi phase (Zhang, Gao, Damoha, & Robertson, 2012).

Controlling the solidification or cooling rates is also a method to effectively reduce the negative effect of intermetallic phase. Several studies have shown that the length and size of β -AlFeSi phase can be refined with faster cooling rate during casting process (Verma, Sundaram, Grant & O'Reilly, 2013). However, controlling the cooling rate will not eliminate the formation of β -AlFeSi. The effect of this method is limited to the refinement of the phase.

Another effective method to control intermetallic formation is heat treatment. Crepeau (1995) in his study found that at high solution temperature, the needle-shape β -AlFeSi phase platelets can be broken into shorter particulates therefore improving the elongation property. However, precaution is needed with this method as solution treatment usually results in surface blistering, especially with the presence of microbubbles from the trapped hydrogen gas during die casting. (Kim, Park, Han, & Lee, 2006).

These methods of controlling and modifying β -AlFeSi intermetallics morphology in die casting aluminum alloy were systematically studied using the PanAluminum database via Pandat thermodynamic simulation software. The nucleation and growth of β -

AlFeSi phase and mechanical properties of modified die-casting alloy were investigated. Optimizing method of minimizing the fraction and controlling morphology of β -AlFeSi phase in Al-Si hypoeutectic alloys are also studied.

1.3 Significance

Three topics are considered significant and addressed in this study. The first significance is the utilization of thermodynamic simulation in designing die casting alloys. Conventionally, a die casting alloy is designed by the mean of the thermodynamic experiment involving numerous samples of different composition. Conducting thermodynamic analysis experimentally can be challenging from the aspect of cost and time consumption. Therefore, simulation work can substantially reduce the work of experiment and be an economical way to design die-casting alloys.

The second significance is the relationship of α -AlFeMnSi and β -AlFeSi intermetallic phases formation sequence to the mechanical properties of the alloy under die casting condition. There are numerous studies that highlight the effect of the morphology of the phases. However, very few of them correlate the formation sequence to the mechanical properties. Therefore, this study attempts to find correlation between controlling phase formation sequence and the mechanical properties.

The third significance pertains to optimizing heat treatment conditions in refining the morphology of the detrimental intermetallic phases. There are very few studies on the effect of heat treatment to the mechanical properties of the alloy. Kim, Park, Han & Lee (2006) found that heat treatment is less favorable in the die casting industry due to the

high solution time due to surface blistering and dimensional instability of die casting parts. This study analyzed the optimal condition of the heat treatment in altering β -AlFeSi intermetallic phase while maintain the high quality of alloys.

1.4 Research Question

The research questions involved are as following:

1. What is the phase formation sequence of iron-containing intermetallic phases in die casting aluminum alloy?
2. What are the desired alloying elements and content to minimize iron-containing intermetallic phases in order to improve the mechanical properties of die casting aluminum alloy?
3. What is the effect of heat treatment on the mechanical properties of the designed alloy?

1.5 Assumptions

Assumptions for this study include:

1. All fabricated casting samples are whole, uniform and with no defects.
2. The mechanical testing and microstructure observation are conducted under the uniform controlled environment.
3. The thermodynamic analysis simulates condition that is close to the real casting condition.

4. During the casting process, insignificant amount of the alloy element is oxidized and considered too small to be element deficiency in the alloy composition.

1.6 Limitations

The limitations for this study include:

1. The thermodynamic simulations are entirely based on Computherm Pandat 2016 software and PanAluminum database.
2. The mechanical testing is restricted by the experimental conditions defined in methodology section.

1.7 Delimitations

The delimitations for this study include:

1. The matrix aluminum alloy that is not confined to die-casting series alloy.
2. Cooling rate control as a method of refining the intermetallic morphology.
3. All the materials and mechanical testing that are not within American Society for Testing and Materials (ASTM) criteria.

1.8 Chapter 1 Summary

In this chapter, the research overview of β -AlSiFe phase morphology control in Al-Si alloy have been introduced as can be found in section 1.1. The purpose, scope, significance and research questions have also been defined and elaborated in section 1.2,

1.3, 1.4 and 1.5 respectively. Finally, in section 1.6 and 1.7, the limitations and delimitations of the research are stated.

CHAPTER 2. REVIEW OF LITERATURE

2.1 Aluminum Alloys

Aluminum is a very widely used material in manufacturing industries due to its versatile features and excellent physical and mechanical properties. Aluminum generally has a Face Centered Cubic (FCC) crystal structure. Pure aluminum as such has relatively ductile property compared to the other metals. In addition, aluminum, due to its metallic bonding, still has considerable strength. Aluminum in such way provides usage for industrial applications that emphasize on both substantial ductility and strength.

Another important property of aluminum that makes it favorable is its very good electrical and thermal conductivity. Aluminum electrical conductivity is almost 70% of Copper electrical conductivity and 60% of Copper thermal conductivity. Aluminum is also excellent in corrosion resistance. Aluminum typically has inert ceramic layer of protection due to the formation of aluminum oxide from the reaction of the molten aluminum with the air (Campbell, 2008).

Aluminum is very commonly alloyed with other elements to form a superior material in terms of the physical and mechanical properties. In terms of the die casting industry, 300-series, sometimes known as Al-Si alloys, such as A380 and A356 are the most widely used aluminum alloys. These alloys are favored mainly because of their exceptional mechanical properties, excellent corrosion resistance and good castability. The 300 series alloys often consist of six elements: Silicon, Iron, Manganese, Copper, Magnesium, and Zinc. It may however be alloyed with numerous other elements to tailor

some specific uses. The effect of adding the aforementioned elements and a few other common elements to cast aluminum alloys is elaborated in the next section.

2.2 The Effect of Alloying Element on β phase

2.2.1 Silicon (Si)

Si is a crucial element that is added to die casting 300-series aluminum alloys. The main purpose of adding Si to the aluminum alloys is to significantly improve the castability, specifically by increasing fluidity. The good fluidity is attributed to the high latent heat of fusion of Si released during the feeding process. Another improved castability parameter that is facilitated by Si addition is the reduction in tendency for hot tearing. During solidification, Si is expanding instead of contracting. The expansion, coupled with reinforcement at the grain boundaries by Cu provide a mechanism for the aluminum alloy to prevent hot tearing from occurring during casting (Kaufman & Rooy, 2004).

2.2.2 Iron (Fe)

Fe is essentially added to die casting alloys to prevent the cast from die soldering. Without Fe, the casted part will have tendency to form chemical bond with the mold, eventually making it difficult to be ejected from the mold. Fe content however needs to be controlled to only a certain threshold amount whereby if exceeded, insoluble intermetallic phases will form inside the microstructure. The intermetallic form is often brittle, hence can be detrimental to the alloy elongation property. In 300-series die casting alloys, the iron-rich content may form either α -AlFeMnSi or β -AlFeSi or more commonly

both phases. Fe in some cases is added to improve the strength of the alloy due to the introduction of the insoluble particles (Kaufman & Rooy, 2004). More details on the effect of Fe on aluminum alloy will be discussed in section 2.3.

2.2.3 Manganese (Mn)

Mn is widely adopted as a replacement for Fe in Al-Si die casting alloys. The similarity of the crystal structures and the radius of atom of Mn and Fe is the reason for the substitution of Fe (Mahta et al., 2005). With the Mn replacement, the needle-like β -AlFeSi phases can be eliminated and replaced with compact size, polygon and star-like α -AlFeSi phase structure (Kores, Vončina, Kosec, & Medved, 2012). The structure improves the tensile and ductility property of Al-Si die-casting alloy. Murali, Raman and Murthy (1994) claimed that β -AlFeSi can be altered into big size α -AlFeSi with high content of Fe and Mn at low cooling condition in Al-Si-Mg alloy.

Ashtari, Tezuka and Sato (2003) studied the effect of interaction between Sr and Mn in A365 series alloy. With only 0.015% of Sr, β -Al₁₅FeSi phase is predominant in the alloy (Ashtari, Tezuka and Sato, 2003). However, α -AlFeSi phase began to appear with the addition of both Sr and Mn. The correct Mn:Fe weight ratio is still not established as the nucleation and growth of phases are influenced by various factors, such as cooling rates, superheating temperatures and other solidification-related factors. However, generally the die casting industry uses the Fe/Mn weight ratio of 1.5 as the most efficient ratio to relief the detrimental effect of β -AlFeSi (Castro-Román et al., 2015).

Adding a small amount of Mn may be effective in substituting Fe, in order to eliminate the formation of β -AlFeSi phase. However, a high Mn addition is undesirable

as it will cause the formation of large polygon called “sludge” therefore increasing the hot tearing susceptibility (Lu, & Dahle, 2005).

2.2.4 Copper (Cu)

The addition of Cu is mainly done to improve both the strength and hardness of the aluminum alloy. During solidification, Cu may react with Al to form an Al-Cu phase. This phase acts as precipitating particle during solution heat treatment therefore become the reinforcement to the grains. Essentially the Al-Cu particles prevent dislocation of grains hence improve the strength of the material. The Al-Cu particles may take the form of either Al_2Cu blocks or a eutectic Al and Al_2Cu (Samuel, 2003).

The introduction of Cu however may reduce the corrosion resistance of the alloy. Due to the chemical properties of Cu, the addition of the element may also increase the hot tearing potential during solidification. Therefore, to counteract the downside aspects of Cu addition, specifically designed mold and feeding system need to be used for alloys with high Cu content (Kaufman & Rooy, 2004).

2.2.5 Magnesium (Mg)

Typically, Mg is used in the Al-Si alloys with a purpose to improve the strength and hardness of the materials, especially the alloys that undergo heat treatment process. Similar to Cu, the strength of the alloy is increased by the mean of precipitation hardening. The Mg particle compounds precipitate along the grain boundaries, hence providing an effective reinforcement to the material by preventing the dislocation of grains. The most common Mg-containing phase is called Q-phase and the compound

takes a form of AlCuMgSi (Hwang, Banerjee, Doty & Kaufman, 2009). The usual issue of dealing with Mg is the high oxidation rate of the element, therefore careful measure must be taken during casting process to avoid safety compromise that is caused by Mg. The use of master alloy is an effective ways to tackle the problem.

2.2.6 Zinc (Zn)

Zn, coupled with Al, forms Al-Zn phase that provides high strength and hardness to the Aluminum Alloy. Typically, the Al-Zn particles are formed after the initial Aluminum dendrites are formed, providing reinforcement to the alloy in similar way as the Cu-containing phase and Mg containing phase do. The alloys with Zn content may also undergo heat treatment process to further reinforce the structure by the mean of precipitation hardening (Dumont, Deschmps & Brechet, 2003).

2.2.7 Chromium (Cr)

Mahta et al. (2005) claimed Cr is a more effective Fe neutralizer than Mn and Co in Al-Si die-casting alloys. An effective Cr: Fe weight ratio of 0.3 transforms almost entire of the β -AlFeSi phase into the favorable α -AlFeSi. The α -AlFeSi phase forms both within the dendrite and at the boundary of the dendrite of the alloy (Mahta et al. 2005).

High amount of alloying using Mn and Cr however can lead to the formation of the hard complex, high temperature resistance intermetallic sludge, $\text{Al}_{15}(\text{FeMnCr})_3\text{Si}_2$. The critical sludge factor is 2.1 for Al-Si alloys, and sludge factor below the threshold point will not result in the formation of the sludge, given the casting temperature is more

than 650°C (Shabestari, 2004). Formation of sludge in the alloy is highly undesirable due to the difficulties to remove it using heat treatment.

2.2.8 Beryllium (Be)

Be is more effective in modifying the AlFeSi phase than Mn (Murali, Raman & Murthy, 1995). Murali, Raman and Murthy (1995) reported that the addition of 0.06-0.27% of Be can reduce the formation of β -AlFeSi phase. The mechanism to transform the β -AlFeSi phase by Be is similar to that of Co, where the AlFeSi phases formed in the dendrite of FCC α -Al (Murali, Raman & Murthy, 1995). Yie, Lee, Lin and Lin (1999) however argued that the addition of Be transforms the β -AlFeSi phases to α -AlFeSi.

2.2.9 Strontium (Sr)

Strontium is effective in modifying the β -AlFeSi phases to α -AlFeSi in wrought alloys. In 6063 alloys, α -AlFeMnSi forms with the addition of at least 0.5 wt% Sr, therefore improving the extrusion ductility of the alloy significantly (Closset et al., 1996). More commonly in the metal casting industry, Sr has been used to phase out the β -AlFeSi formation in die casting alloys. Various studies have shown that Sr can effectively suppress the formation of β -AlFeSi phase (Lu, & Dahle, 2005). Trace Sr addition of 0.05wt% can both transfer β -phase to α -AlFeMnSi and refine β -AlFeSi phase by the reaction of fragmentation (Shabestari, 2004). Ashtari, Tezuka and Sato (2003) in their study however concluded that Sr can only reduce the size and amount of β -phase but not transform β -AlFeSi to α -AlFeSi.

A number of studies found provide contrasting opinions with regard to the mechanism of morphology transformation of AlFeSi phase by Strontium. Mulazimoglu et al. (1994) claimed that the absorption of Sr on the primary α -Al₈Fe₂Si preventing the dissolution of Fe, subsequently preventing the formation of β -AlFeSi. Closset et al. (1996) and Cho, Lee, Oh and Dahle (2008) in their studies suggested that the reduction of β -AlFeSi is caused by the nucleation sequence modification. The Sr addition leads to the full saturation of Fe and Si, hence facilitating the formation of β -AlFeSi in advance of α -Al, subsequently be the nucleate substrate of fcc α -Al.

2.2.10 The summary of effect of alloying element

The advantages and disadvantages of the aforementioned elements in die casting alloys are summarized in Table 1.

Table 1: The advantage and disadvantage of the alloying element

Element	Advantage	Disadvantage
Si	Improve fluidity, hot tearing resistance, reduce shrinkage	Leading to formation of α -AlFeMnSi and β -AlFeSi
Fe	Preventing die soldering	Leading to formation of α -AlFeMnSi and β -AlFeSi
Mn	Reducing formation of β -AlFeSi	Formation of sludge
Mg	Imrpove strength and hardness	Costly
Cu	Improve strength and hardness	Reduce corrosion resistance
Cr	Effectively transform β -AlFeSi to α -AlFeMnSi	Formation of sludge
Be	Effectively transform β -AlFeSi to α -AlFeMnSi	Costly, Be-Fe intermetallic formation
Sr	Effectively transform β -AlFeSi to α -AlFeMnSi	Intermetallic formation

2.3 α and β Intermetallic Phases

In this section, both the α -AlFeMnSi and β -AlFeSi intermetallic phases will be elaborated further to justify the importance of addressing the phases in this research. The intermetallic phase is an iron bearing phase that forms as a primary phase in aluminum alloys when the percentage of Fe exceeds a certain amount. Researchers have agreed that the solubility limit of iron in aluminum alloy is 0.05wt% (Mondolfo, 1976). Exceeding the solution limit results in, while solidifying, iron in most Al-Si die-casting alloys bonds with other elements forming other intermetallic phases, namely the binary AlFe and ternary AlFeSi phases (Khalifa, Samuel, & Gruzleski, 2003).

Multiple studies have found that the AlFe and AlFeSi phases in Al-Si die-casting alloys make take various forms and crystal structure. The identified forms of Fe-rich phases in aluminum alloy and their crystal structure are summarized in Table 2. The two most common AlFeSi intermetallic phases found in die casting AlSi alloys are α -phase and β -phase. The α -AlFeSi may exist in the form of α -Al₁₂Fe₃Si₂, α -Al₈Fe₂Si or α -Al₁₅Fe₃Si₂ (Khalifa, Samuel, & Gruzleski, 2003). There is an argument among scientists about the crystal structure of α -AlFeSi. The study by Kral, McIntyre and Smillie (2004) claimed that the α -phase has a BCC structure. Meanwhile, the alternative structure of the α -phase from the study by Crepeau (1995) is HCP. The morphology of the α -phases is usually star-like or polygon, but commonly known as Chinese Script (Lu & Dahle 2005). This structure is superior to the platelet or needle-like β -AlFeSi on Al-Si alloy's ductility due to the absence of stress concentration.

Table 2: Identified Fe-containing phases in aluminum alloys

Fe-containing Intermetallic	Crystal structure	Reference
Al_mFe	BCT	(Khalifa, Samuel & Gruzleski, 2003)
Al_6Fe	Orthorhombic	(Khalifa, Samuel, & Gruzleski, 2003)
Al_xFe	C-centered orthorhombic	(Young & Clyne, 1981)
$\theta-Al_3Fe$	Monoclinic	(Khalifa, Samuel, & Gruzleski, 2003)
$\theta-Al_{13}Fe_4$	Monoclinic	(Khalifa, Samuel, & Gruzleski, 2003)
$\alpha-Al_8Fe_2Si$	Hexagonal Bcc	(Khalifa, Samuel, & Gruzleski, 2003)
$\alpha-Al_{12}Fe_3Si_2$	Hexagonal Bcc	(Khalifa, Samuel, & Gruzleski, 2003)
$\beta-Al_5FeSi$	Monoclinic B-face centered	(Lu and Dahle, 2005; Shabestari, 2004)
$\delta-Al_4FeSi_2$	Tetragonal	(Crepeau, 1995; Khalifa, Samuel, & Gruzleski, 2003)
q1-AlFeSi	C-centered orthorhombic	(Khalifa, Samuel, & Gruzleski, 2003)
q2-AlFeSi	Monoclinic	(Khalifa, Samuel, & Gruzleski, 2003)
$\gamma-Al_8FeSi$	C-centered monoclinic	(Khalifa, Samuel, & Gruzleski, 2003)

Meanwhile, the β -AlFeSi phase may exist in the form of $\text{Al}_9\text{Fe}_2\text{Si}_2$ or Al_5FeSi , whereby the later form is the most agreed upon stoichiometric of the β phase. There are several versions of the structure of the β - Al_5FeSi (from here-on will be introduced as β -AlFeSi) as proposed by a number of previous studies. However, most researchers agree on the monoclinic structure of the β -AlFeSi (Crepeau, 1995). Alternatively, some researchers considered the β -AlFeSi structure as orthorhombic (Carpenter & LePage, 1993; Zheng, Vincent & Steeds, 2000). β -AlFeSi has the most detrimental structure of all the Al-Fe-Si intermetallic phases due to the ununiformed platelet morphology, which is brittle and has stress concentration. The presence of β -AlFeSi phase therefore often severely deteriorates the toughness of Aluminum-Silicon casting alloys, hence highly unfavorable in the die casting industry (Zheng, Vincent & Steeds, 2000).

The length β -AlFeSi phase governs the mechanical properties. The ability of the alloy to elongate reduces as the β -AlFeSi gets longer. Study by Caceres and Taylor (2006) found that shorter β -AlFeSi phase create less path for crack initiation to propagate. This is due to, as a short needle breaks, there are very few or non-existence of linkage across the path for the other system to propagating fracture (Caceres & Taylor, (2006). Therefore, refining the β -AlFeSi needle size is a viable method to improve the mechanical properties of die casting alloys.

2.4 The Justification of β Phase Research

The main reason why β phase is a crucial issue that requires attention in this research lies in the phase mechanical properties. The hardness of β phase is much larger in relation to the surrounding aluminum matrix, thus greatly affecting the elongation

property of the aluminum alloy. Table 3 enlists the physical properties of the micro-constituents commonly found in A380 alloy (Seifeddine, Johansson & Svensson, 2008). The hardness of the β phase is much higher by 447.6% by comparison to the aluminum matrix.

Table 3: Physical properties of Al matrix and β phase

Phase	Average Hardness (GPa)	Elastic Modulus
Al Matrix	2.1	92
β -Phase	11.7	194

Another significant factor to the detrimental effect by the β -AlFeSi phase is the morphology it takes form in. In two-dimension flat plane, the morphology of this phase is described as needle-like structure or sometimes referred as mono-clinical structure. However, when observed in three-dimension, the phase has plate-like structure. The aforementioned morphology in a die casting alloy creates high stress concentration area when the alloy is put under tensile loading (Yang et al., 2015).

Numerous literatures on the effect of the content of Fe on the properties of the alloys has been published. Most researchers agree that Fe has little effect on the mechanical properties with an emphasis on the condition that the Fe content is kept under a low level. However, the mechanical properties of the alloy start to significantly deteriorate when the iron content surpasses a critical point of 0.7% due to brittle β -AlFeSi intermetallic formation (Khalifa, Samuel & Gruzleski, 2003).

The critical point of iron content can be altered by controlling the alloying elements and cooling rates (Mbuya, Odera & Ng'ang'a, 2003). The critical point is also

attributed to the silicon content in Al-Si alloy (Taylor, 1995). The starting nucleation temperature of the β -AlFeSi decreases with the increase of Si content (Taylor, 1995). Lowering the Fe content is the most viable way to develop superior Al-Fe-Si die-casting alloys. By the American Foundry Society (AFS) standard, the traditional die casting alloys such as A360 and A380 may contain up to 2% iron. However, most of the recent AFS die-casting alloys contain only up to 1.3% iron (Donahue, 2011). The current practice involving on high iron die casting aluminum alloy is to replace Fe with other elements, mostly manganese (Mn) (Hartlieb, 2013). This is the common method to solve the Fe intermetallic problem in Al-Si die casting alloy.

The first low Fe structural die casting alloy, Silafont-36 was developed by Rheinfelden, Germany in 1990 (Hartlieb, 2013). The iron content of the alloy is lowered to a maximum of 0.15%. Mn is used to replace iron for die soldering resistance and the content is in the range of 0.5% to 0.8%. In Japan, the ADC3SF aluminum alloy (also commonly labelled as W3 alloy) was developed by using even lower Mn content (0.3-0.4%).

Mercury Marine discovered the use of strontium (Sr) as an alternative to Mn to increase die-soldering resistance of casting alloys and utilized it for the Mercalloy series of die casting alloys (AA367, 368, and 362). The use of Sr allows lowering the Mn content further to only about 0.3%. In recent years, Mn and Sr are widely used to replace the Fe for die soldering resistance purpose, hence reducing the undesirable impacts of Fe needles on the mechanical properties of the Al-Si die casting alloys (Hartlieb, 2013).

2.5 The Nucleation and Growth of β Phase

To understand the β -AlFeSi, it is important to understand the nucleation sequence of Al-Si alloys due to the ability of the alloy to form primary alpha and beta phases. Little literature describes specifically the nucleation and growth of this phase. Cao and Campbell (2004) reported that the AlFeSi phase in Aluminum-Silicon alloys is formed by the nucleation on the double oxide layers film. The film surface reacts during the pouring and casting, hence inducing a surface turbulence.

The inner side of the oxide film is dry and unbounded due to the air that is trapped inside. The outer side on the other hand is in contact with the unsolidified molten alloy therefore it is only possible AlFeSi phase nucleation site. Cao and Campbell also outlined the relationship of nucleation site and hierarchy of the Al-Si-Mg die casting alloys as shown in Figure 1. The relationship shows that oxide layer can be nucleate substrates of all AlFeSi phase (Cao & Campbell, 2004).

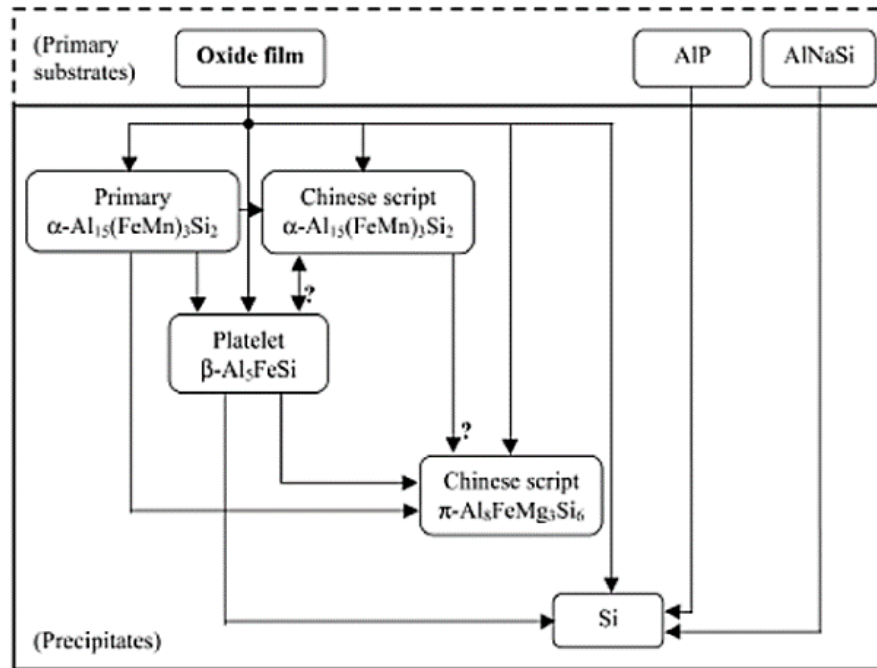


Figure 1: Possible nucleation hierarchy in AlSiMg alloys containing Fe and Mn contents (Reproduced from Cao and Campbell (2004))

2.6 Cooling Rate

Controlling the cooling rate has been an alternative viable method to control the formation of β -AlFeSi phase. Numerous studies have established that the β -AlFeSi phase is a stable phase at low cooling rates for the entire range of Fe and Si variation. The α -AlFeSi phase however, exists as metastable α -AlFeSi at high cooling rate (Iglesias, Frantz & Gantois, 1977; Narayanan, Samuel & Gruzleski, 1994). The stability of the AlFeSi phase depends on the critical transit cooling rate. Generally, critical transit cooling rate will increase with the Fe content (Mascre, 1955). The increase of cooling rate will decrease the formation temperature of β -AlFeSi phase until it is lower than the eutectic temperature (Castro-Román et al., 2015).

2.7 Heat Treatment

Another method to improve the mechanical property by the mean of altering the β -AlFeSi morphology is through the heat treatment. However very few researchers describe the effect of heat treatment to the β -AlFeSi phase conclusively. As explained in section 2.3, the length of β -AlFeSi phase governs the mechanical property of the alloy (Caceres & Taylor, 2006). Heat treatment can be applied to β -AlFeSi containing alloy to break the length of the phase. During the heat treatment at high temperature, the needle-shape β -AlFeSi phase platelets are broken into shorter, granulated particulates at the imperfect sites of the crystals (Crepeau, 1995).

Al-Fe-Si phases nonetheless cannot be easily transformed with heat treatment (Crepeau, 1995). This is because in practice, heat treatment needs high temperature due to the low Fe diffusion rate Fe in Al. Wang, Xu and Han (2016) address the effect of heat treatment to the morphology of the intermetallic in A380 alloy. The study concludes that morphology of AlFeSi phases can be altered with high solution temperature and solution time. 2 hours of solution time at 515°C solution temperature are the best parameters in decomposing the β -AlFeSi phase in A380 (Wang, Xu & Han, 2016). The morphology changes with solution time are described in Figure 2.

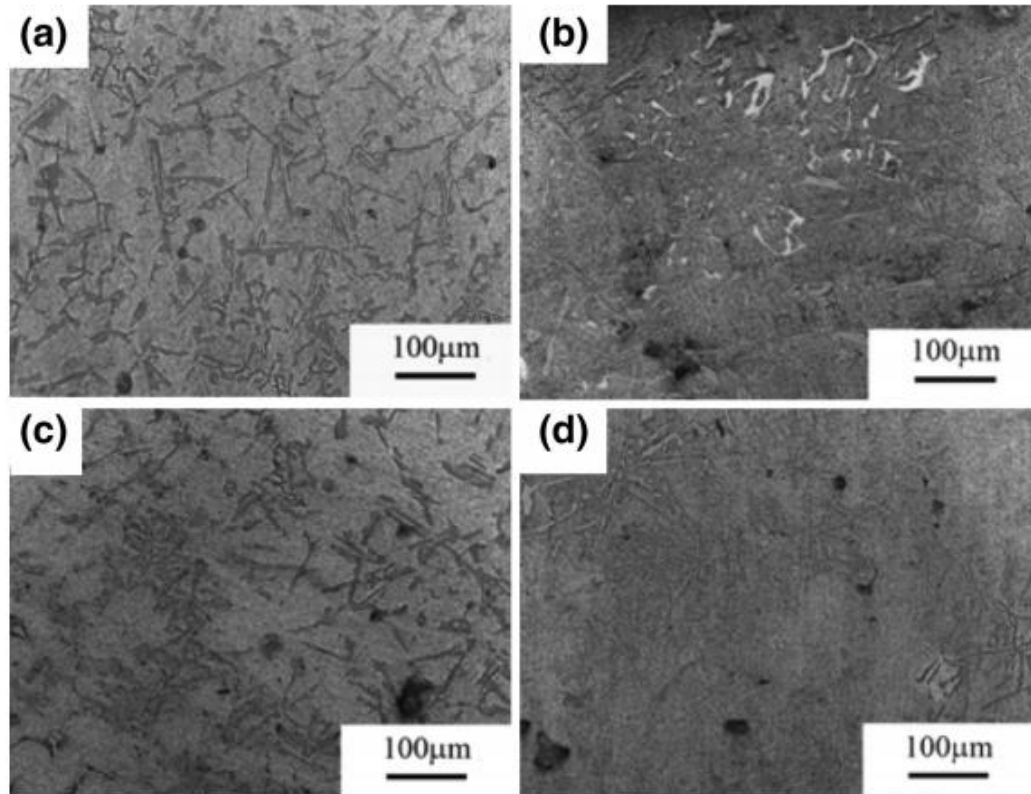


Figure 2: Morphology of the AlFeSi phases at 525°C for (a) 0.5 h; (b) 1 hour; (c) 2 hour; (d) 4 hour (Reproduced from Wang, Xu and Han (2016))

Practically, the requirement of high temperature has caused the heat treatment method to not be a preferred method in the die casting industry for alloy refinement. High solution temperature may cause surface blistering to the alloy during the heat treatment thus deteriorating the mechanical properties of the alloy. However, the blistering issue can be avoided if high quality casting is done whereby low tendency of microbubbles trapped in the casting part. The high solution temperature, while dissolving the β -AlFeSi, can melt the grain boundaries at the same time. Therefore, heat treatment can be expected to also reduce the strength of an alloy (Wang, Xu & Han, 2016).

2.8 Sludge Factor and Soldering Factor Limit

During die casting solidification process, sludge, and intermetallic phase contaminant may be formed within the cast and sleeve. The sludge takes a form of polyhedral structure and block-like brittle morphology of $Al_{12}(FeMnCr)_3Si_2$. Due to the morphology of the sludge, it is regarded as detrimental to the mechanical properties of the alloy and machining of the part. The sludge decreases the elongation property, thus the overall Quality Index of the alloy. The sludge also decreases the effective usage life of the machining tool due to the very hard particles (Shabestari, 2004).

Sludge formation amount is greatly affected by the content amount of iron, manganese and chromium. Although most of the time chromium is regarded as only an impurity, it is present in most die casting aluminum alloys and thus seen as a cause for sludge formation. Equation 2.1 represents the sludge factor with regard to the Fe, Mn and Cr weight percentage (Taylor, 2012). Sludge Factor is used to indicate the amount of sludge formed within the alloy. The critical sludge factor is 2 for Al-Si alloys, and sludge factor below the threshold point will not result in the formation of the sludge, given the casting temperature is more than $650^{\circ}C$ (Shabestari, 2004). Formation of sludge in the alloy is highly undesirable due to the difficulties to remove it using heat treatment.

$$Sludge\ Factor = Fe\ wt\% + 2 * Mn\ wt\% + 3 * Cr\ wt\% \quad (2.1)$$

Another important consideration in designing the alloy is the soldering factor. Soldering is the phenomenon whereby the cast alloy, during solidification, sticks to the die or core surface due to the chemical bonding of some elements or phases of the cast on the mold. The adhesion of the metal on the mold causes defects on the part or difficulties

in ejection of the part. Soldering can also increase die wear if not avoided. The soldering factor is governed by the amount of iron, manganese and strontium in the alloy. Equation 2.2 shows the soldering factor based on the Fe, Mn and Sr content. The recommended value of soldering factor for a high-quality die casting alloy is above 0.8 (Zhu, Schwam, Wallace & Birceaunu, 2004).

$$\text{Soldering Factor} = \text{Fe wt\%} + \text{Mn wt\%} + 10 * \text{Sr wt\%} \quad (2.2)$$

In designing alloy composition, both factors can be combined to guide the viable range of Fe and Mn in order to avoid the formation of sludge and soldering issue. Figure 3 shows the sludge factor and soldering factor lines for composition of Fe versus Mn. The blue region is the feasible region of consideration for acceptable values of sludge factor (Sludge Factor = 2) and soldering factor (Soldering Factor = 0.8) when Sr is 0.06%. Subsequently, the feasible region gets larger if the Sr content is lower down. The alloy must be designed within this feasible region in order to avoid the cast from having both sludge formation and soldering issue during the casting process.



Figure 3: Sludge factor and soldering factor for composition of Fe to Mn at different Sr content

2.9 Chapter 2 Summary

The overview of die casting aluminum alloys has been discussed briefly in section 2.1. The problem of β -AlFeSi phase in Al-Si die-casting alloy is elaborated in this literature review. The importance of minimizing the formation of β -AlFeSi phase has been highlighted in section 2.4. Three methods to refine β -AlFeSi: alloying element, heat treatment and cooling rate control have been discussed. Among the three methods outlined, element alloying is the most effective way to refine the β -AlFeSi phase. The effect of the alloying element has been discussed in section 2.2.10.

Another controlling method is heat treatment. Multiple studies have proven that β -AlFeSi can dissolve at high solution temperature as discussed in section 2.7. Heat

treatment would not introduce other impurity, but it needs high solution temperature and blistering may occur. Optimizing the utilization of these methods will be the focus of this research.

CHAPTER 3. RESEARCH METHODOLOGY

3.1 Introduction to Research Methodology

The primary objective of the research is to reduce the detrimental effect of β -AlFeSi phase to the mechanical properties, especially the elongation property of the die-casting alloys. To carry out the research, a thermodynamic simulation was utilized in studying the Al-Fe-Si phase effect in Al-Si die-casting alloy. According to the literature review, alloy composition is the most significant factor that influence the formation of the β -AlFeSi phase in die-casting alloys. Computherm Pandat software was used to simulate the thermodynamics equilibrium in Al-Si die-casting alloy at different alloy compositions. Based on the simulation results, five alloys at different compositions were proposed.

Experimental work was designed to validate the simulation results. The designed alloys were casted using the ASTM E8M - 04 standard aluminum alloy permanent mold casting into the tensile bar samples. The as cast samples were mechanically tested by using the tensile test machine to analyze the elongation and strength properties of the alloys. The as cast samples were also polished and observed under optical microscope for the purpose of microstructure characterization of the alloys.

The samples also underwent heat treatment at different conditions to study the optimal condition for improving the mechanical properties of the alloys. Similar to the as cast samples, the heat-treated samples were mechanically tested to study the effect of heat treatment on the mechanical properties of the alloys. The heat-treated samples were also

observed under microscope to record how heat treatment affects the morphology of the alloys.

3.2 Research Type

This research is a combination of quantitative and qualitative research. From the quantitative aspect, the project attempts to see if controlling the composition of the alloy has any effect to the mechanical properties of the aluminum alloy. Meanwhile, from the qualitative aspect, the project attempts to explain how transforming the morphology of the needle-like β -AlFeSi intermetallic phase can affect the mechanical properties of the alloy at the microstructure level.

3.3 Thermodynamics Simulation

The thermodynamics simulations were derived by using the Pandat Software Version 2016 copyright CompuTherm LLC. The software can produce the equilibrium phase diagrams and solidification curves based on an alloy composition/composition range. Meanwhile, the database used in this simulation is PanAluminum2016 database provided by the CompuTherm LLC. This database covers all common elements in the diecasting Aluminum alloys, namely Aluminum (Al), Silicon (Si), Manganese (Mn), Iron (Fe), Copper (Cu), Strontium (Sr), Magnesium (Mg), Potassium (K), Zinc (Zn), Cadmium (Ca), and Titanium (Ti).

The justification of the simulation work lies in the following aspects. Conducting thermodynamics analysis experimentally is challenging and time consuming. However,

simulation can substantially reduce the work of experiment. Instead of conducting experiment for hundreds of alloy compositions, Pandat simulation can produce the results in a much shorter time. The simulation can also give prediction of the phase formation and transformation during solidification. This is especially useful in this research as substantial amount of work is done to minimize the formation of the unfavorable intermetallic phases. In addition, thermodynamics calculation using the validated database gives fairly good results and provides a good estimation of workable range of alloy composition. A quaternary phase diagram produced by the mean of Pandat simulation is compared to an experimental phase diagram and the simulated result is shown to be closed to the experimental one.

While only the equilibrium condition can be simulated in Computherm Pandat software, the result of the simulation can give a general idea of the solidification behavior of alloys with certain compositions, thus can be utilized to optimize the range of alloy composition. In every simulation, only one of the specified elements was varied, while other elements are kept constant. The database that was used is PanAluminum, which is the most recent database designed for die-casting aluminum alloy.

The simulations were calculated based on the equilibrium, Lever and Scheil condition. Previous study by Wang (2014) enlists Si, Fe, Mg, Cu and Mn as the principal elements of A380 alloy, while other elements, including Zn, Sr, Na, Ca, Ti, and K, are treated as minor elements. Only the composition of principal elements will be varied due to significant effects on the formation of AlFeSi phase. The variation range of each element were determined based on the literature review. The details are given in Table 4.

Table 4: The variation range of principal elements of A380 alloy

Element	Si	Fe	Mg	Cu	Mn
Variation	5.0 –	0.4 –	0.1 –	1.0 –	0.2 –
Range (wt%)	13.0	2.0	1.0	4.0	2.0

The solidification path was simulated to model the solidification process of aluminum alloy to further understand the sequence of the phase formation during solidification. In this analysis, phase diagram information for multicomponent die casting aluminum alloys were coupled to solidification model to predict the solidification path. The Al-Fe-Si ternary phase diagrams and Al-Fe-Si-Mn quaternary liquid projections were calculated using Pandat software. The solidification paths of the die-casting alloys of certain compositions were plotted on the quaternary phase diagram. The sequence of reactions during solidification process was then matched with the solidification path to determine the phase formation on the solidification path.

3.4 Material Design

Based on the thermodynamic simulation result, five alloys of different composition were developed and casted into tensile bar specimens for mechanical testing and microstructure characterization purpose. Table 5 shows the nominal content (by mass percentage) of the five alloys designed based on the region identified on the liquidus projection of Al-Fe-Si-xMn phase diagram that inhibit formation of β -AlFeSi. The method of establishing the element fraction of each designed alloy is further elaborated throughout Chapter 4. The designed alloys are introduced in this research as Alloy #1, Alloy #2, Alloy #3, Alloy #4 and Alloy #5.

Table 5: Designed composition of alloys for mechanical characterization

Alloy	Si (wt%)	Fe (wt%)	Mn (wt%)	Cu (wt%)	Mg (wt%)	Zn (wt%)	Al (wt%)
#1	8	0.15	0.2	3.3	0.3	2.2	Balance
#2	10	0.15	0.2	3.3	0.3	2.2	Balance
#3	10	0.15	0.4	3.3	0.3	2.2	Balance
#4	8	0.5	0.2	3.3	0.3	2.2	Balance
#5	8	1	0.4	3.3	0.3	2.2	Balance

The base material used in the casting process is a commercial die casting A380 aluminum alloy, a hypoeutectic Al-Si alloy with a relatively low liquidus temperature at 600 °C and solidus temperature at 520 °C. The experimental alloy was prepared by using Mn pellets, Al-Mg, Al-Fe and Al-Cu master alloys. The composition of A380 alloy is specified in Table 6.

Table 6: Composition of A380 alloy

Element	Si	Fe	Mg	Cu	Mn	Ni	Zn	Al
wt%	9.0	1.0	0.2	3.5	0.4	0.3	0.35	Bal.

The aluminum ingots and master alloys of each element were melted in the electro-melt furnace at 750°C, then slowly homogenized and cooled down to 670°C for casting. The molten alloy was then casted into the standard tensile mold to produce the standard tensile bar specimens. Every composition alloy was casted into the aluminum alloy standard mold casting. The purpose was to produce the tensile bar according to the ASTM E 8M - 04 standard, the most common industrial standard used to determine the mechanical properties of the alloy. Figure 4 and table 7 specify the dimension of the

standard tensile bars as outlined by the ASTM standard. 100 samples were casted for each composition in this research.

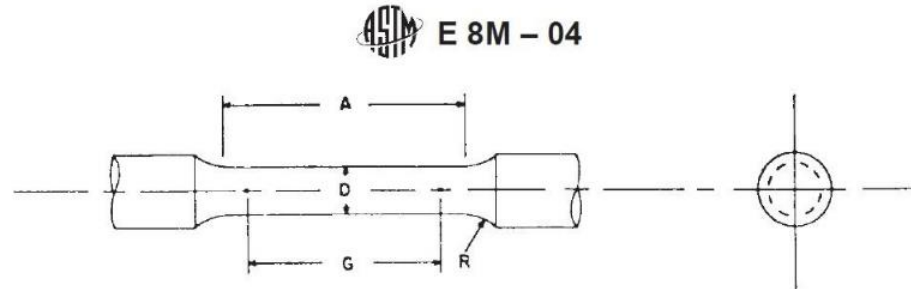


Figure 4: Specification of standard tensile bar for ASTM E 8M – 04

Table 7: Specification of Dimensions for standard tensile bar for ASTM E 8M – 04

Feature	Dimensions (mm)
Gage Length, G	30.0 ± 0.1
Diameter, D	6.0 ± 0.1
Radius of filler, R	6
Length of reduced section, A	36

For each composition, the casted samples were grouped to two categories: as-cast samples and heat-treated samples. The as-cast samples were used to see the effect of modifying the critical composition of die casting alloy to the mechanical properties and microstructure of the alloy. For this purpose, 15 samples were allocated for every composition. Meanwhile, the heat-treated samples were used to see the effect of heat treatment at various time to the mechanical properties and microstructure of the alloy. For this purpose, 36 samples were allocated for every composition.

3.5 Heat Treatment

A method to control the length formation of the β -AlFeSi as found in literature is through the heat treatment. Heat treatment can be applied to β -AlFeSi containing alloy to break the length of the phase. During the heat treatment at high temperature, the needle-shape β -AlFeSi phase platelets are broken into shorter, granulated particulates at the imperfect sites of the crystals (Crepeau, 1995).

Al-Fe-Si phases nonetheless could not be easily transformed with the heat treatment. This is because heat treatment needs high temperature due to the low Fe diffusion rate Fe in Al. High temperature may cause blistering to the alloy during the heat treatment thus worsen the mechanical properties of the alloy (Crepeau, 1995).

To avoid blistering issue, a modified T4 condition of heat treatment was designed and applied to the alloy samples. Solidus temperature were calculated for every alloy using Pandat Computherm software. Subsequently, solution temperature for the heat treatment was designed to be 30°C below the calculated solidus temperature of each alloy as outlined in Table 8.

Table 8: Solidus Temperature and Solution Temperature for heat treatment

Alloy	Solidus Temperature (°C)	Solution Temperature (°C)
#1	533.4	503
#2	535.8	506
#3	535.6	506
#4	509.5	480
#5	509.5	480

The alloy specimens of each composition underwent solution heat treatment at the prescribed temperature for 1 hour, 2 hours, 4 hours, 8 hours, 16 hours and 32 hours. Each of the samples that were heat treated at various time were mechanically tested and microstructurally analyzed to record the effect of the heat treatment to the mechanical properties and microstructure of the alloy.

3.6 Mechanical Properties Analysis

All the tensile specimens underwent the tensile test by tensile test machine to determine the engineering stress and the strain of the alloy until the specimens reach the mode of failure. From the stress strain curve graph, the mechanical elongation and strength in terms of the UTS of the alloy of a particular composition were calculated.

In this analysis, the independent variables were the composition of the alloy and the heat treatment conditions, while the dependent variable was the strength of the alloy. The result of the mechanical test was statistically analyzed to determine if the null hypothesis, that controlling the composition of Al-Si alloy has no effect to the mechanical properties of the alloy, can be rejected.

3.7 Microstructure Analysis

The microstructure characterization is a local characterization from a micro level to explain how the composition of the alloy effect the formation of α -AlFeSi and β -AlFeSi intermetallic phases, thus influencing the mechanical properties of the alloy. In

the microstructure analysis, the as-cast samples from each composition of the alloy were polished carefully.

This section addresses the microstructural observation and analysis of the experimental samples of the five different alloys. The alloys that had been casted into the tensile bars were cut and sub-grouped into two categories. The first category is the fractured samples and the second category is the polished samples. The fractured samples were taken from the fractured tensile bars (obtained from the mechanical testing) and cut using diamond blade saw into 5mm depth samples. These samples were used to observe the behavior of the fracture of the alloys.

The polished samples on the other hand were obtained from the tensile bars that are not mechanically tested. The samples were cut using the diamond blade saw into 5mm depth samples at the middle section of the bar. All the polished samples were then mounted on epoxy mounting using hot compression mounting process by LECO Bakelite. The mounting process was done to improve handling of the materials and protect the integrity of the edge and surface area.

The mounted samples were manually polished by using silicon carbide pads of 240, 400, 600 and 1200 grit in the sequence order. The samples were then manually polished using TEMO 0.5 Micron diamond polish lapping paste compound for their final polish. Carl Zeiss Axioscope 7 optical microscope was used as the microscope to observe the morphology of the polished samples. The microstructure pictures were taken by using the Axiocam 305 color camera and the measurements were done by using the Zen-Zeiss imaging software.

The α -AlFeMnSi and β -AlFeSi intermetallic phases analysis is the focus of the study as they are the main influence on the mechanical property of the The existence of α -AlFeMnSi and β -AlFeSi intermetallic phases was apparent in the microscopic observation of all the five different alloys. Figure 5 shows the example of a microscopic image with α -AlFeMnSi and β -AlFeSi intermetallic phases. The α -AlFeMnSi intermetallic phase is the Chinese-script like structure as observed on the right side of the image. Meanwhile the β -AlFeSi intermetallic phase is the needle-like structure as observed on the left side of the image.

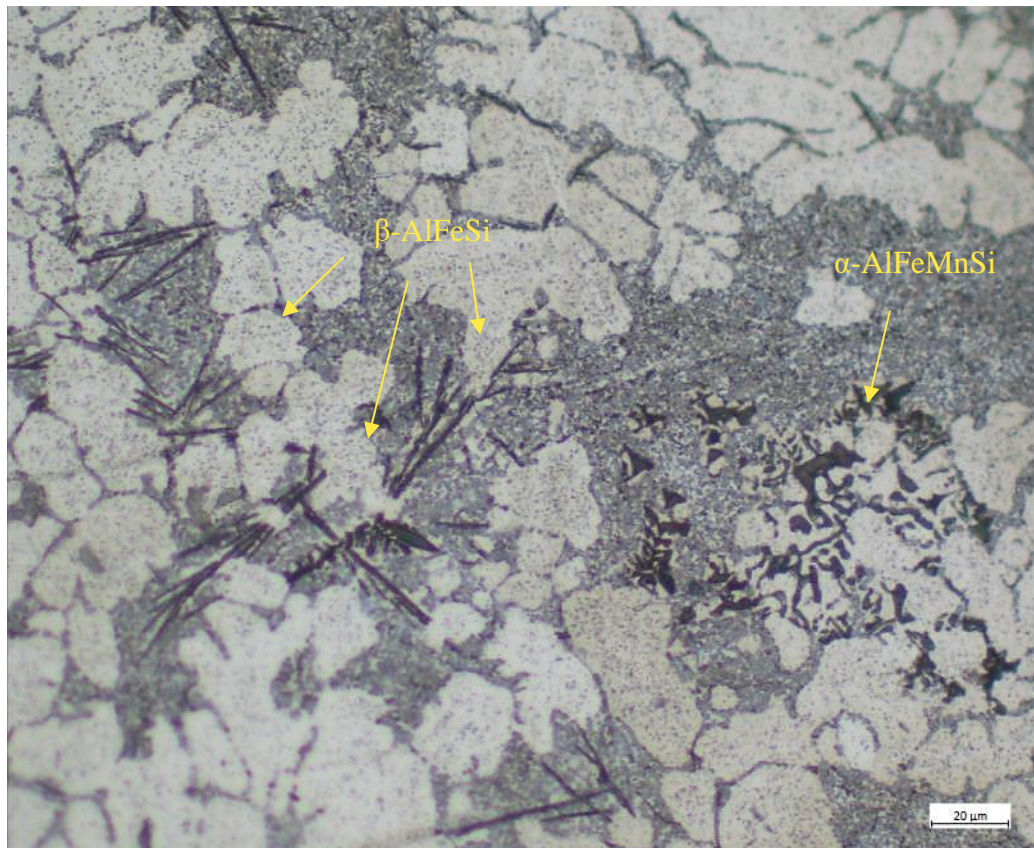


Figure 5: Intermetallic phases observed in the designed alloy under optical microscope

β -AlFeSi intermetallic phases were measured by taking five fields with observed needles. The five needles were measured and averaged, combining with the other field to

establish the length of the beta phase for a given composition. The α -AlFeMnSi intermetallic phases, if observed, were measured by identifying the entire length of the branch spacing. The entire length measured was divided by the branch number to estimate the average spacing of the alpha phase. The measurement will then be combined with the measurements from the other four fields to establish the length of the alpha phase for a given composition.

Scanning Electron Microscopy (SEM) analysis was conducted to observe the fracture surface of each designed alloy. The fracture surface morphology at the 2000X magnification can be utilized to explain the fracture behavior of the materials. SEM was also used to characterize the transformation of eutectic silicon structure with increasing heat treatment time. MIRA3 Tescan SEM machine in Chrysler Kokomo Casting Plant was used to carry out the fracture analysis.

3.8 Chapter 3 Summary

Thermodynamics simulation and casting experiment were used to study on the Al-Fe-Si phase in Al-Si diecasting alloy. PanAluminum database in Computherm Pandat software was used to simulate the thermodynamics condition during solidification process of diecasting alloy. According to the simulation results, experiments were design and five different alloy castings were made by controlling alloy compositions. Microstructure and mechanical testing were carried out to analyze the effect of morphology control to the mechanical properties of the alloys. The effect of heat treatment to the mechanical properties and microstructure of the alloy were also studied by introducing the modified T4 heat treatment to the designed alloys.

CHAPTER 4. THERMODYNAMIC SIMULATION

4.1 Introduction of Thermodynamic Simulation

The chapter presents and discusses the results of the thermodynamic simulation analysis done within the scope of this research. The results can give an estimation of the feasible range of aluminum alloy composition.

In section 4.2, the experimental results of tensile testing for varied compositions are shown. The results conclude the optimal composition for the aluminum alloy in terms of the quality index. Meanwhile, the experimental results of tensile testing for varied heat treatment conditions are presented in section 4.3.

The final section of this chapter, section 4.4 focuses on the results of microscopic observation of the metallurgy of the alloys at different compositions and heat treatment conditions. The observations are used to explain the mechanical testing results obtained in section 4.2 and section 4.3.

4.2 The Effect of Single Element to Phase Formation Sequence

In studying the effect of single element change, one element was varied (using the range of composition according to American Foundry Society standard), while the other elements were kept constant at the nominal composition of the A380 aluminum alloy. The simulation output was the binary phase diagram and the region/range of phase formation is the main focus of the analysis. The elements varied were the principle elements of the die casting aluminum alloy, namely Si, Fe, and Mn. Other elements in the

die casting alloy such as Mg, Sr, Zn, Sr, K, Ca and Ti do not have significant effect on the formation of AlFeSi intermetallic phase (Wang, 2014), therefore were not considered in this analysis section.

4.2.1 Silicon (Si)

Si is a major element in die casting alloy due to its ability to increase the fluidity of the alloy and reduce the shrinkage porosity. Due to that, die casting alloys such as A380 tend to have relatively high percentage by weight of Si compared to other types of aluminum alloy. However, a higher Si content alters the sequence of phase formation, especially that of the AlFeSi intermetallic phase.

Figure 6 illustrates the binary Al-xSi phase diagram for solidification of A380 for the range of 5% to 12% which is the common range of Si for die casting alloys according to American Foundry Society standard. The diagram shows that for this range, the primary α -AlFeMnSi phase will be formed first. In another words, for Al-Si die casting alloys where Si must be maintained within the range of 5 – 12% to provide fluidity, the formation of primary α -AlFeMnSi phase is inevitable for equilibrium casting environment. This confirms the literature findings from study by Samuel & Samuel (1996).

However, when the Si content is below approximately 9.7%, the formation of primary α -AlFeMnSi phase is followed by the nucleation of FCC α -Al. Meanwhile, when the Si content is 9.5% to 12%, the formation of the primary phase is followed by the nucleation of β -AlFeSi. Therefore, while it may be favorable to have higher Si content due to fluidity and hot tearing resistance advantage, it leads to the formation of secondary

detrimental β -AlFeSi phase which severely affect the mechanical property. FCC α -Al, α -AlFeMnSi, β -AlFeSi and Si are the only four solid phases formed during solidification.

The nucleation sequence of the alloy for Si range of 5% to 12% are recorded in Table 9.

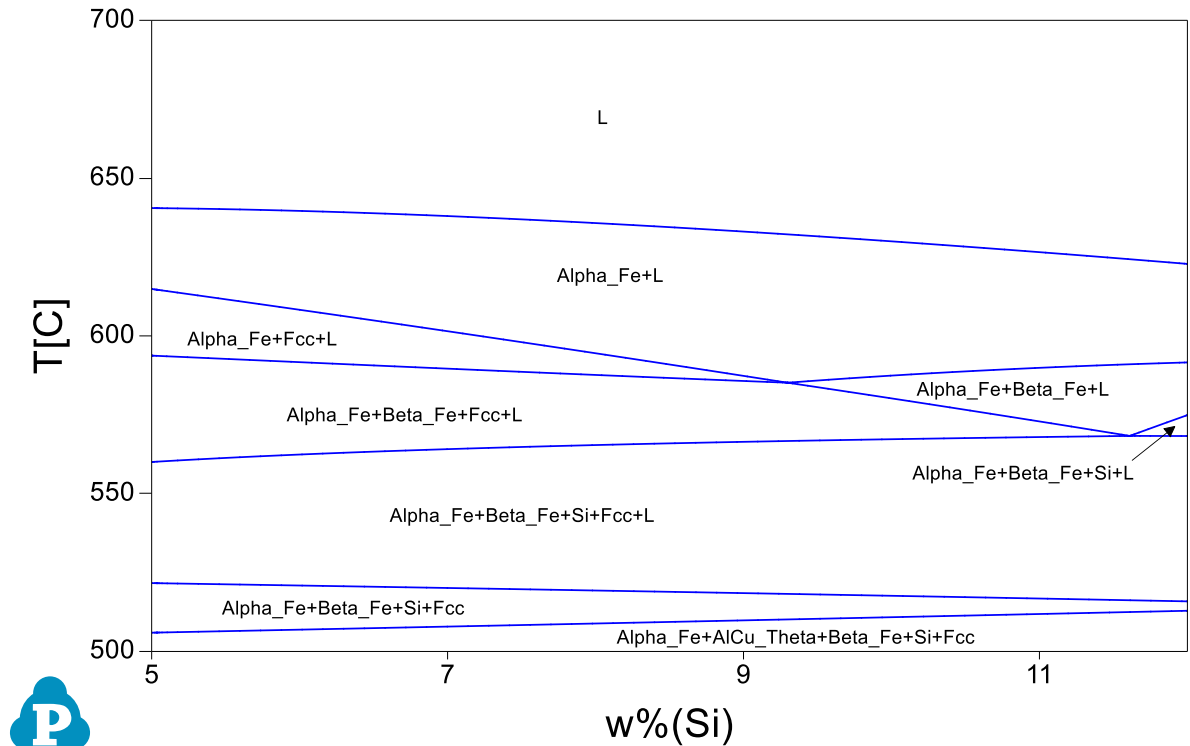


Figure 6: Binary phase diagram of A380 alloy-xSi

Table 9: Nucleation sequence of A380 alloy-xSi

Nucleation Sequence	Si wt%		
	5 – 9.5	9.5 – 11.5	11.5 – 12
1	α -AlFeMnSi	α -AlFeMnSi	α -AlFeMnSi
2	FCC α -Al	β -AlFeSi	β -AlFeSi
3	β -AlFeSi	FCC α -Al	Si
4	Si	Si	FCC α -Al
5	Al ₂ Cu	Al ₂ Cu	Al ₂ Cu

4.2.2 Iron (Fe)

Multiple literatures show that Fe is a crucial element that affects the formation of intermetallic phases in Al-Si alloy. In this section, the effect of Fe to the sequence of phase formation was studied using the Al-xFe binary phase diagram. Figure 7 shows the Al-xFe phase diagram for the range of 0 to 2% Fe, which is a typical range for die casting alloys by the American Foundry Society (AFS) standard. Meanwhile, the nucleation sequence of the alloy for the range of 0 to 2% Fe are recorded in Table 10.

The nucleation sequence shows that different content of Fe yield changes to the sequence. It is interesting to note that although Fe is the major cause for formation of β -AlFeSi, the phase does not precipitate until Fe content reaches 0.48%. For the range 0 to 0.15, the FCC α -Al precipitates first, followed by the formation of other phases. In contrast, if the Fe is more than 0.15, α -AlFeMnSi will first nucleate.

If the Fe level is more than 1.2%, both α -AlFeMnSi and β -AlFeSi intermetallic phases will form before the nucleation of α -Al. This is especially undesirable because it gives longer time for the β -AlFeSi to nucleate and grow in larger size, subsequently negatively affecting the mechanical properties of the alloy. The result agrees with finding by Donahue (2011) that suggests the Fe level for die casting alloys to be kept lower than 1.3%. Therefore, in designing the alloy, keeping the Fe content low is favorable to avoid the nucleation of the intermetallic phase, especially the β -AlFeSi phase. FCC α -Al, α -AlFeMnSi, β -AlFeSi and Si are the only four solid phases formed during solidification.

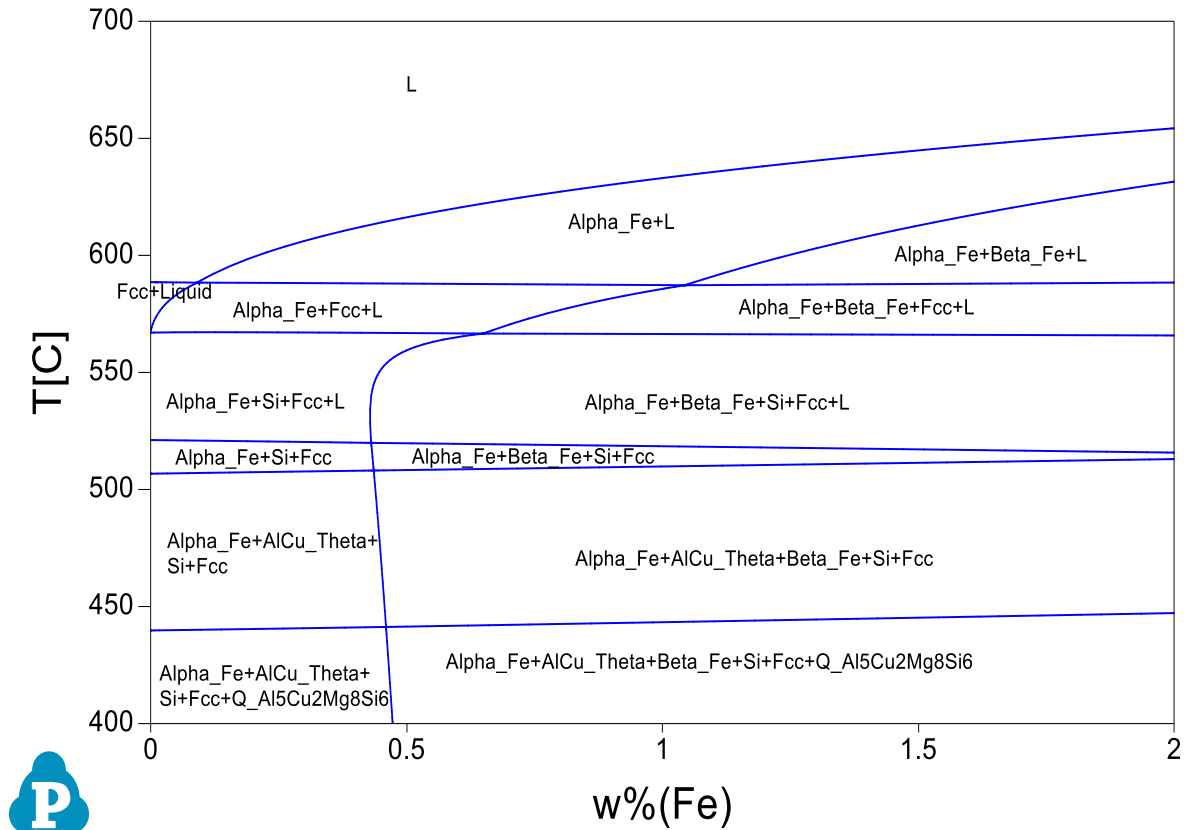


Figure 7: Binary phase diagram of A380 alloy-xFe

Table 10: Nucleation sequence of A380 alloy-xFe

Nucleation Sequence	Fe content (wt%)				
	0 – 0.15	0.15 – 0.48	0.48 – 0.65	0.65 – 1.2	1.2 - 2
1	FCC α -Al	α -AlFeMnSi	α -AlFeMnSi	α -AlFeMnSi	α -AlFeMnSi
2	α -AlFeMnSi	FCC α -Al	FCC α -Al	FCC α -Al	β -AlFeSi
3	Si	Si	Si	β -AlFeSi	FCC α -Al
4	Al ₂ Cu	Al ₂ Cu	β -AlFeSi	Si	Si
5	AlCuMgSi	AlCuMgSi	Al ₂ Cu	Al ₂ Cu	Al ₂ Cu
6	-	-	AlCuMgSi	AlCuMgSi	AlCuMgSi

4.2.3 Manganese (Mn)

Mn has been regarded as an effective Fe corrector to naturalize the detrimental effect of Fe due to the high similarity of Mn and Fe atomic structures (Colwell & Kissling, 1961). Therefore, this research intends to see if Fe can effectively be replaced by Mn, hence minimizing the formation of the detrimental β -AlFeSi phase. To analyze the nucleation sequence, Al-xMn binary phase diagram was simulated for the range of 0 to 2% Mn as shown in Figure 8. Meanwhile, the nucleation sequence of the alloy for the range of 0 to 2% Mn are recorded in Table 11.

The simulated phase diagram displays the opposite trend compared to increasing Fe content. Here, the tendency to form the β -AlFeSi phase decreases with the increase of Mn content. For 0 - 0.2% Mn, β -AlFeSi phase forms as the primary phase, hence unfavorable as primary β -AlFeSi will lower the elongation property. Meanwhile, the α -AlFeMnSi will form as the primary phase if the Mn content is within the range of 0.2 to 2%. Therefore, in designing the alloy composition, it is proposed that Mn content to be kept above 0.2%.

The ratio of Mn to Fe is also vital in controlling the formation of the β -AlFeSi. Within the range of 0.9 to 2% Mn, the formation of β -AlFeSi phase was eradicated. The range underlies within the range of ratio Mn:Fe more than 0.9. Therefore, it is proposed that the ratio of Mn:Fe to be above 0.9 when designing the alloy composition.

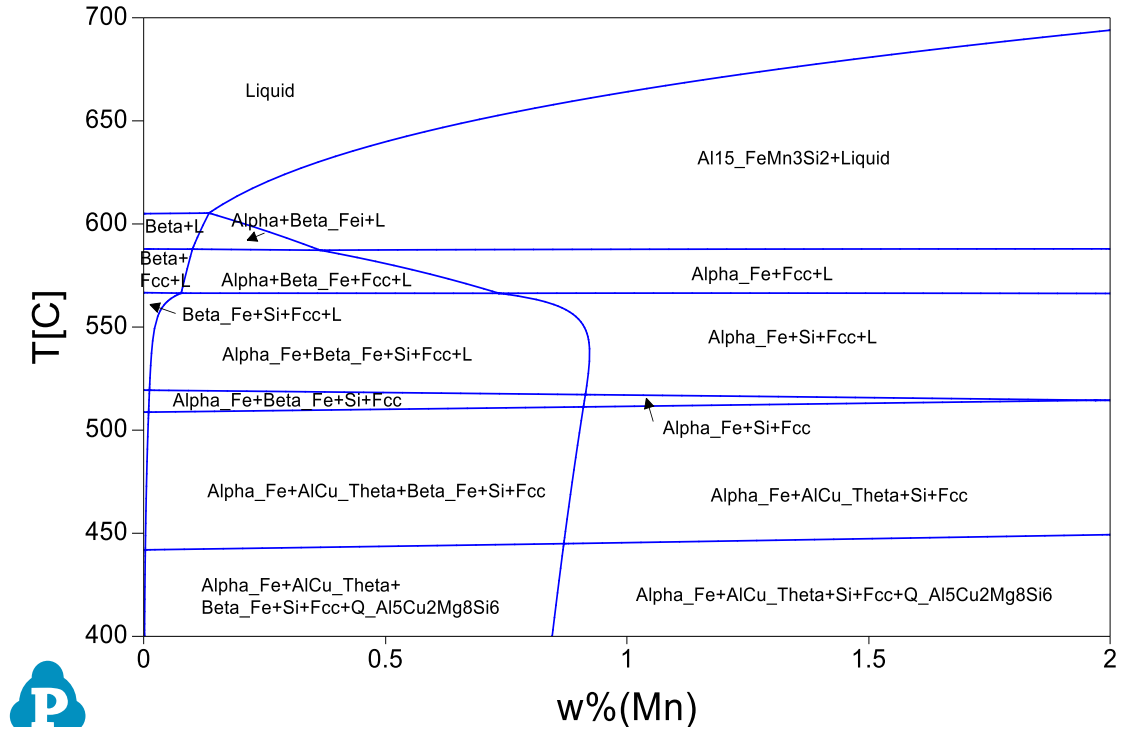


Figure 8: Binary phase diagram of A380 alloy-xMn

Table 11: Nucleation sequence of A380 alloy-xMn

Nucleation Sequence	Mn content (wt%)						
	0 – 0.1	0.1 – 0.15	0.15 – 0.2	0.2 – 0.37	0.37 – 0.75	0.75 – 0.9	0.9 - 2
1	β -AlFeSi	β -AlFeSi	β -AlFeSi	α -AlFeSi	α -AlFeSi	α -AlFeSi	α -AlFeSi
2	FCC α -Al	FCC α -Al	α -AlFeSi	β -AlFeSi	FCC α -Al	FCC α -Al	FCC α -Al
3	Si	α -AlFeSi	FCC α -Al	FCC α -Al	β -AlFeSi	Si	Si
4	Al ₂ Cu	Si	Si	Si	Si	β -AlFeSi	Al ₂ Cu
5	AlCuMg Si	Al ₂ Cu	AlCuMg Si				
6	-	AlCuMg Si	AlCuMg Si	AlCuMg Si	AlCuMg Si	AlCuMg Si	-

4.3 The Solidification Path of Die Casting Alloys

The Al-Fe-Mn-Si system was particularly analyzed in this study. In each standardized die-casting alloy with given silicon content, the amount of iron and manganese present play important roles in establishing mechanical properties of the material being produced. It is therefore of a special interest to investigate the precipitation of Fe- and Mn- containing phases.

Figure 9 illustrates the Al-Fe-Si liquidus projection (Mn content is 0%). The projection shows that there is no primary Al-Fe-Si phase formation if the Fe composition is lower than 0.5%. Meanwhile, line (a) is the boundary line whereby the formation of both α -AlFeSi and β -AlFeSi phases occur. The boundary line is important as it indicates the limitation of Fe and Si composition in the alloy, for which it determines the phase formation sequence during the alloy solidification.

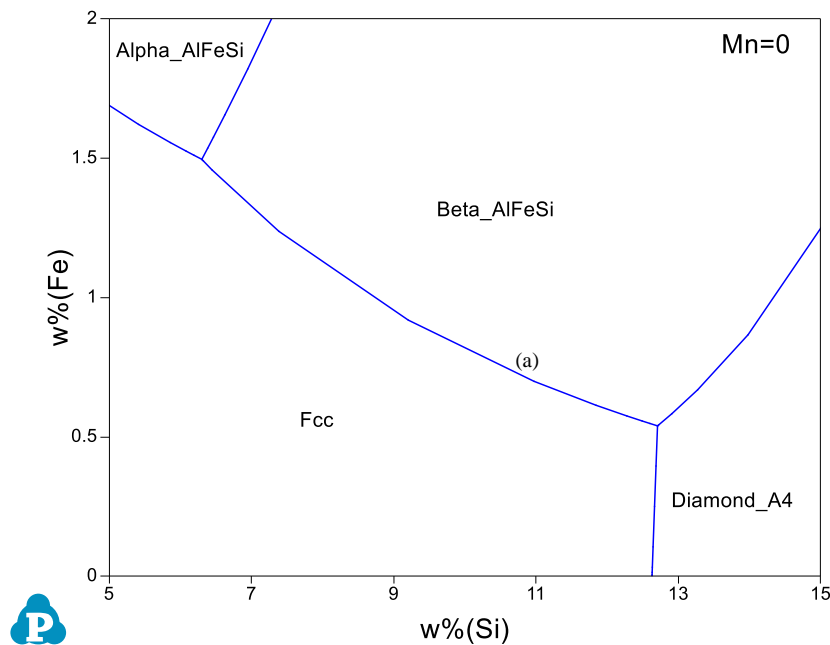


Figure 9: Al-Fe-Si liquidus projection

This Al-Fe-Si-0%Mn liquidus projection agrees with the finding by Backerud (1994). Figure 10 shows the Backerud's Al-Fe-Si liquidus projection. In his study, Backerud constructed the similar liquidus projection of Al-Fe-Si ternary system from the value obtained in elaborated thermodynamics experiments.

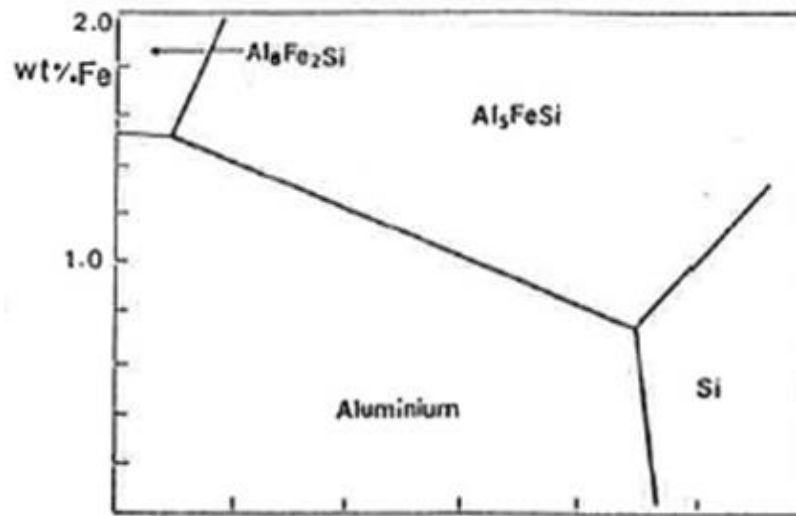


Figure 10: Backerud's Liquidus Projection (Reproduced from Backerud (1994))

Commercially available die casting alloys, A360 and B360 were used to model the solidification paths analysis. The comparison between the two alloys were done because these alloys have distinct difference in terms of the Fe content, while the other major elements are similar. Table 12 details the composition of both alloys. Phase diagram information for these alloys were coupled to solidification model to predict the solidification path. The Al-Fe-Si ternary phase diagrams and Al-Fe-Si-Mn quaternary liquid projections were calculated using Pandat software. The solidification paths of the selected die-casting alloys were plotted on the quaternary phase diagram. The sequence

of reactions during solidification process was then matched with the solidification path to determine the phase formation on the solidification path.

Table 12: Composition of A360 and B360

Alloy	Composition (wt%)						
	Si	Fe	Mn	Cu	Mg	Zn	Ni
A360	9.5	1.3	0.3	0.6	0.5	0.5	0.5
B360	9.5	0.4	0.3	0.6	0.5	0.2	0.1

Figure 11 represents the composition of A360, and the blue line illustrates its solidification path. The solidification path starts within the β -AlFeSi region, therefore the formation of β -AlFeSi occurs at the beginning of the solidification process. Line (i) indicates the formation of β -AlFeSi, which occurred until the through between the α -AlFeSi and β -AlFeSi phases is reached. During this phase, the Fe fraction is reduced to form the β -AlFeSi, while Si content maintains its fraction. The reaction continues with the formation of secondary α -AlFeSi and β -AlFeSi along the boundary line (ii) until the ternary eutectic composition was reached. Fe, Mn and Si fraction are consumed within this phase. The solidification continues with the formation of Al, Si and α -AlFeSi in the ternary eutectic at point (iii). The complete nucleation sequence of A360 is shown in the Table 13. The sequence of formation starts with the formation of α -AlFeSi and β -AlFeSi, followed by Al and finally Si.

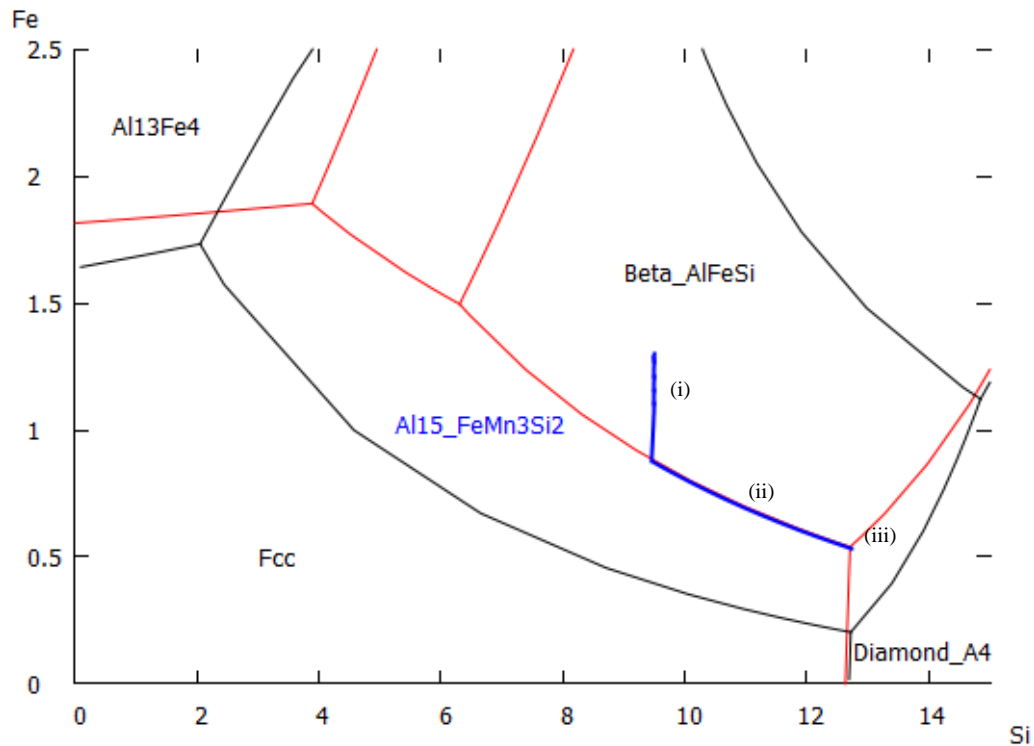


Figure 11: The solidification path of A360 alloy

Table 13: Reaction during solidification of A360 alloy

Temp (K)	Reactions during Solidification
906.79	$\text{Liq} \rightarrow \text{Al}_{15}\text{FeMn}_3\text{Si}_2 (\alpha)$
880.92	$\text{Liq} \rightarrow \text{Al}_{15}\text{FeMn}_3\text{Si}_2 (\alpha) + \text{AlFeSi} (\beta)$
871.36	$\text{Liq} \rightarrow \text{Al}_{15}\text{FeMn}_3\text{Si}_2 (\alpha) + \text{AlFeSi} (\beta) + \text{Al}$
848.56	$\text{Liq} \rightarrow \text{Al}_{15}\text{FeMn}_3\text{Si}_2 (\alpha) + \text{AlFeSi} (\beta) + \text{Al} + \text{Si}$

Meanwhile, Figure 12 represents the composition of B360, and the green line shows its solidification path. B360 has the same composition as A360, except having lower Fe content. The solidification path starts within the α -AlFeSi region, hence the α -AlFeSi phase is a more dominant phase formation. Line (iv) illustrates the formation of α -AlFeSi and Al until the through between the α -AlFeSi and Si is reached. During this phase, the Si fraction is reduced to form the α -AlFeSi, while Fe content maintains its fraction.

The reaction continues with the formation of secondary α -AlFeSi, Al and Si along the boundary line (v) until the ternary eutectic composition is reached. During this phase, the Al and Mn fractions are consumed while Si fraction is constant, therefore the Fe fraction is increased. The solidification continues with the formation of β -AlFeSi in the ternary eutectic at point (vi). The nucleation sequence of B360 alloy is shown in Table 14. The sequence of formation starts with the formation of α -AlFeSi and Al, followed by Si and finally β -AlFeSi.

The reduction of Fe can shift β -AlFeSi to α -AlFeSi phase. Fe addition above the α -AlFeSi and β -AlFeSi boundary line introduces the β -AlFeSi at the start of solidification process, hence became a large phase within the solidified aluminum alloy. In contrary, the β -AlFeSi forms last at the end of solidification process, therefore the formation is very minimal. By comparison, the result of the simulation shows that for A360, the β -AlFeSi fraction formed is 0.02954, while for B360 which has less Fe content, the β -AlFeSi fraction is reduced to 0.00526.

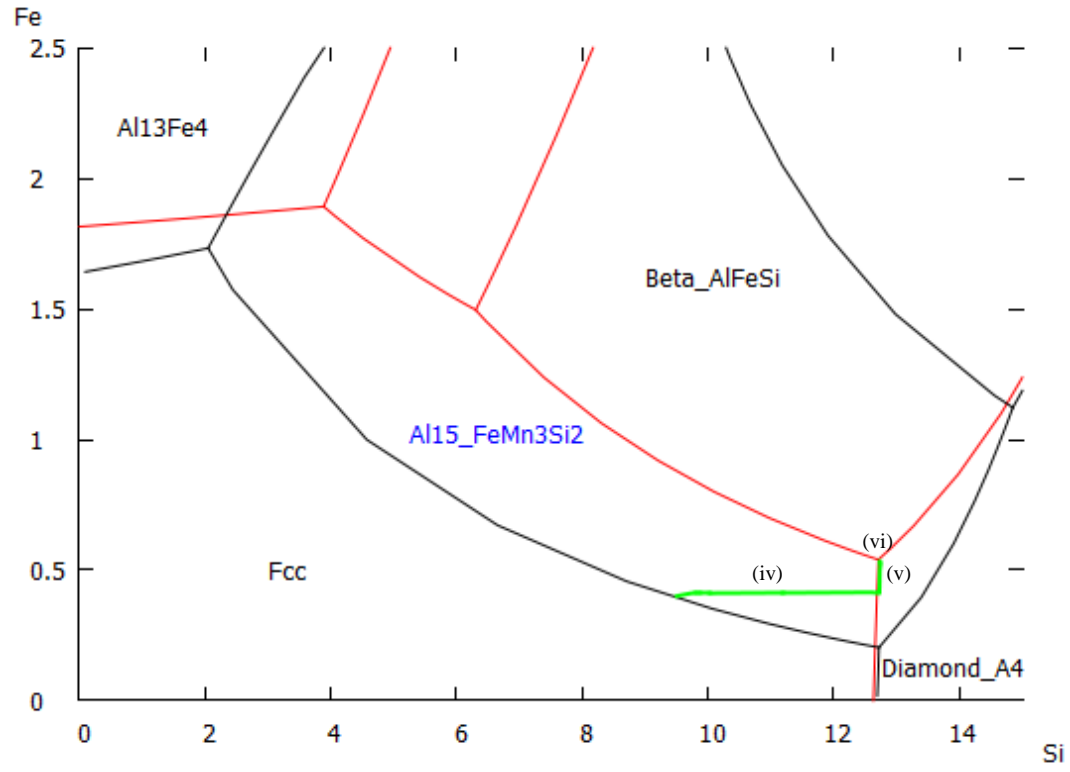


Figure 12: The solidification path of B360 alloy

Table 14: Reaction during solidification of B360 alloy

Temp (K)	Reactions during Solidification
872.21	Liq → Al ₁₅ FeMn ₃ Si ₂ (α)
871.80	Liq → Al ₁₅ FeMn ₃ Si ₂ (α) + Al
848.77	Liq → Al ₁₅ FeMn ₃ Si ₂ (α) + Al + Si
848.56	Liq → Al ₁₅ FeMn ₃ Si ₂ (α) + Al + Si + AlFeSi (β)

4.4 Solidification Path for Common Commercial Die Casting Alloys

The Al-Fe-Mn-Si system was further analyzed in this study. In each standardized die casting alloy with given silicon content, the amounts of iron and manganese present play important roles in establishing mechanical properties of the material being produced. It is therefore of a special interest to investigate the precipitation of Fe- and Mn-containing phases. To understand how the composition affect the solidification path and its correlation to the beta phase fraction and mechanical properties, solidification paths of common commercial die casting alloys were mapped on the liquidus projection. The compositions of the alloys being analyzed are listed in Table 15.

Table 15: Compositions of commercial die casting alloys

Alloy	Composition (wt%)						
	Si	Fe	Mn	Cu	Mg	Zn	Ni
A360	9.5	1.3	0.3	0.6	0.5	0.5	0.5
B360	9.5	0.4	0.3	0.6	0.5	0.2	0.1
D380	8.5	1.3	0.5	3.5	0.2	1.0	0.5
F380	8.5	0.4	0.3	3.5	0.2	1.0	0.1
381	9.5	1.3	0.5	3.5	0.13	3.8	0.5
A381	9.5	0.4	0.3	3.5	0.13	3.8	0.1
A383	10.5	1.3	0.5	2.5	0.2	3.0	0.3
C383	10.5	0.4	0.3	2.5	0.2	3.0	0.1
C384	11.25	1.3	0.5	3.5	0.2	3.0	0.5
D384	11.25	0.4	0.3	3.5	0.2	3.0	0.1

The solidification path for all selected die-casting alloys were plotted on the Al-Si-Fe-Mn quaternary liquidus projection as shown in Figure 13. The alloys exhibit the

similar path trends as A360 and B360, whereby the Fe content affects the the β -AlFeSi formation. From the calculation of β -AlFeSi fraction, it is observed that D380 form β -AlFeSi the most, followed by the A360, 381, A383 and C384. As β -AlFeSi is formed along the the α -AlFeSi and β -AlFeSi boundary line, it can be deduced that the longer the path through the the α -AlFeSi and β -AlFeSi boundary line, the higher the fraction of β -AlFeSi phase formation. For example, A360 alloy, undergoing the longer path through the boundary line, has 0.0295 β -AlFeSi fraction, while A383 alloy, with shorter path through the boundary line, has 0.0254 β -AlFeSi fraction.

Meanwhile, the simulation result shows that the pairing die-casting alloys with lower percentage of Fe form much less β -AlFeSi. A383 alloy forms 0.0254 of β -AlFeSi fraction, while its pairing alloy, C383 alloy which had lower Fe content only forms 0.0052 of β -AlFeSi fraction. The reduction of β -AlFeSi fraction with the reduction of Fe content is consistent for all the selected die-casting alloy being analyzed.

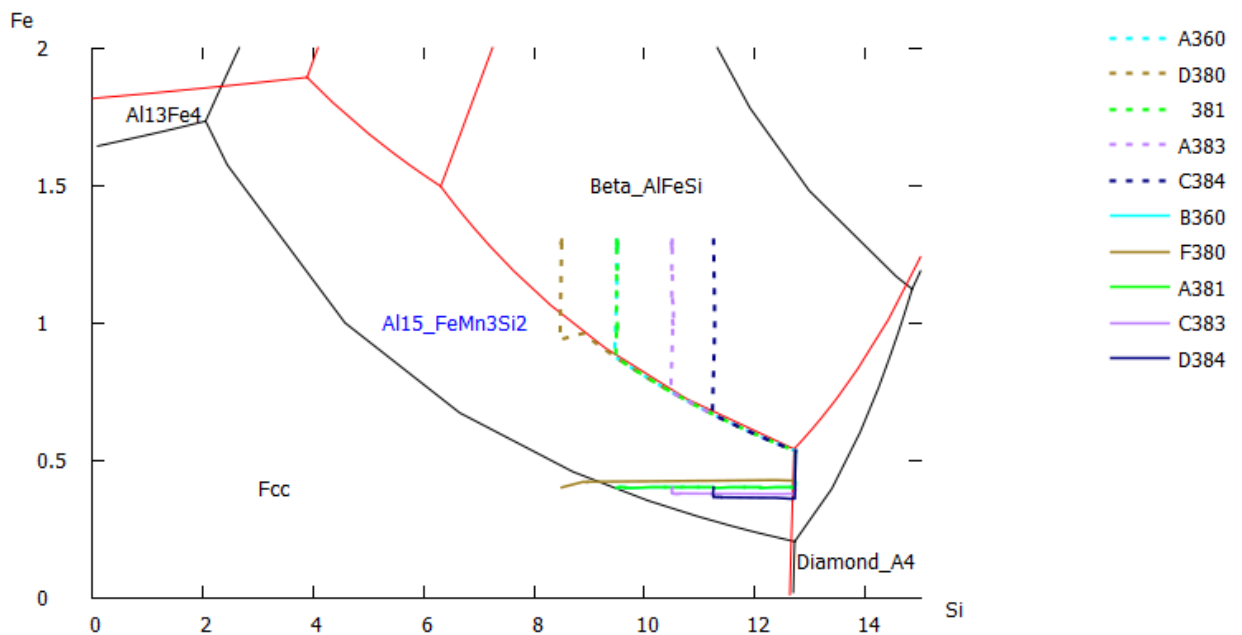


Figure 13: Solidification Path of DC Alloys by Thermodynamic Simulation

Figure 14 shows the comparison between β -AlFeSi phase fraction from the result of simulation with the Quality Index of the die casting alloys from the study by Donahue (2016) for three pairing die casting alloys. For every pair of alloys, the lower the β -phase formation, the higher the Quality Index is. For example, B360 has lower Fe content compared to A360, resulting in lower β -AlFeSi phase fraction by 81.2%.

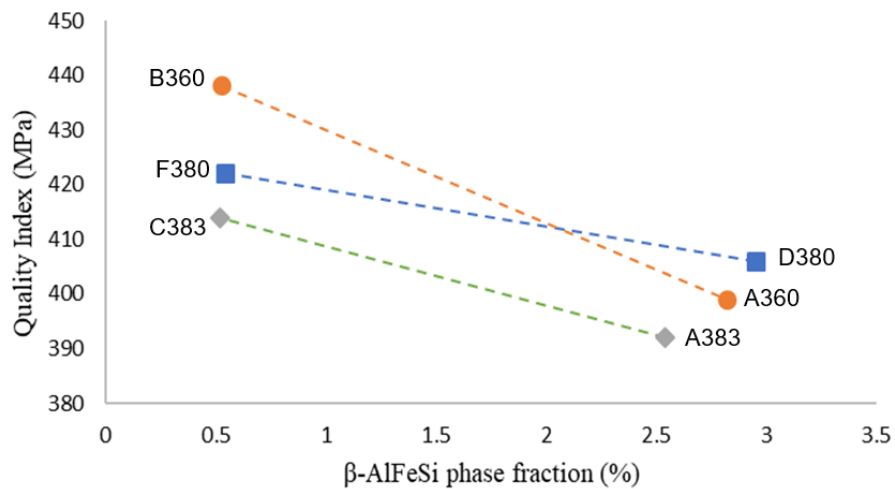


Figure 14: Quality Index by β -AlFeSi phase fraction

4.5 Proposed Alloy Composition based on Thermodynamic Analysis

The method of thermal dynamic simulation to predict the α -AlFeSi and β -AlFeSi phase formation of the aluminum die-casting alloy indicates the following deductions:

1. The addition of Fe in the composition of the alloy favors the formation of the β -AlFeSi phase.
2. The fraction of β -AlFeSi formation is dictated by whether the composition is above or below the α -AlFeSi and β -AlFeSi boundary line. If the Fe level is

above the boundary line, the β -AlFeSi phase is larger due to it being formed at the starting of the solidification.

3. The β -AlFeSi phase always forms subsequently after the α -AlFeSi phase.
4. Reducing Fe content in the alloy tends to reduce the the β -AlFeSi phase fraction more substantially than the α -AlFeSi phase.
5. The longer the solidification path through the the α -AlFeSi and β -AlFeSi boundary line, the higher the fraction of β -AlFeSi phase formation.
6. Reducing the β -AlFeSi phase formation increases the Quality Index of the alloy.

Based on the deduction on solidification path analysis, five alloys of different compositions were proposed to be fabricated. The alloys compositions are enlisted in Table 16. The proposed alloys have compositions with varied Si, Fe, Mn and Al content, while keeping the other elements, Cu, Mg and Zn to be consistent at nominal A380 alloy compositions.

Table 16: Proposed composition of the alloys

Alloy	Si (wt%)	Fe (wt%)	Mn (wt%)	Cu (wt%)	Mg (wt%)	Zn (wt%)	Al (wt%)
#1	8	0.15	0.2	3.3	0.3	2.2	Balance
#2	10	0.15	0.2	3.3	0.3	2.2	Balance
#3	10	0.15	0.4	3.3	0.3	2.2	Balance
#4	8	0.5	0.2	3.3	0.3	2.2	Balance
#5	8	1	0.4	3.3	0.3	2.2	Balance

The justification of selection of Alloy #1 composition lies on the deduction that lowering the content of Fe will be unfavorable to the formation of β -AlFeSi. The content

of Fe for this alloy is 0.15%, much lower than the Fe content A380 which is 1%. Alloy #1 also has lowest content of Si at 8%. Based on literature review, low Si content will lead to less formation of the brittle eutectic Silicon structure, hence favoring higher elongation. At 0.2% Mn, Alloy #1 also has the lowest Mn content. Mn is one of the elements that contributes in the formation of α -AlFeMnSi phase. Figure 15 shows the solidification path of Alloy #1 as predicted by the thermodynamic simulation.

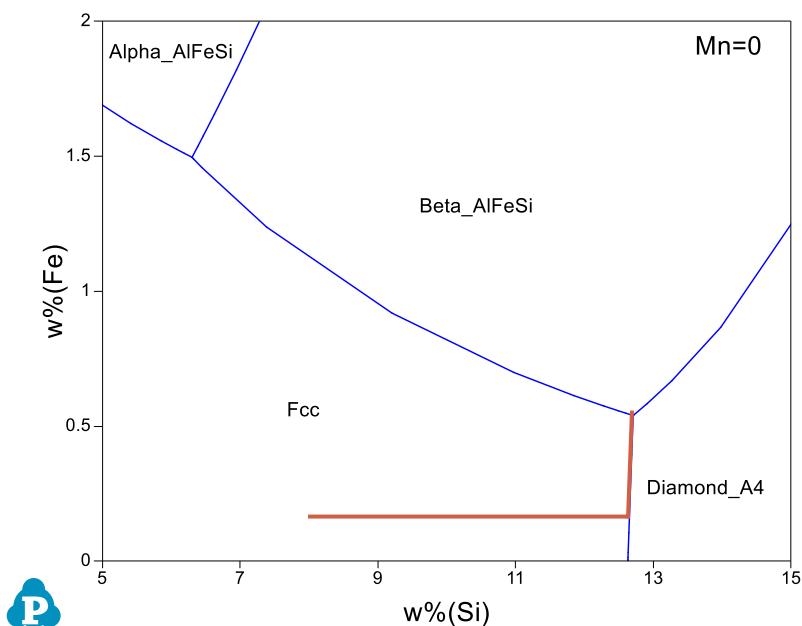


Figure 15: Solidification Path of Alloy #1

Meanwhile, composition of Alloy #2 is selected to observe the effect of increasing the Si content to the mechanical properties and morphology of the alloy. At 10% Si, Alloy #2 has Si content that is higher by 2% than Alloy #1, while the percentages of the other elements are similar to those of Alloy #1. With higher Si content, Alloy #2 is predicted to yield less elongation, attributed by the higher formation of eutectic Silicon in the alloy. The increase of Si will also not affect the formation of the

intermetallic phases. Figure 16 shows the solidification path of Alloy #2 as predicted by the thermodynamic simulation.

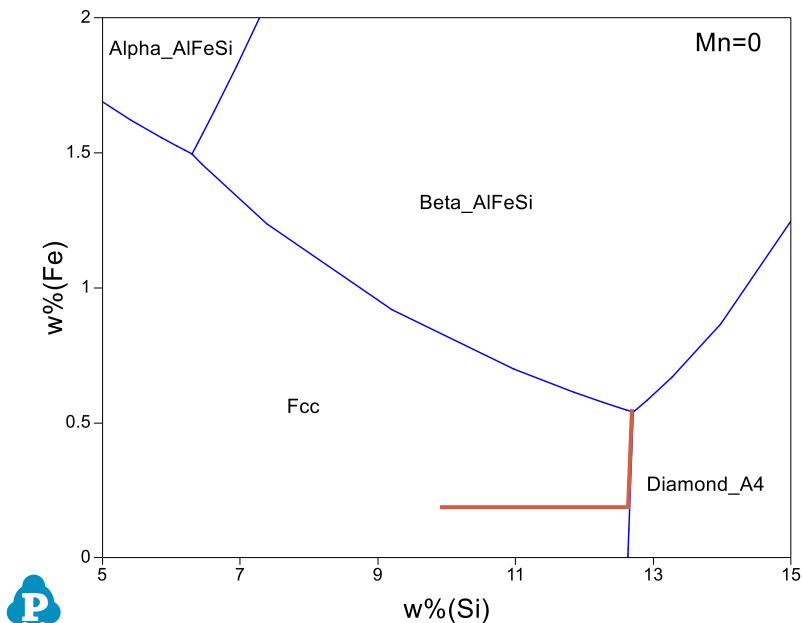


Figure 16: Solidification Path of Alloy #2

Composition of Alloy #3 is designed to observe the effect of increasing Mn content to the mechanical property of the alloy. At 0.4% Mn, the Mn content for Alloy #3 is double than that of Alloy #2. While Mn is an effective Fe naturalizer, high Mn content can lead to issues such as formation of alpha phase and the sludge contaminant. Therefore, it is of an interest to see how having higher Mn level can affect the mechanical properties as well as the microstructure of the alloy. Figure 17 shows the solidification path of Alloy #3 as predicted by the thermodynamic simulation.

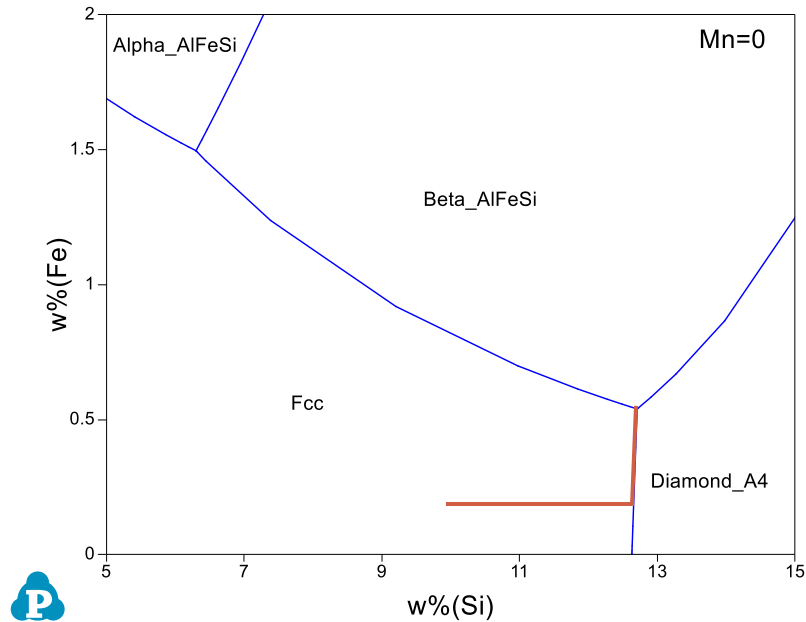


Figure 17: Solidification Path of Alloy #3

Meanwhile, composition of Alloy #4 is proposed to see the effect of increasing Fe content to the mechanical property and microstructure of the alloy. By comparison to Alloy #1, Alloy #4 has a much higher Fe level at 0.5%, while the percentage of the other elements are similar. The high Fe content is predicted to form larger needle-like β -AlFeSi intermetallic phase, subsequently leading to lower elongation and less superior mechanical property as compared to Alloy #1. Figure 18 shows the solidification path of Alloy #4 as predicted by the thermodynamic simulation.

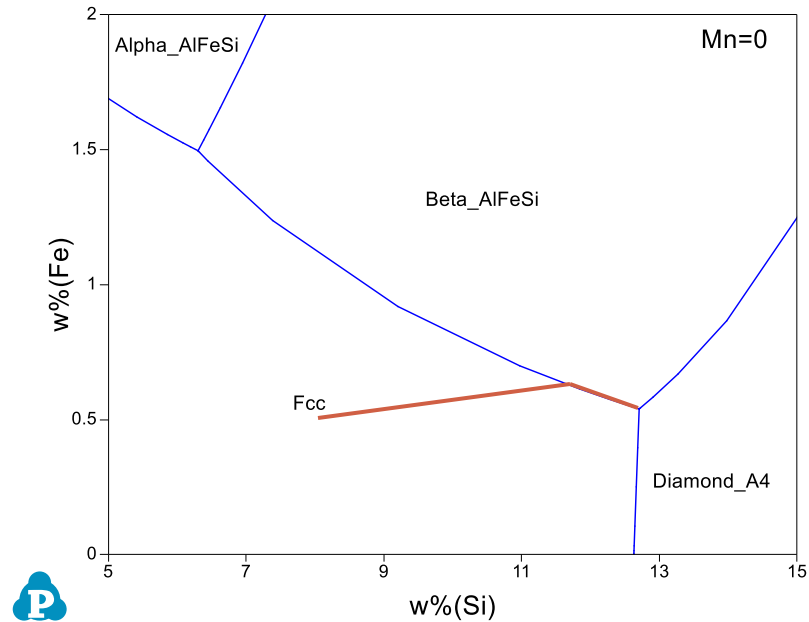


Figure 18: Solidification path of Alloy #4

Alloy #5 can be considered as a control group as it was designed with composition almost similar to the composition of A380. Therefore, it can be expected that this alloy will yield result that is closed to the properties of A380. By comparison to Alloy #4, Alloy #5 has double the content of both Fe and Mn. However, the ratio of Fe to Mn was kept constant with Alloy #4. Therefore, comparison of Alloy #5 and Alloy #4 can explain if increasing both Fe and Mn while keeping the ratio constant has any significant effect to the mechanical properties and morphology of the alloy. Figure 19 shows the solidification path of Alloy #5 as predicted by the thermodynamic simulation.

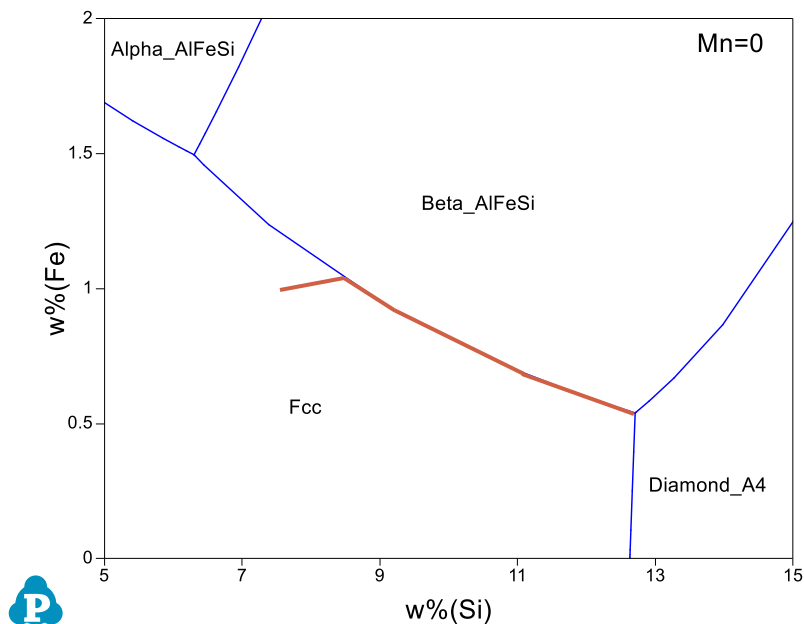


Figure 19: Solidification path of Alloy #5

4.6 Chapter 4 Summary

In this chapter, the idea of utilizing thermodynamic simulation in designing alloy composition was explored. Pandat Software was used in carrying out the thermodynamic simulations. The first section of the simulation deals with binary phase diagrams of A380 alloy to study the effect of single element to phase formation sequence. The analysis provides conclusion that Si, Fe and Mn are the elements that actively affect the formation of the intermetallic α -AlMnFeSi and β -AlFeSi phases. The changes in the composition of these elements change the phase nucleation sequence, subsequently affecting the mechanical properties of the alloy.

The second section of thermodynamic simulation analyzes the solidification path on the Al-Fe-Si-Mn liquidus projection. The solidification path analysis shows that fraction of β -AlFeSi formation is dictated by whether the composition was above or below the α -AlFeSi and β -AlFeSi boundary line. If the Fe level is above the boundary line, the β -AlFeSi phase is larger due to it being formed at the beginning of the solidification. The longer the solidification path through the α -AlFeSi and β -AlFeSi boundary line, the higher the fraction of β -AlFeSi phase formation. The analysis draws conclusion that the addition of Fe in the composition of the alloy favors the formation of the β -AlFeSi phase.

CHAPTER 5. EXPERIMENTAL RESULTS

5.1 Introduction of Experimental Results

In this section, the results of experiment conducted on the alloy samples of five different compositions and different heat treatment conditions are elaborated. The experimental results are presented from two tests that were done on the samples:

- a. mechanical testing
- b. microstructural analysis

In section 5.1, the experimental results of tensile testing for varied compositions of as-cast alloys are shown. The results will conclude the optimal composition for the aluminum alloy in terms of the quality index. Meanwhile, the experimental results of tensile testing for varied heat treatment conditions are presented in section 5.2.

The final section of this chapter, section 5.3 focuses on the results of microscopic observation of the metallurgy of the alloys at different compositions and heat treatment conditions. The observations are used to explain the mechanical testing results obtained in section 5.1 and section 5.2.

5.2 Mechanical Testing for Alloys at Different Compositions

Mechanical testing of selected compositions of die casting alloy was done mainly to verify the simulation results that have been presented in section 4.1. The testing was also conducted to show that by controlling the composition, the elongation of the alloy can be improvised. Another aspect that was investigate in the mechanical testing is the effect of

composition to the strength and quality index of the alloy. The quality index was calculated by using the equation 4.1 (Sui, Wang & Ye, 2015)

$$Q = UTS(MPa) + 150 \log(\delta) \quad (4.1)$$

Figure 20 shows the result of elongation for the five alloys of different composition, while Figure 21 shows the results of the UTS and Quality Index for the five alloys. From the result, it can be concluded that Alloy #1 yields the best elongation property, followed by Alloy #2, Alloy #3, Alloy #4 and Alloy #5. In terms of the strength, Alloy #4 displays the highest UTS, followed by Alloys #5, Alloy #3, Alloy #2 and Alloy #1. In terms of overall quality of the alloys, Alloy #1 yields the highest Quality Index, followed by Alloy #2, Alloy #4, Alloy #3 and Alloy #5. Table 17 summarizes the elongation, UTS and Quality Index results with the nominal values of Fe, Mn and Si weight percentage.

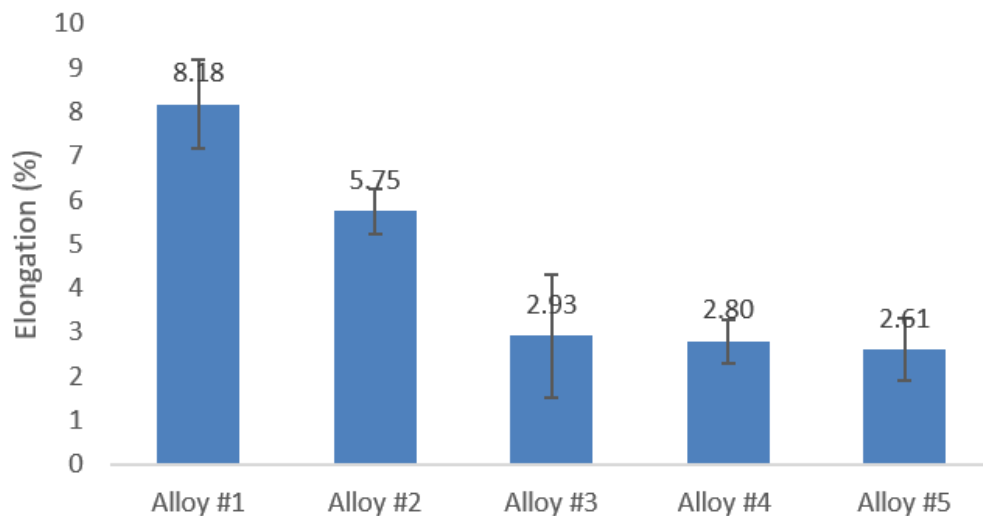


Figure 20: Elongation for five designed alloys

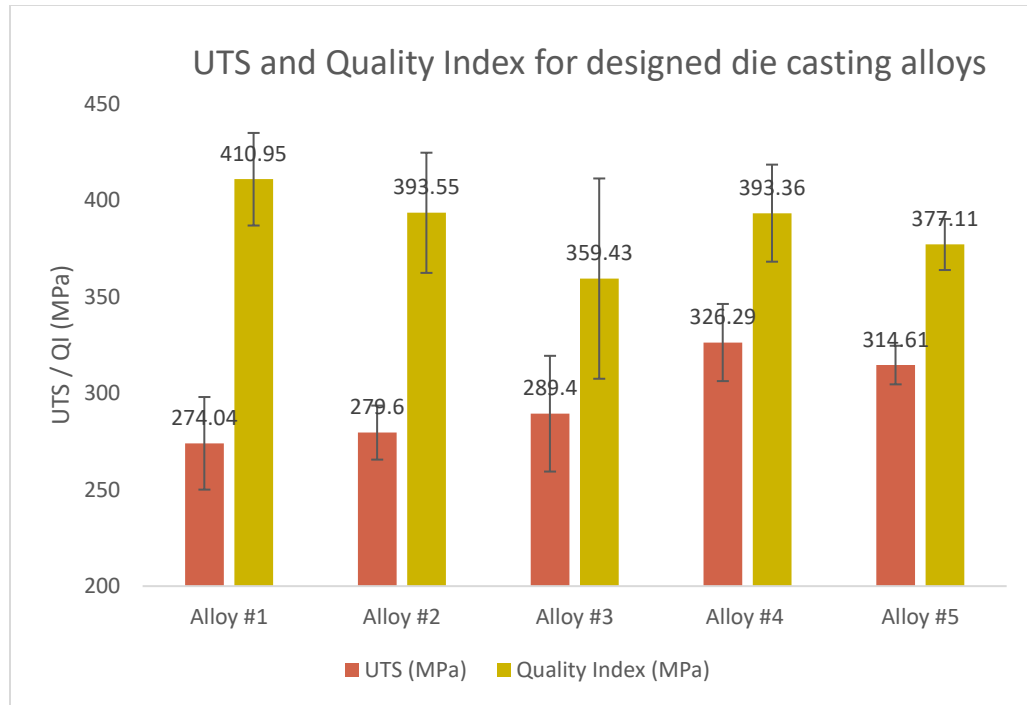


Figure 21: UTS and Quality Index for designed die casting alloys

Table 17: Summary of elongation, UTS and Quality Index results with the nominal values of Fe, Mn and Si composition

Alloy	Si wt %	Fe wt %	Mn wt %	Elongation (%)	UTS (MPa)	QI (MPa)
#1	8	0.15	0.2	8.18 %	274.04	410.95
#2	10	0.15	0.2	5.75 %	279.60	393.55
#3	10	0.15	0.4	2.93 %	289.4	359.43
#4	8	0.5	0.2	2.80 %	326.29	393.36
#5	8	1	0.4	2.61 %	314.61	377.11

By comparison to A380, Alloy #1 improves the elongation property by 133.7%.

The significant improvement in elongation property of Alloy #1 can be attributed to the low content of Si, Fe and Mn. Among the five alloys, Alloy #1 has the lowest weight percentage of the elements (8% Si, 0.15% Fe and 0.2% Mn). Substantial amount of Fe has been reduced in Alloy #1 composition compared to the Fe percentage in A380

(reduction by 88.5%). Meanwhile the Mn content in Alloy #1 is half the nominal content of Mn in A380, and Si content in Alloy #1 is similar to that of in A380. These result in lowering the formation of both α -AlFeMnSi and β -AlFeSi intermetallic phases.

At 8% weight percentage, the silicon content in Alloy #1 is also lower than in the other alloys, hence less formation of eutectic Silicon structure. The eutectic silicon coral-like structure contributes in increasing the brittleness and lowering the elongation of an alloy. The effect of Si content to the elongation property of the alloy is apparent when Alloy #1 is compared to Alloy #2. Alloy #1 and Alloy #2 only difference was the Si percentage, where Alloy #2 had a higher content of Si than Alloy #1 by 2%, whereas the other contents are kept constant. The 2% increase of Si percentage in Alloy #2 reduces the elongation by 29.7%. It can also be noted that the increase in Si content does not significantly affect the strength of the alloy. Therefore, the quality index of Alloy #1 is better than that of Alloy #2, mainly contributed by the elongation property of the alloy.

The effect of Mn to the elongation property can be seen by comparing Alloy #1 to Alloy #3. Alloy #1 and Alloy #3 only difference is the Mn percentage. Alloy #2 content of Mn is double the Mn content in Alloy #1, whereas the other contents are kept constant. Doubling the Mn content tremendously reduces the elongation property by 64.2%. The reduction in elongation can be attributed to the higher phase fraction of the brittle α -AlFeMnSi intermetallic phase presence in the alloy #3, despite lower β -AlFeSi phase formation. From simulation result, doubling the Mn increases phase formation of α -AlFeMnSi by a factor of approximately 2.3.

The effect of Fe to the elongation property can be seen by the comparison of Alloy #1 and Alloy #4. Alloy #4 has Fe content 3.3 times higher than Alloy #1, while all the other elements are kept constant. The elongation of Alloy #4 is lower than elongation of Alloy #1 by 65.8%. Fe has a significant influence in the decrease of the elongation property of the alloy. The elongation decrease can be attributed to the presence of the brittle, needle-like structure of β -AlFeSi intermetallic phase. The simulation result shows that the increase of Fe content increases the phase fraction of β -AlFeSi formation tremendously, as described by the equation 4.2.

$$f_{\beta-AlFeSi} = -0.444x_{Fe}^3 + 1.89x_{Fe}^2 + 0.4854x_{Fe} - 0.0085 \quad (4.2)$$

Despite the negative effect on the elongation property, the brittle structure of the β -AlFeSi phase provides some strengthening to the alloy, albeit only a slight increase. The UTS of Alloy #4 is higher by 19.1% than Alloy #1. The morphology of plate-like β -AlFeSi creates stress risers when the alloy is given stress, resulting in the increase of UTS.

Alloy #4 and Alloy #5 can be compared to observe effect of doubling both the Fe and Mn content, while keeping the ratio of Fe:Mn constant at 5:2. Doubling both Fe and Mn content only reduces both elongation and UTS by 6.79% and 3.58%. The decrease is considerably low especially when comparing with the effect of doubling only Fe content or doubling Mn content. The result showed that doubling both Fe and Mn does not have significant effect on both the elongation and strength properties of the alloy if the ratio of Fe to Mn is kept constant.

Multiple Linear Regression analysis was done on the available tests data to correlate the percentage elongation and UTS with the composition of Si, Fe and Mn. From the analysis, the linear regression equation for elongation can be expressed as in Equation 4.3. The regression shows that the elongation is negatively affected by the amount of Fe, Mn and Si. The addition of Si, Fe and Mn decreases the elongation value.

$$\text{Elongation (\%)} = 16.62 - 1.013 \text{ Si} - 4.98 \text{ Fe} - 4.67 \text{ Mn} \quad (4.3)$$

The linear regression equation for UTS can be expressed as in Equation 4.4. From the analysis, the UTS value is significantly affected by the amount of Fe and Mn rather than Si. Addition of both Si and Fe increases UTS value of the alloy, while addition of Mn negatively affect the UTS.

$$\text{UTS(MPa)} = 279.35 + 0.897 \text{ Si} + 52.45 \text{ Fe} - 38.87 \text{ Mn} \quad (4.4)$$

5.3 Microstructure Analysis of Alloys of Different Compositions

This section addresses the microstructural observation and analysis of the experimental samples of the five different alloys. The alloys that were casted into the tensile bars were cut and sub-grouped into two categories. The first category is the fractured samples and the second category is the polished samples. The fractured samples were taken from the fractured tensile bars (obtained from the mechanical testing) and cut using diamond blade saw into 5mm depth samples. These samples were used to observe the behavior of the fracture of the alloys.

The polished samples on the other hand were obtained from the tensile bars that are not mechanically tested. The samples were cut using the diamond blade saw into 5mm depth samples at the middle section of the bar. All the polished samples were then mounted on epoxy mounting using hot compression mounting process by LECO Bakelite. The mounting process was done to improve handling of the materials and protect the integrity of the edge and surface area.

The mounted samples were manually polished by using silicon carbide pads of 240, 400, 600 and 1200 grit in the sequence order. The samples were then manually polished using TEMO 0.5 Micron diamond polish lapping paste compound for their final polish. Carl Zeiss Axioscope 7 optical microscope is used as the microscope to observe the morphology of the polished samples. The microstructure pictures were taken by using the Axiocam 305 color camera and the measurements were done by using the Zen-Zeiss imaging software.

The α -AlFeMnSi and β -AlFeSi intermetallic phases analysis is the focus of the study as they are the main influence to the mechanical property of the alloys. The existence of α -AlFeMnSi and β -AlFeSi intermetallic phases is apparent in the microscopic observation of all the five different alloys. Figure 22 shows the example of a microscopic image with α -AlFeMnSi and β -AlFeSi intermetallic phases. The α -AlFeMnSi intermetallic phase is the Chinese-script like structure as observed on the right side of the image. Meanwhile the β -AlFeSi intermetallic phase is the needle-like structure as observed on the left side of the image.

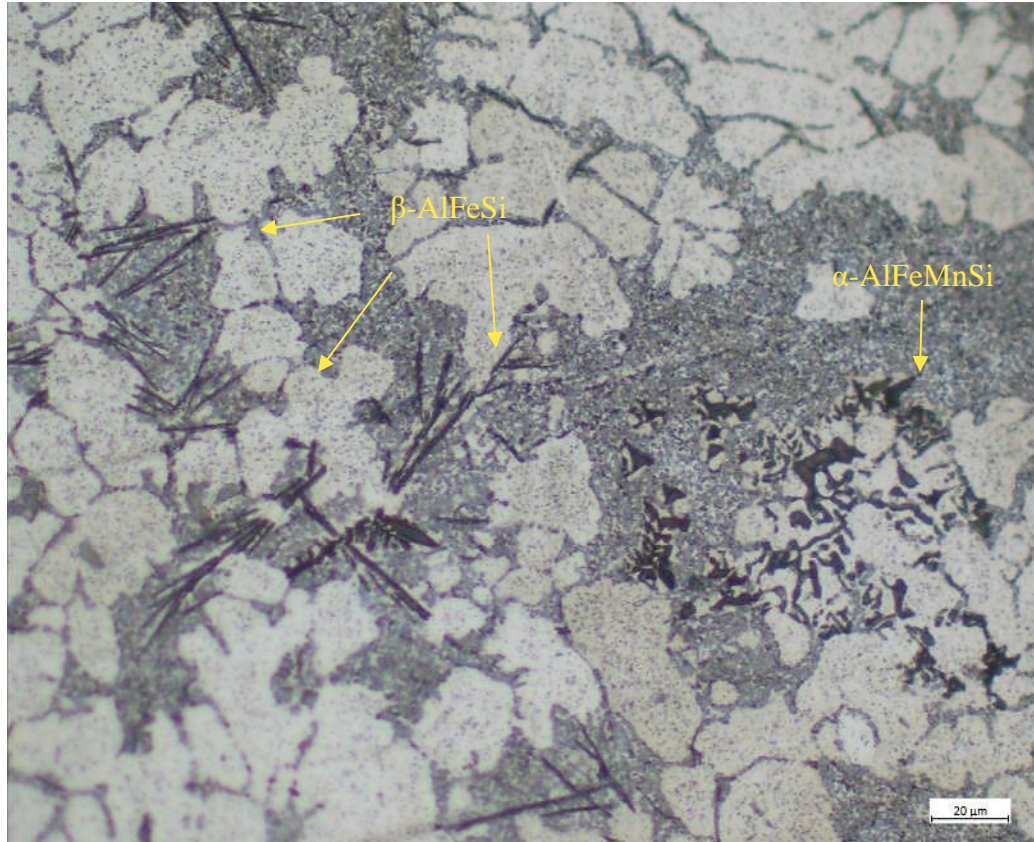


Figure 22: Microscopic image with α -AlFeMnSi and β -AlFeSi intermetallic phases.

β -AlFeSi intermetallic phases were measured by taking five fields with observed needles. The five needles were measured and averaged, combining with the other field to establish the length of the beta phase for a given composition. The α -AlFeMnSi intermetallic phases, if observed, were measured by identifying the entire length of the branch spacing. The entire length measured was divided by the branch number to estimate the average spacing of the alpha phase. The measurement was then combined with the measurements from the other four fields to establish the length of the alpha phase for a given composition.

5.3.1 Microstructure of Alloy #1

The results of simulation show that Alloy #1 has the most ideal composition in terms of reducing the formation of intermetallic phase. The alloy has the lowest content of Si (8%), Fe (0.15%) and Mn (0.2%) as compared to the other designed alloys. In terms of its mechanical properties, Alloy #1 has the best elongation property at 8.18% and lowest UTS (274.04 MPa). Figure 23 shows an overview of the microstructure of the polished as-cast Alloy #1 at 500X magnification.

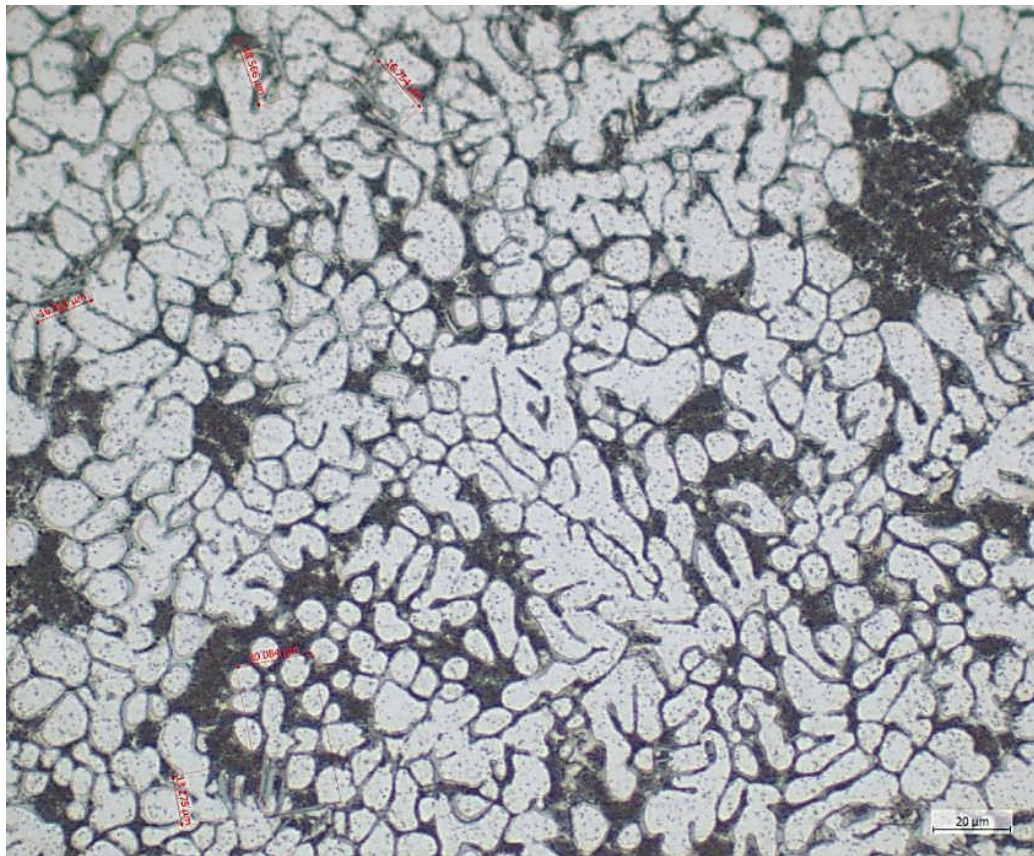


Figure 23: Microstructure of the as-cast Alloy #1 at 500X

In general, the phase formations of the Chinese-script α -AlFeMnSi and needle-like β -AlFeSi intermetallics appear to be the more dispersed in terms of the dispersion

than their counterparts in the other designed alloys. The intermetallic phases also appear to be the smallest and shortest compared to the intermetallic formed in the other alloys. Further analysis reveals that block-like Cu-phases particles are formed in Alloy #1, providing reinforcements and improvement to the alloy strength.

The measurement of alpha and beta phases average spacing provides quantifiable evidence of the effect of the intermetallic formation to the mechanical property of the alloy as shown in Table 18. For Alloy #1, the average spacing for α -AlFeMnSi is 5.42 μm , while the average length for β -AlFeSi is 15.45 μm . The data points represent the frequency of occurrence of each phase in five different fields. From the number of data points, it can be seen that the formation of β -AlFeSi outnumbers the formation of α -AlFeMnSi in Alloy #1 with the ratio of 18:3, indicating that β -AlFeSi is the dominant intermetallic phase formed in the alloy.

Table 18: Intermetallic phase measurement from Alloy #1

Intermetallic Phase	α -AlFeMnSi	β -AlFeSi
Average Length (μm):	5.42	15.45
Data Points:	3	18

Figure 24 show the SEM images for the fracture surface observation at 2000X magnification. Dimple ruptures are apparent in the observation of the fracture surface. The dimple fractures indicate that ductile cracking occurrence along the fracture path. Alloy #1 appears to be physically dimpled when examined under high magnification due to the tensile fractures in the tensile tests.

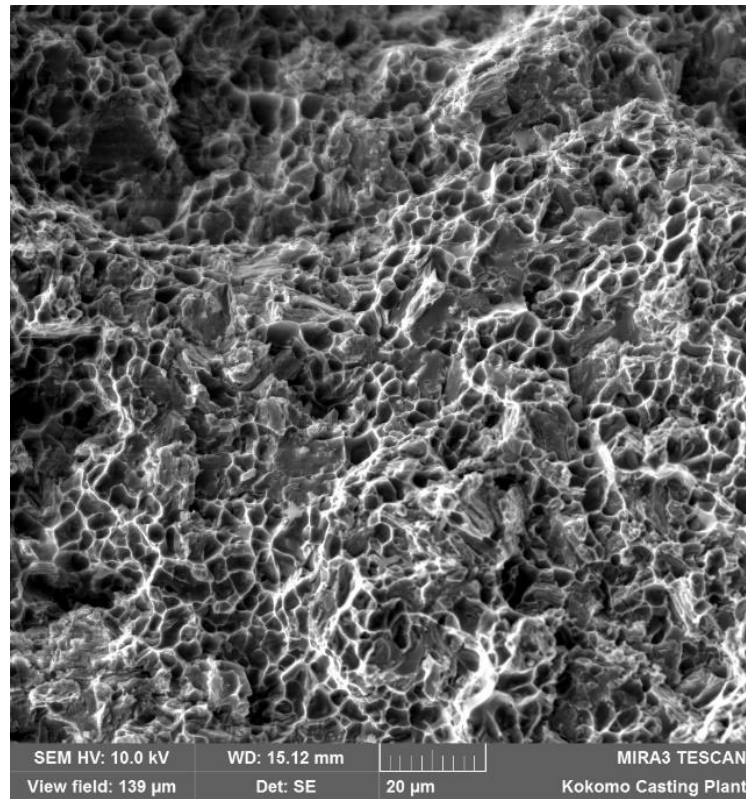


Figure 24: Fracture surface of Alloy #1 at 2000X magnification

5.3.2 Microstructure of Alloy #2

Alloy #2 has relatively low Fe and Mn content and high Si percentage. The alloy has a higher content of Si than Alloy #1 (10%), while the Fe (0.15%) and Mn (0.2%) are similar to that of Alloy #1. In terms of its mechanical properties, Alloy #2 has the second highest elongation property at 5.75% and second lowest UTS (279.60 MPa). Figure 25 shows an overview of the alloy morphology of the polished Alloy #2 at 500X magnification.

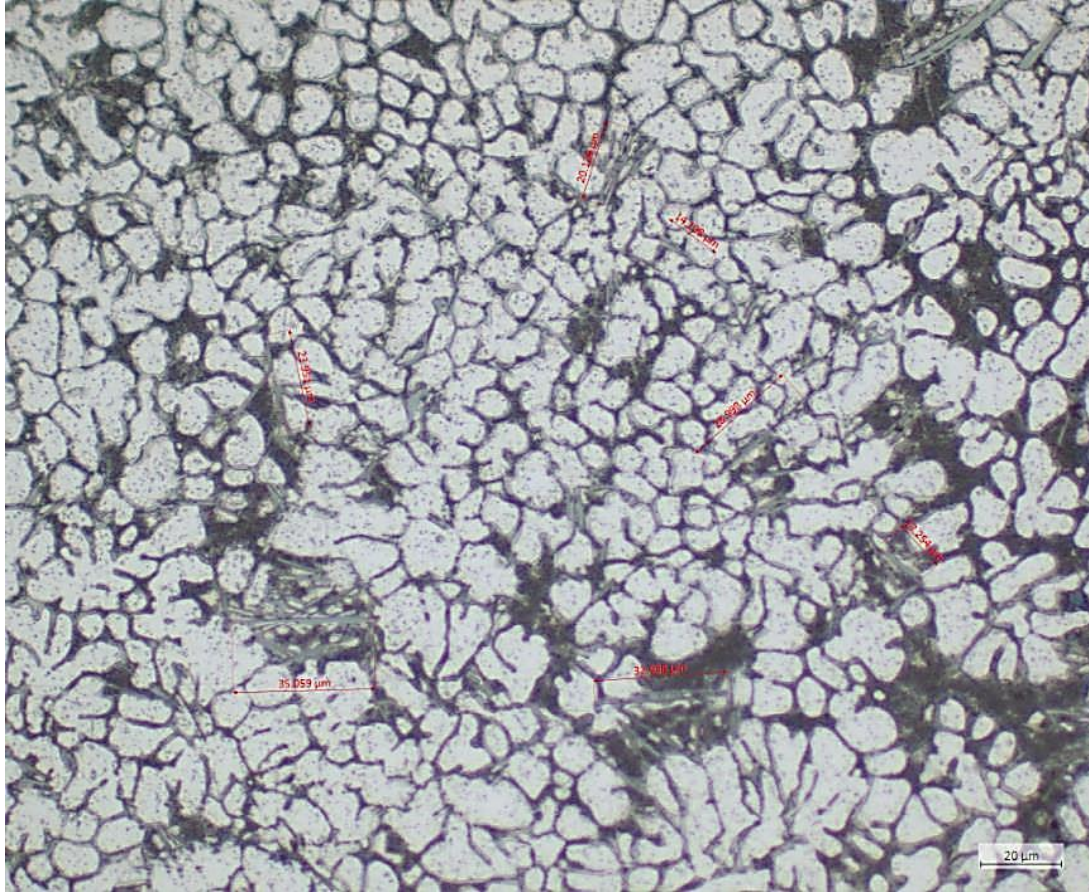


Figure 25: Microstructure of the as-cast Alloy #2 at 500X

In general, the phase formations of the Chinese-script α -AlFeMnSi and needle-like β -AlFeSi intermetallics appear to be uniformly dispersed in similar manner as Alloy #1. The intermetallic phases also appear to be the short and comparable to the size of intermetallic phases measured in Alloy #1. Table 19 details the measurement of alpha and beta phases average spacing of Alloy #2. The average spacing recorded for α -AlFeMnSi is 3.67 μm , while the average length for β -AlFeSi is 17.31 μm . The data points represent the frequency of occurrence of each phase in five different fields. From the number of data points, it can be seen that the formation of β -AlFeSi outnumbers the formation of α -

AlFeMnSi with the ratio of 15:4, indicating that β -AlFeSi is the dominant intermetallic phase formed in Alloy #2.

Table 19: Intermetallic phase measurement from Alloy #2

Intermetallic Phase	α -AlFeMnSi	β -AlFeSi
Average Length (μm):	3.67	17.31
Data Points:	4	15

Figure 26 shows the SEM images for the fracture surface observation at 2000X magnification. Similar to Alloy #1, dimple ruptures are apparent in the observation of the fracture surface of Alloy #2. The dimple fractures indicate that ductile cracking occurrence along the fracture path. Alloy #2 appears to be physically dimpled when examined under high magnification due to the tensile fractures in the tensile tests, thus confirming the mechanical test result that shows the ductile behavior of the material.

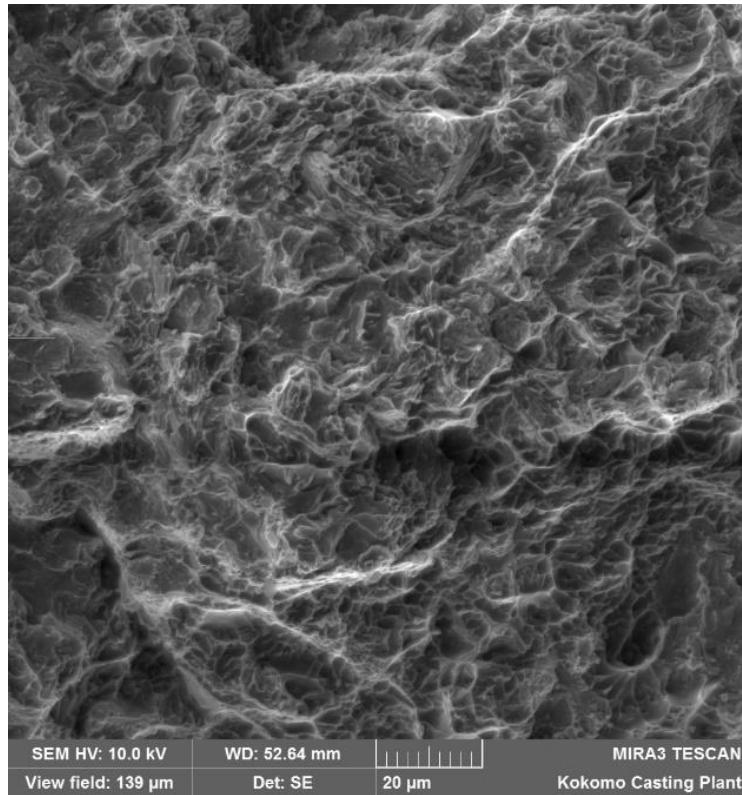


Figure 26: Fracture surface of Alloy #2 at 2000X magnification

5.3.3 Microstructure of Alloy #3

Alloy #3 has relatively low Fe content and high Si and Mn percentage among the designed alloys. The alloy has similar percentage of Si (10%) and Fe (0.15%), while double the Mn content (0.4%) compared to Alloy #2. In terms of its mechanical properties, Alloy #3 has a significant reduction of elongation property at 2.93% compared to Alloy #1 and Alloy #2 and UTS of 289.40 MPa. Figure 27 shows an overview of the alloy morphology of the polished Alloy #3 at 500X magnification.

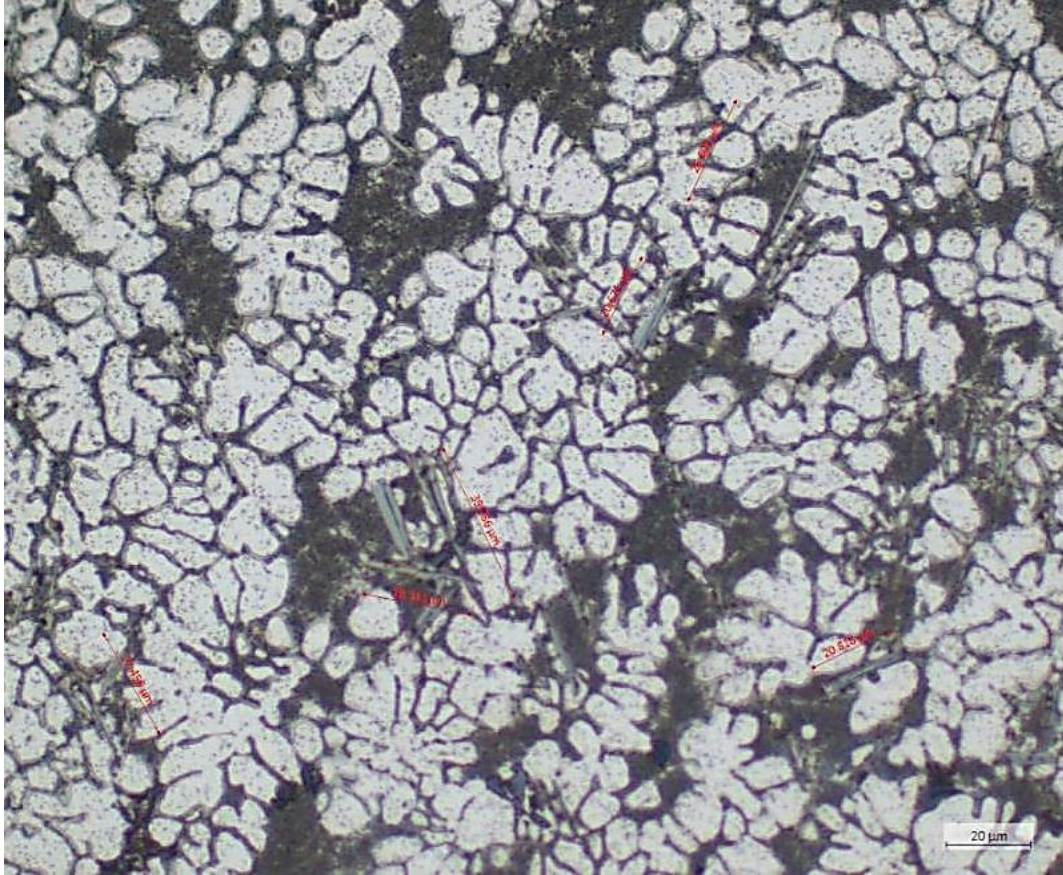


Figure 27: Microstructure of the as-cast Alloy #3 at 500X

In general, the phase formations of the Chinese-script α -AlFeMnSi and needle-like β -AlFeSi intermetallics appear to be the more uniformly dispersed than their counterparts in the other designed alloys. The intermetallic phases also appear to be the smallest and shortest compared to the intermetallic formed in the other alloys. Further analysis reveals that block-like Cu-phases particles are formed in Alloy #3 to provide some additional reinforcements to the alloy strength.

Table 20 details the measurement of alpha and beta phases average spacing of Alloy #3. For this alloy, the average spacing for α -AlFeMnSi is 4.73 μm , while the average length for β -AlFeSi is 23.56 μm . From the number of data points, it can be seen

that the formation of β -AlFeSi outnumbers the formation of α -AlFeMnSi with the ratio of 21:6, indicating that β -AlFeSi is the dominant intermetallic phase formed in Alloy #3.

Table 20: Intermetallic phase measurement from Alloy #3

Intermetallic Phase	α -AlFeMnSi	β -AlFeSi
Average Length (μm):	4.73	23.56
Data Points:	6	21

Figure 28 shows the SEM images for the fracture surface observation at 2000X magnification. Compared to the fracture surfaces of Alloy #1 and Alloy #2, dimple ruptures are observed but less apparent in the observation of the fracture surface of Alloy #3 and there is large area of the surface that appears reasonably smoother. The observed pattern indicates that while ductile cracking occurs along the fracture path, there is also significant part that fractures in brittle manner. The observation confirms the mechanical test result that shows the low elongation property of Alloy #3 relative to Alloy #1 and Alloy #2.

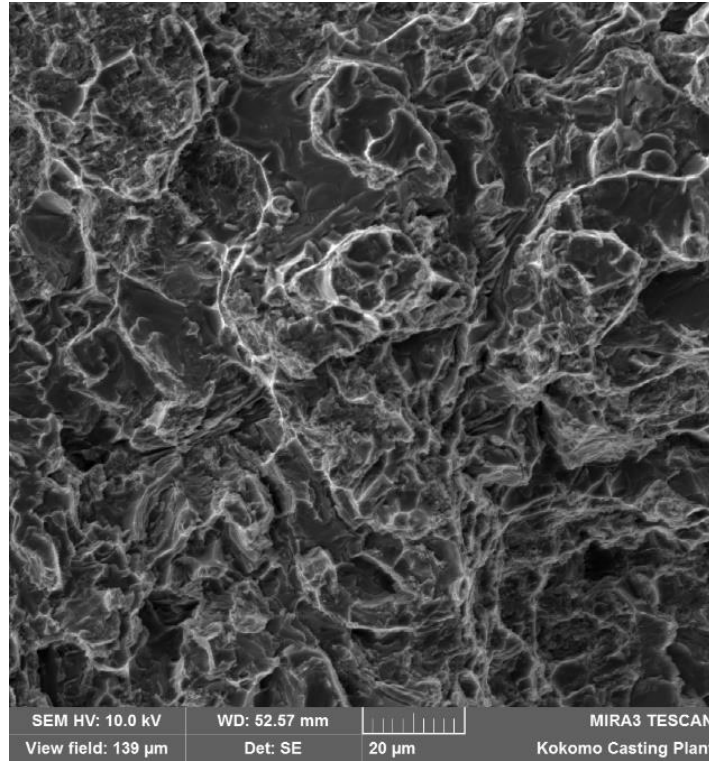


Figure 28: Fracture surface of Alloy #3 at 2000X magnification

5.3.4 Microstructure of Alloy #4

Alloy #4 has relatively high Fe (0.5%) percentage among the designed alloys. The alloy has similar percentage of Si (8%) and Mn (0.2) compared to Alloy #1. In terms of its mechanical properties, Alloy #4 has a significant reduction of elongation property at 2.80% compared to Alloy #1 and high UTS of 326.29 MPa. Figure 29 shows an overview of the alloy morphology of the polished Alloy #4 at 500X magnification.

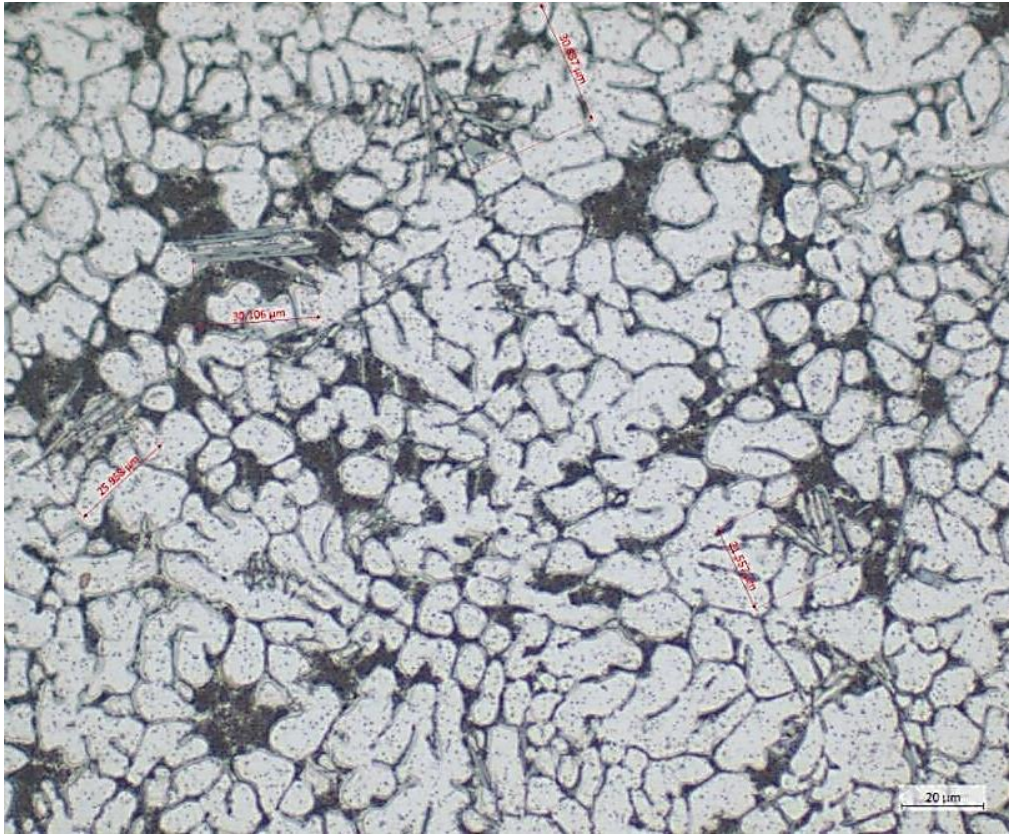


Figure 29: Microstructure of the as-cast Alloy #4 at 500X

In general, the phase formations of the Chinese-script α -AlFeMnSi and needle-like β -AlFeSi intermetallics tend to form near each other and appear to be the less dispersed than their counterparts in the other designed alloys. The intermetallic phases also appear to be significantly longer compared to the intermetallic formed in Alloy #1, Alloy #2 and Alloy #3. Block-like Al-Cu phases particles were also formed in Alloy #4, providing additional reinforcements to the alloy.

Table 21 details the measurement of alpha and beta phases average spacing of Alloy #4. For Alloy #4, the average spacing for α -AlFeMnSi is 3.37 μm , while the average length for β -AlFeSi needle is 27.08 μm . From the number of data points, formation of β -AlFeSi significantly outnumbers the formation of α -AlFeMnSi with the

ratio of 20:2, indicating that β -AlFeSi is the dominant intermetallic phase formed in Alloy #2.

Table 21: Intermetallic phase measurement from Alloy #4

Intermetallic Phase	α -AlFeMnSi	β -AlFeSi
Average Length (μm):	3.37	27.08
Data Points:	2	20

Figure 30 show the SEM images for the fracture surface observation of Alloy #4 at 2000X magnification. Similar to Alloy #3, dimple ruptures are observed but less apparent in the observation of the fracture surface of Alloy #4. There is large area of the surface observed reasonably smoother than the others. The observed pattern indicates that there is also significant part that fractures in brittle manner while ductile cracking occurs along the fracture path. The observation confirms the mechanical test result that shows the low elongation property of Alloy #4.

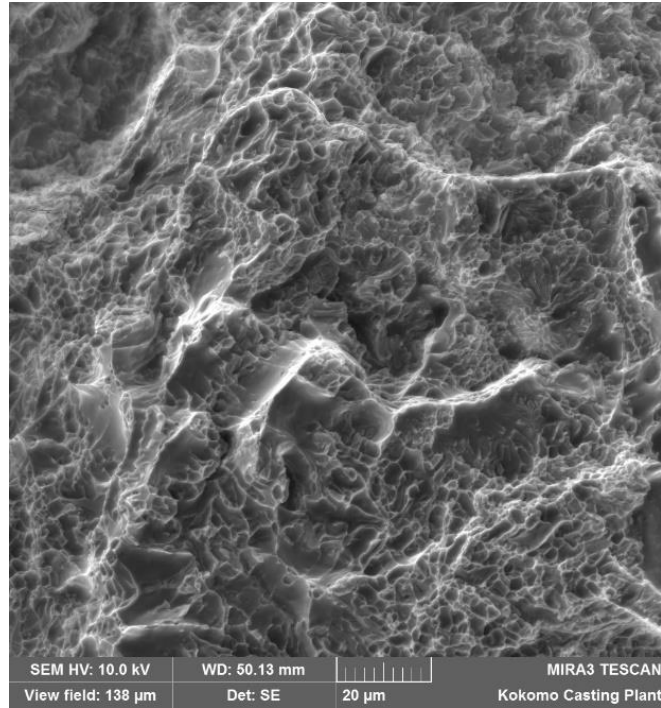


Figure 30: Fracture surface of Alloy #4 at 2000X magnification

5.3.5 Microstructure of Alloy #5

Alloy #5 has the highest Fe content (1%). It also has high Si and Mn percentage among the designed alloys at 8% and 0.4% respectively. In terms of its mechanical properties, Alloy #5 has the lowest elongation property at 2.61% compared to the other designed alloys and high UTS of 314.61 MPa. Figure 31 shows an overview of the alloy morphology of the polished Alloy #5 at 500X magnification.

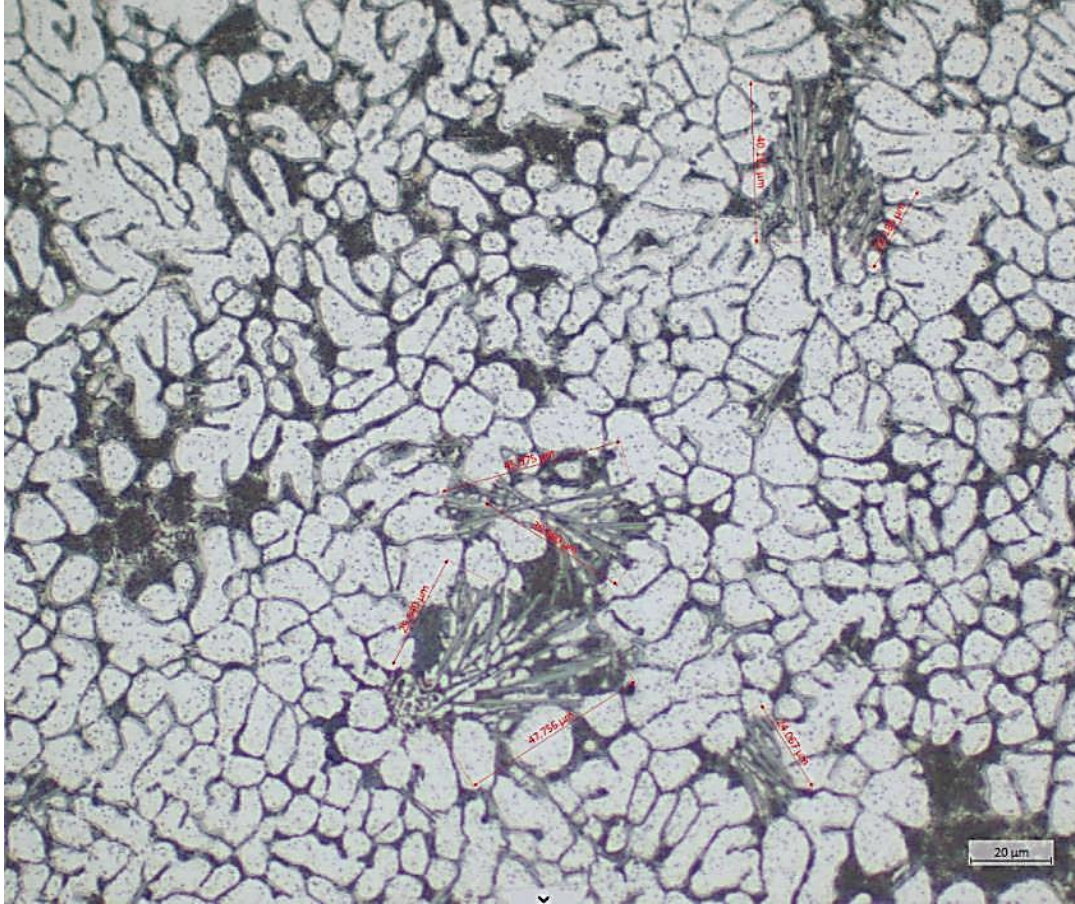


Figure 31: Microstructure of the as-cast Alloy #5 at 500X

In general, the phase formations of the Chinese-script α -AlFeMnSi and needle-like β -AlFeSi intermetallics appear to be the more dispersed than their counterparts in the other designed alloys. The intermetallic phases also appear to be the smallest and shortest compared to the intermetallic formed in the other alloys. Further analysis reveals that block-like Cu-phases particles are formed in Alloy #5 to provide reinforcements to the alloy strength.

For Alloy #5, the average spacing for α -AlFeMnSi is 2.51 μm , while the average length for β -AlFeSi needle is 38.41 μm . Among all designed alloys, Alloy #5 has the longest β -AlFeSi length. From the number of data points, the formation of β -AlFeSi

outnumbers the formation of α -AlFeMnSi with the ratio of 30:2, indicating that β -AlFeSi is the significantly dominant intermetallic phase formed in Alloy #5. It was observed that the formation of α -AlFeMnSi was very few compared to its formation in Alloy #1 and #2.

Table 22: Intermetallic phase measurement from Alloy #5

Intermetallic Phase	α -AlFeMnSi	β -AlFeSi
Average Length (μm):	2.51	38.41
Data Points:	2	30

Figure 32 shows the SEM images for the Alloy #5 fracture surface observation 2000X magnification. As a control group alloy, dimple ruptures are observed but less apparent in the observation of the fracture surface of Alloy #5. There is large area of the surface observed reasonably smoother than the others. The observed pattern indicates significant part that fractures in brittle manner while ductile cracking occurs along the fracture path. The observation confirms the mechanical test result that shows the low elongation property of Alloy #5.

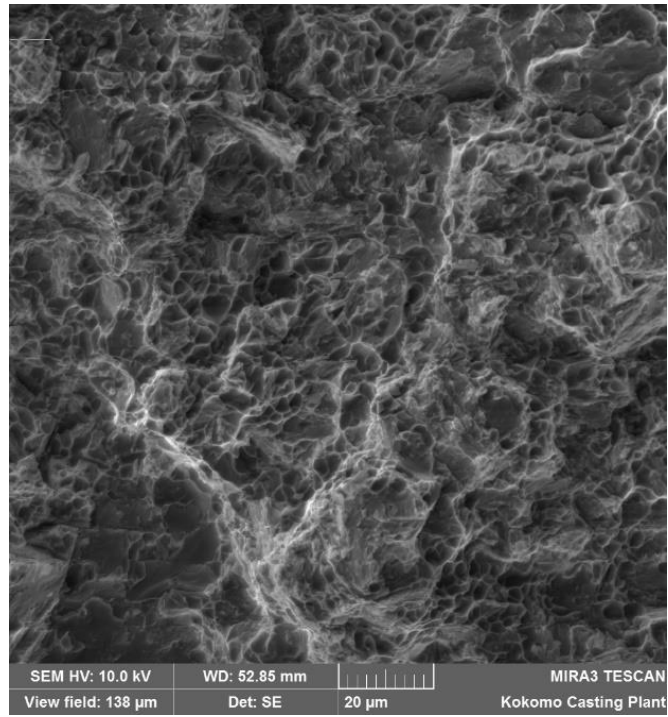


Figure 32: Fracture surface of Alloy #5 at 2000X magnification

5.3.6 Effect of β -AlFeSi length to the Elongation

Elongation of the alloy tends to be affected by the the β -AlFeSi phase fraction more substantially than the α -AlFeSi phase. The regression analysis on the correlation of elongation to the microscopic measurement discovers that the elongation is significantly affected by the β -AlFeSi length and insignificantly affected by the α -AlFeMnSi spacing. This section addresses the correlation between elongation and the beta phase needle length. Figure 33 summarizes the effect of β -AlFeSi length to the elongation of the as-cast samples.

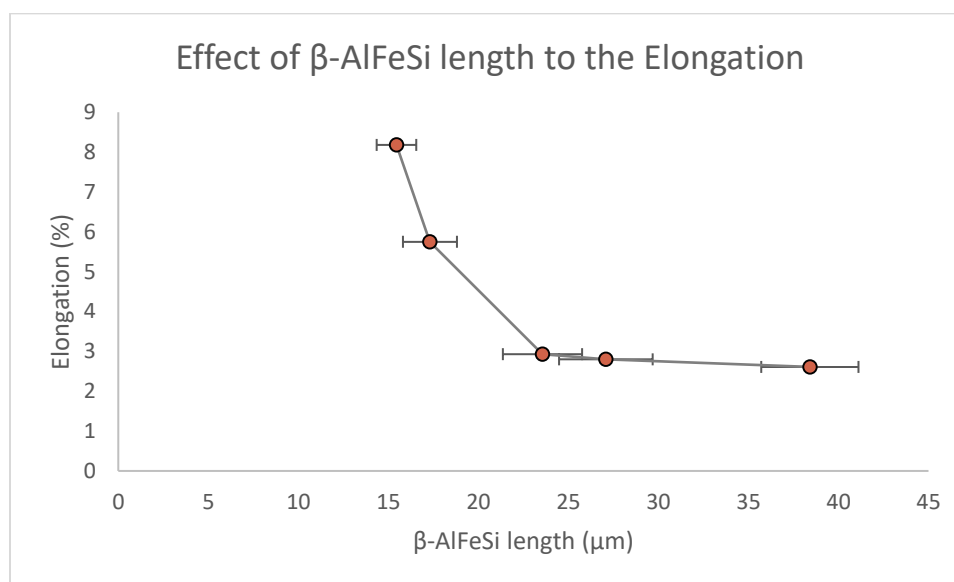


Figure 33: Effect of β -AlFeSi length to the elongation

Generally, the increase in β -AlFeSi length negatively affect the elongation. The elongation drops significantly from 8.18% to 2.93% as the β -AlFeSi length increases from 15.45 μm to 23.56 μm . This shows that for the range of length of β -AlFeSi, the phase significantly contributes to the elongation property of the alloy. In contrast, when the β -

AlFeSi length increases from 23.56 μm to 38.41 μm , there is only slight decrease of elongation has been observed. It can be deduced that the change of β -AlFeSi length significantly affect the elongation property when it is below 23 μm .

5.4 Mechanical Testing for Alloys at Different Heat Treatments

Heat treatment at various conditions were done on the alloy samples to study the effect of heat treatment to the mechanical property of the alloy, especially the elongation property. Crepeau (1995) in his study concluded that during the heat treatment at high temperature, the needle-shape β -AlFeSi phase platelets can be broken into shorter, granulated particulates at the imperfect sites of the crystals.

The most common issue with applying heat treatment to the die casting alloy is blistering, due to the high solution heat treatment temperature. To avoid blistering issue, a modified T4 condition of heat treatment was designed and applied to the alloy samples. Solidus temperature were calculated for every alloy using CompuTherm Pandat software. Subsequently, solution temperature for the heat treatment was designed to be 30 $^{\circ}\text{C}$ below the calculated solidus temperature. Table 23 shows the solution temperature used for each alloy during the heat treatment.

Table 23: Solidus Temperature and Solution Temperature

Alloy	Solidus Temperature (°C)	Solution Temperature (°C)
#1	533.4	503
#2	535.8	506
#3	535.6	506
#4	509.5	480
#5	509.5	480

The alloy specimens of each composition underwent solution heat treatment at the prescribed temperature for 1 hour, 2 hours, 4 hours, 8 hours, 16 hours and 32 hours. Each of the samples that were heat treated at various time were mechanically tested and microstructurally analyzed to record the effect of the heat treatment to the mechanical properties and microstructure of the alloy.

5.4.1 Modified T4 heat treatment on Alloy #1

Figure 33 presents the effect of heat treatment solution time to the elongation property of the Alloy #1 while Table 24 summarizes the mechanical properties in terms of UTS, Elongation and Quality Index for different heat treatment solution time. The result generally shows that T4 heat treatment with 503°C solution temperature improves the elongation of the alloy. The elongation property for the alloys that have been heat treated from 1 hour to 32 hours is higher than the as-cast alloy. The elongation property of Alloy #1 increases at a great rate as it is heat treated up to two hours. The elongation is maximum at 15.72% at 2 hours solution time, accounting 92.2% improvement from the as cast alloy elongation. As the alloy is heat treated longer than 2 hours for up to 32 hours, the elongation value steadily declines from 15.72% to 11.27%.

Meanwhile, the UTS value of the alloy steadily decreases with heat treatment time. Quality Index, which measures the combined property of elongation and UTS, is maximum at 2 hours of heat treatment time. The high value of Quality Index is mainly contributed by the high percentage elongation at the heat treatment condition. It can be deduced that the optimal heat treatment condition for Alloy #1 is 2 hours solution time at 503°C solution temperature.

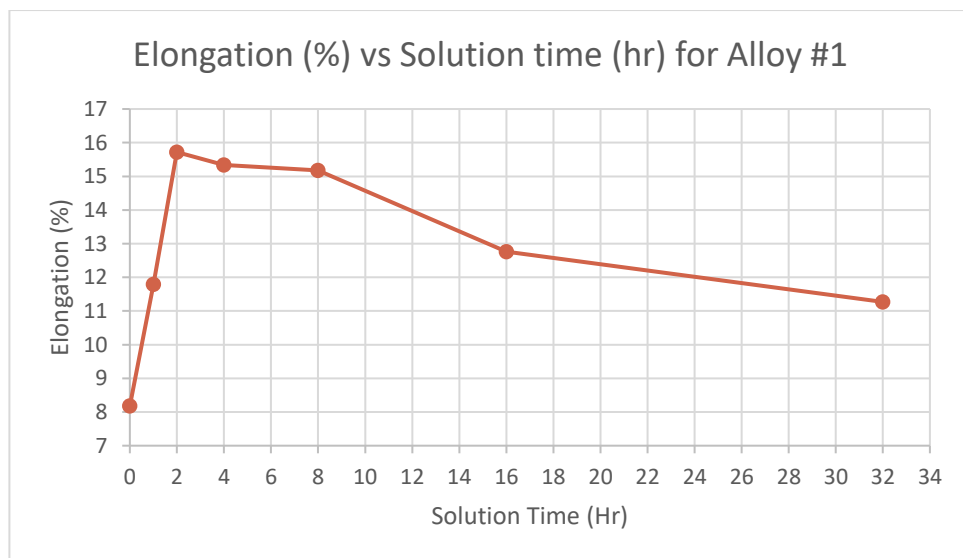


Figure 34: Effect of solution time to elongation of Alloy #1

Table 24: Summary of mechanical properties of Alloy #1 at different solution time

Solution Time (hour)	Elongation (%)	UTS (MPa)	Quality Index (MPa)
As cast	8.18	274.04	410.95
1	11.79	257.38	418.11
2	15.72	245.18	424.65
4	15.34	245.04	422.91
8	15.18	244.76	421.95
16	12.76	243.59	409.47
32	11.27	243.62	401.41

5.4.2 Modified T4 heat treatment on Alloy #2

Figure 34 presents the effect of heat treatment solution time to the elongation property of the Alloy #2. Meanwhile, Table 25 summarizes the mechanical properties in terms of UTS, Elongation and Quality Index for different heat treatment solution time. The mechanical testing result generally shows that T4 heat treatment with 506°C solution temperature improves the elongation of Alloy #2. The elongation property for the alloys that have been heat treated from 1 hour to 32 hours is higher than the as-cast alloy at all heat treatment condition. Unlike Alloy #1, the elongation of Alloy #2 is maximum at 11.36% when Alloy #2 is heat treated for 4 hours. The increment of percentage elongation accounts for 97.6% improvement from the as cast alloy. As the alloy is heat treated longer than 4 hours for up to 32 hours, the elongation value declines from 11.36% to 8.33%. However, there is a slight increase of elongation for heat treatment time from 8 hours to 16 hours.

Meanwhile, similar to Alloy #1, the UTS value of alloy #2 generally drops with heat treatment time. Quality Index, which measures the combined property of elongation and UTS, is highest at 4 hours of heat treatment time. The high value of Quality Index is mainly contributed by the high percentage elongation at the heat treatment condition. Therefore, it can be deduced that for Alloy #2, the optimal heat treatment condition is 4 hours solution time at 506°C solution temperature.

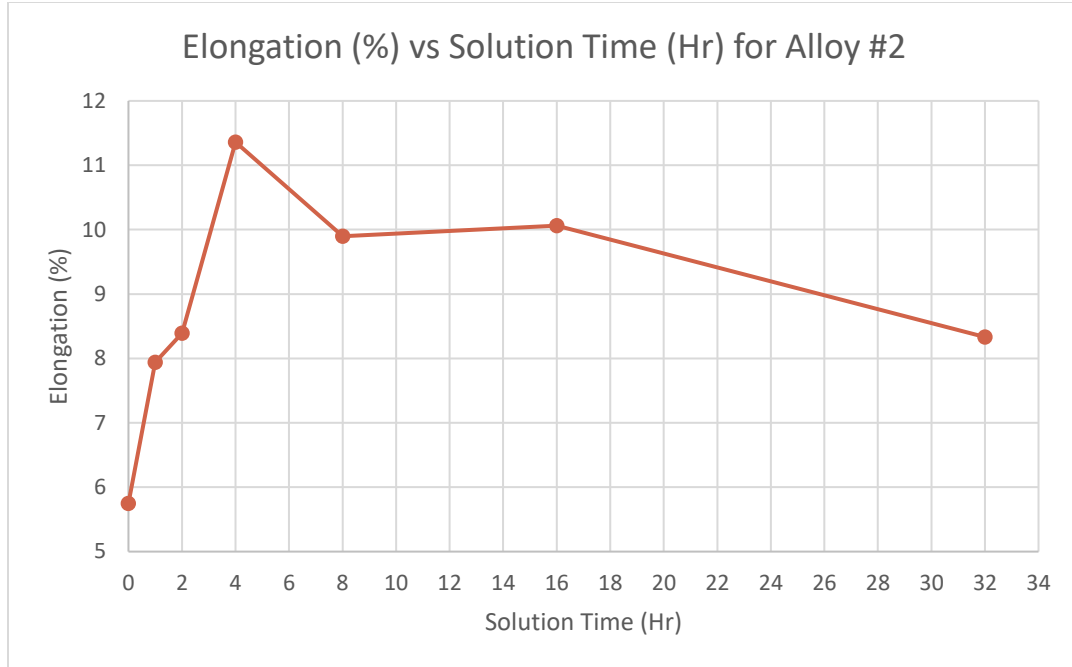


Figure 35: Effect of solution time to elongation of Alloy #2

Table 25: Summary of mechanical properties of Alloy #2 at different solution time

Solution Time (hour)	Elongation (%)	UTS (MPa)	Quality Index (MPa)
As cast	5.75	279.6	393.55
1	7.94	268.52	403.49
2	8.39	263.63	402.19
4	11.36	275.09	433.40
8	9.9	265.12	414.47
16	10.06	252.99	403.38
32	8.33	247.16	385.26

5.4.3 Modified T4 heat treatment on Alloy #3

Figure 35 presents the effect of heat treatment solution time to the elongation property of the Alloy #3, while Table 26 summarizes its mechanical properties in terms of UTS, Elongation and Quality Index at different heat treatment solution time. The solution temperature used in the heat treatment for Alloy #3 is 506°C. Generally, the mechanical testing result shows that heat temperature improves the elongation of Alloy #2 up to 16 hours of solution time. The elongation property for the alloys that have been heat treated from 1 hour to 16 hours is higher than the as-cast alloy at all heat treatment condition. However, unlike Alloy #1 and Alloy #2, the elongation of Alloy #3 is lower than as cast at 32 hours solution time. Similar to Alloy #2, the maximum elongation is recorded at 4 hours solution time. The increment of percentage elongation accounts for 83.3% improvement from the as cast alloy. As the alloy is heat treated longer than 4 hours for up to 32 hours, the elongation degrades from 5.37% to 2.91%.

Alloy #3 follows similar trend displayed by Alloy #1 and Alloy #2, where its UTS value generally drops with heat treatment time. Quality Index, measuring the combined property of elongation and UTS, is highest at 4 hours of heat treatment time. The high value of Quality Index is mainly contributed by the high percentage elongation at the heat treatment condition. It can be concluded that the optimal heat treatment condition for Alloy #3 is 4 hours solution time at 506°C solution temperature.

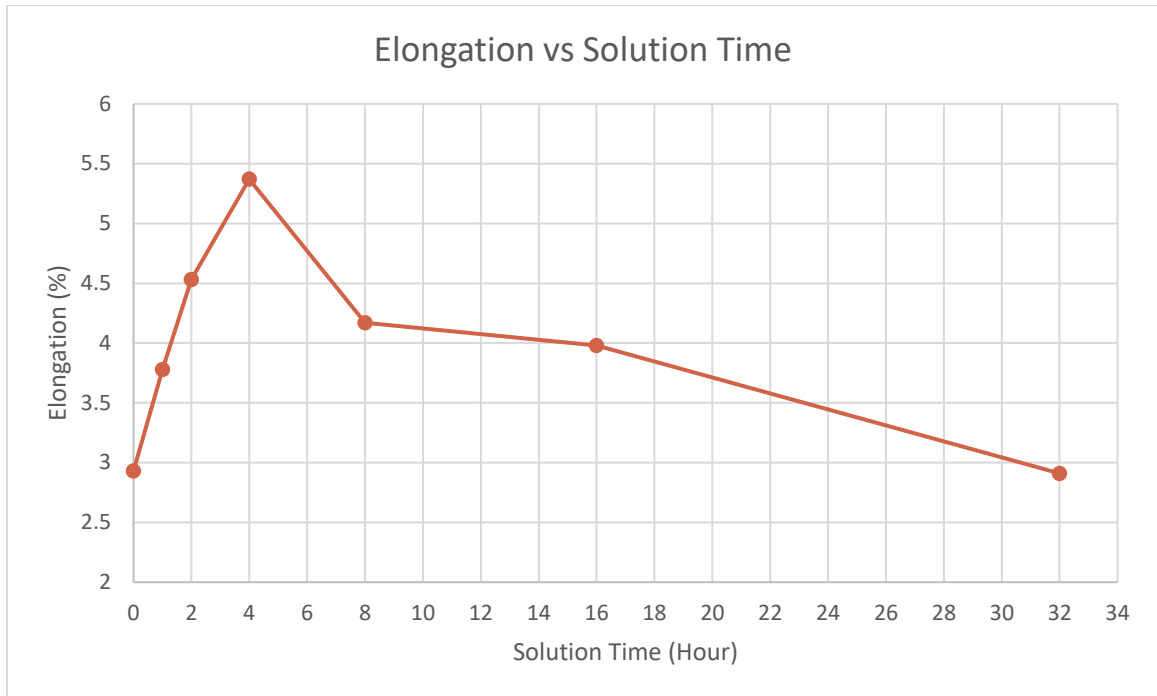


Figure 36: Effect of solution time to elongation of Alloy #3

Table 26: Summary of mechanical properties of Alloy #3 at different solution time

Solution Time (hour)	Elongation (%)	UTS (MPa)	Quality Index (MPa)
As cast	2.93	289.4	359.43
1	3.78	273.27	359.89
2	4.53	275.08	373.49
4	5.37	266.16	375.66
8	4.17	268.89	361.91
16	3.98	262.06	352.04
32	2.91	260.82	330.40

5.4.4 Modified T4 heat treatment on Alloy #4

Figure 36 presents the effect of heat treatment solution time to the elongation property of the Alloy #4 while Table 27 summarizes the mechanical properties in terms of UTS, Elongation and Quality Index for different heat treatment solution time. The result generally shows that T4 heat treatment with 480°C solution temperature improves the elongation of the alloy. The elongation property for the alloys that have been heat treated from 1 hour to 32 hours is higher than the as-cast alloy. The elongation property of Alloy #1 increases as it is heat treated up to 8 hours. The elongation is maximum at 5.33% at 8 hours solution time, accounting 90.4% improvement from the as cast alloy #4 elongation. As the alloy is heat treated longer than 8 hours for up to 32 hours, the elongation value declines from 5.33% to 3.10%.

Meanwhile, the UTS value of the alloy steadily decreases with heat treatment time. Quality Index, which measures the combined property of elongation and UTS, is maximum at 2 hours of heat treatment time. Despite maximum elongation at 8 hours solution time, the high value of Quality Index at 2 hours is mainly due to the higher contribution of UTS value at the heat treatment condition comparative to the elongation. It can be deduced that the optimal heat treatment condition for Alloy #1 is 2 hours solution time at 480°C solution temperature.

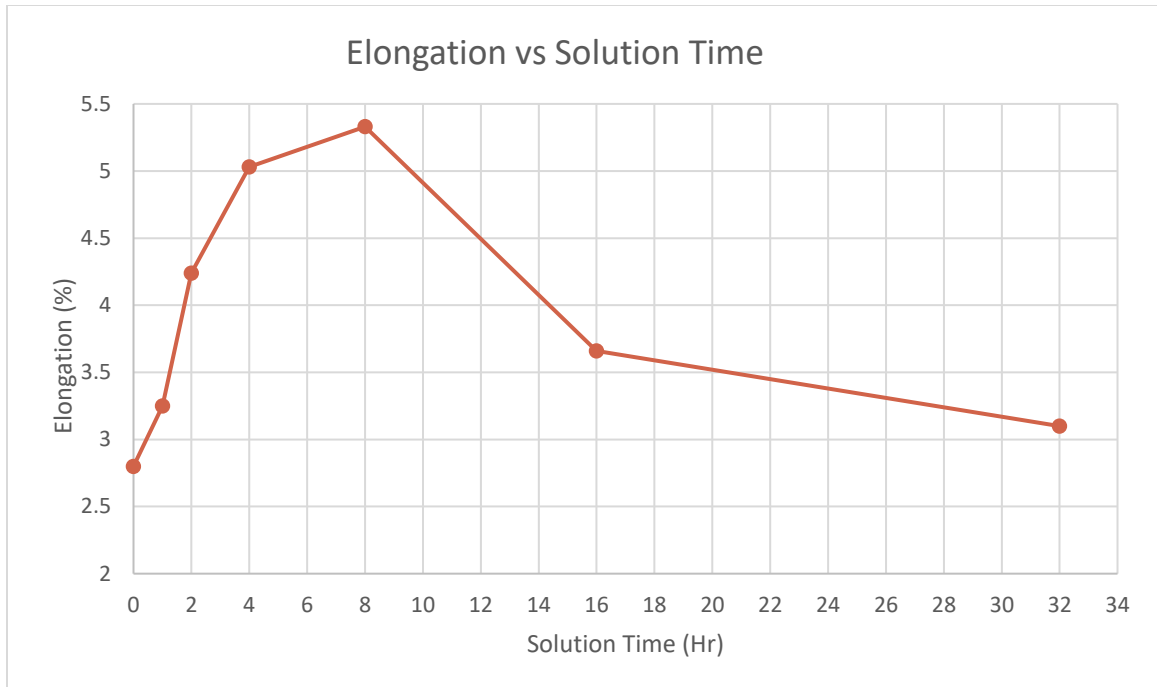


Figure 37: Effect of solution time to elongation of Alloy #4

Table 27: Summary of mechanical properties of Alloy #4 at different solution time

Solution Time (hour)	Elongation (%)	UTS (MPa)	Quality Index (MPa)
As cast	2.8	326.29	393.36
1	3.25	322.36	399.14
2	4.24	323.21	417.31
4	5.03	304.08	409.32
8	5.33	285.85	394.86
16	3.66	278.72	363.24
32	3.1	271.56	345.26

5.4.5 Modified T4 heat treatment on Alloy #5

Among the five designed alloys, as cast Alloy #5 has the lowest elongation property. Figure 37 presents the effect of heat treatment solution time to the elongation property of the Alloy #5 while Table 28 summarizes its mechanical properties in terms of UTS, Elongation and Quality Index for different heat treatment solution time. The result generally shows that T4 heat treatment with 480°C solution temperature improves the elongation of the alloy. The elongation property for the alloys that have been heat treated from 1 hour to 32 hours is higher than the elongation of as-cast alloy. The elongation of Alloy #5 increases at an exponential rate as it is heat treated up to 8 hours. The elongation is maximum at 4.97% at 8 hours solution time, accounting 90.4% improvement from the as cast alloy elongation. As the alloy is heat treated longer than 8 hours for up to 32 hours, the elongation value steadily declines from 4.97% to 3.31%.

Meanwhile, similar to the other alloys, the UTS value of the alloy steadily decreases with heat treatment time. Quality Index is maximum at 8 hours of heat treatment time, mainly contributed by the high percentage elongation at the heat treatment condition. It can be deduced that the optimal heat treatment condition for Alloy #5 is 8 hours solution time at 480°C solution temperature.

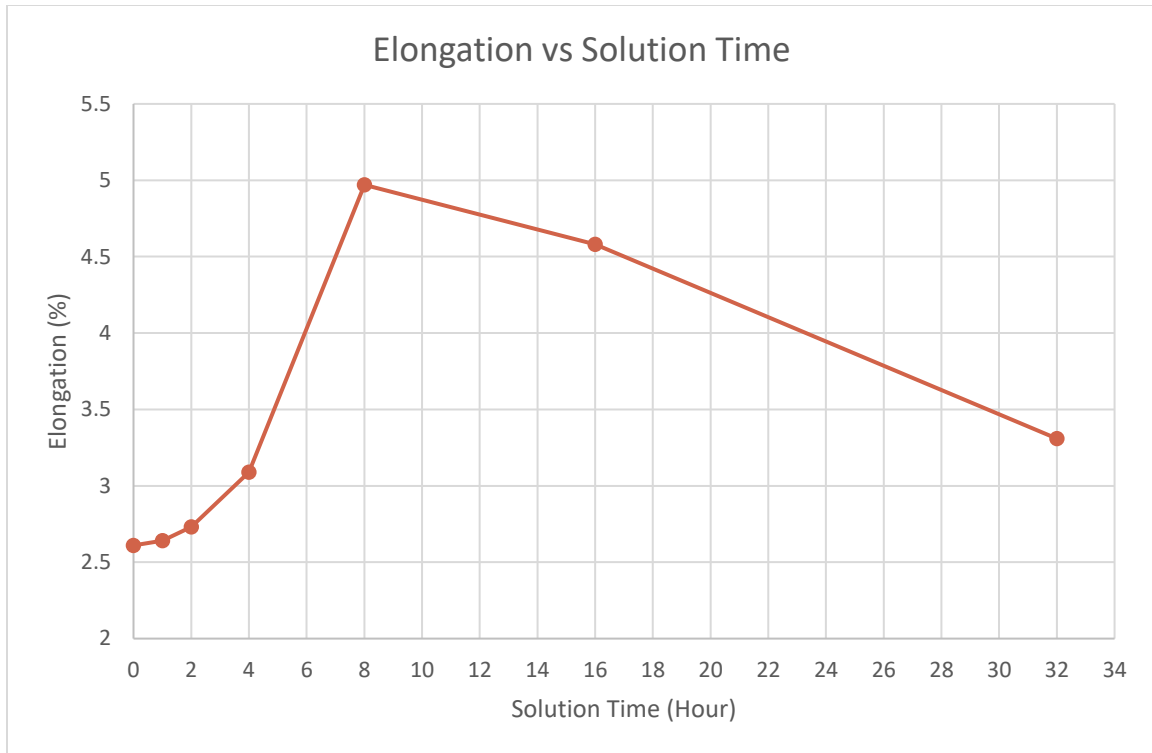


Figure 38: Effect of solution time to elongation of Alloy #5

Table 28: Summary of mechanical properties of Alloy #5 at different solution time

Solution Time (hour)	Elongation (%)	UTS (MPa)	Quality Index (MPa)
As cast	2.61	314.61	377.11
1	2.64	305.03	368.27
2	2.73	305.6	371.02
4	3.09	297.84	371.33
8	4.97	281.07	385.52
16	4.58	272.14	371.27
32	3.31	271.08	349.05

5.4.6 Microscopic Observation on Effect of Heat Treatment

In this section, the observation on morphology of Alloy #5 is presented. Sample #5 was selected as among all five designed alloys because the as cast Alloy #5 contains the highest recorded length (by average) of β -AlFeSi phase, therefore it is of an interest to study how the heat treatment affects the length of the phase.

Table 29 represents the measurement of the β -AlFeSi length in Alloy #5 samples with different heat treatment time. The observation shows that there is no significant change on length of β -AlFeSi for the 1 hour and 2 hours heat treated samples compared to the as cast samples as can be seen in Figure 39 and 40. However, the length of β -AlFeSi starts to decrease significantly when the heat treatment duration is 4 hours as depicted in Figure 41. The length of β -AlFeSi at 8 hours solution heat treatment is approximately half of that of as cast. The length of the phase is further reduced for 16 and 32 hours as shown in Figure 43 and 44.

Table 29: β -AlFeSi length of Alloy #5 samples with different heat treatment time

Heat Treatment Time (hour)	β -AlFeSi length (μm)
0	38.41
1	36.73
2	34.59
4	23.53
8	16.75
16	8.54
32	9.43

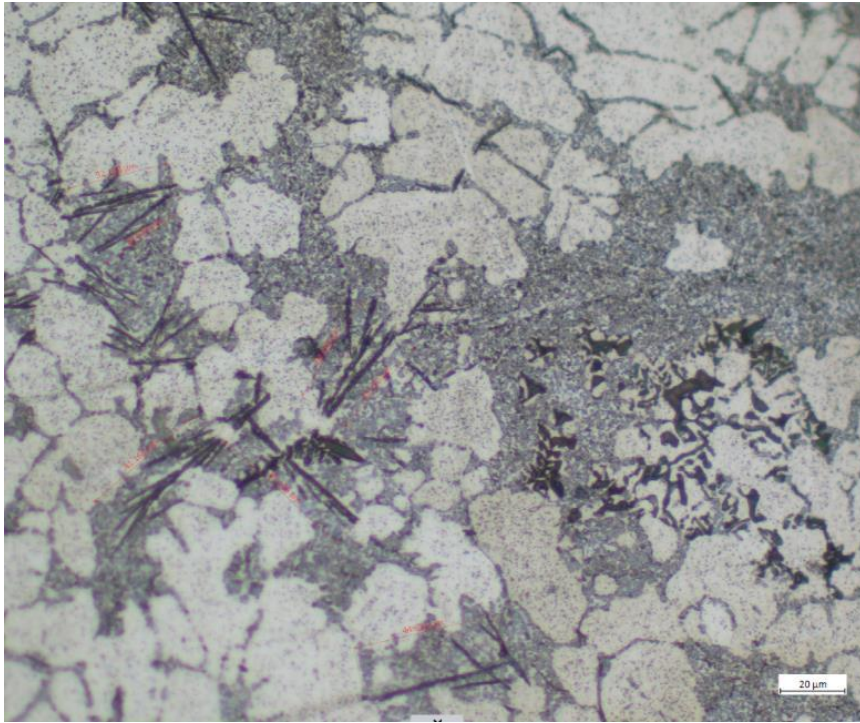


Figure 39: Optical sample of Alloy #5 at 1 hour solution time (500X)

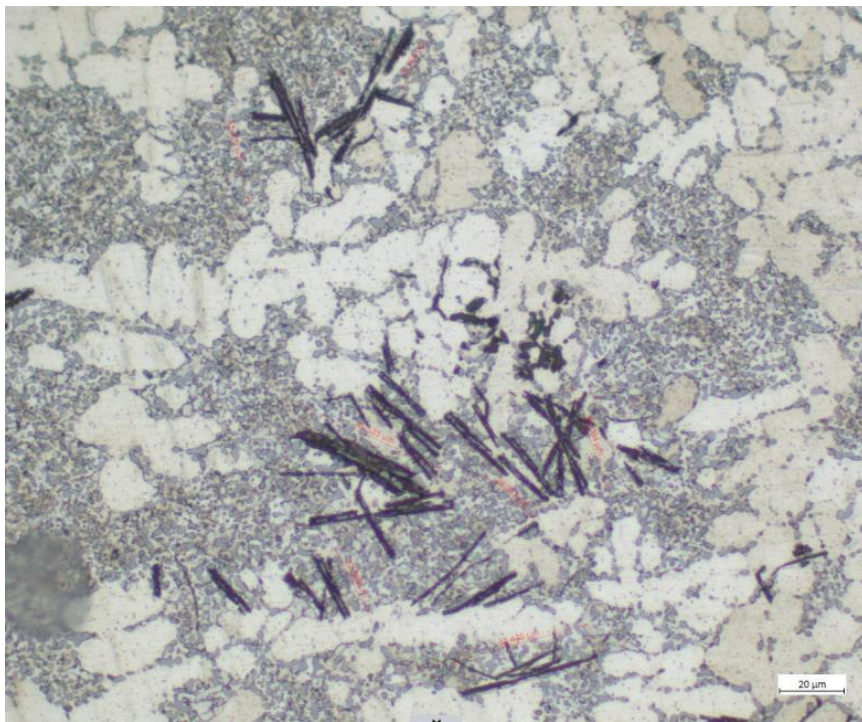


Figure 40: Optical sample of Alloy #5 at 2 hour solution time (500X)

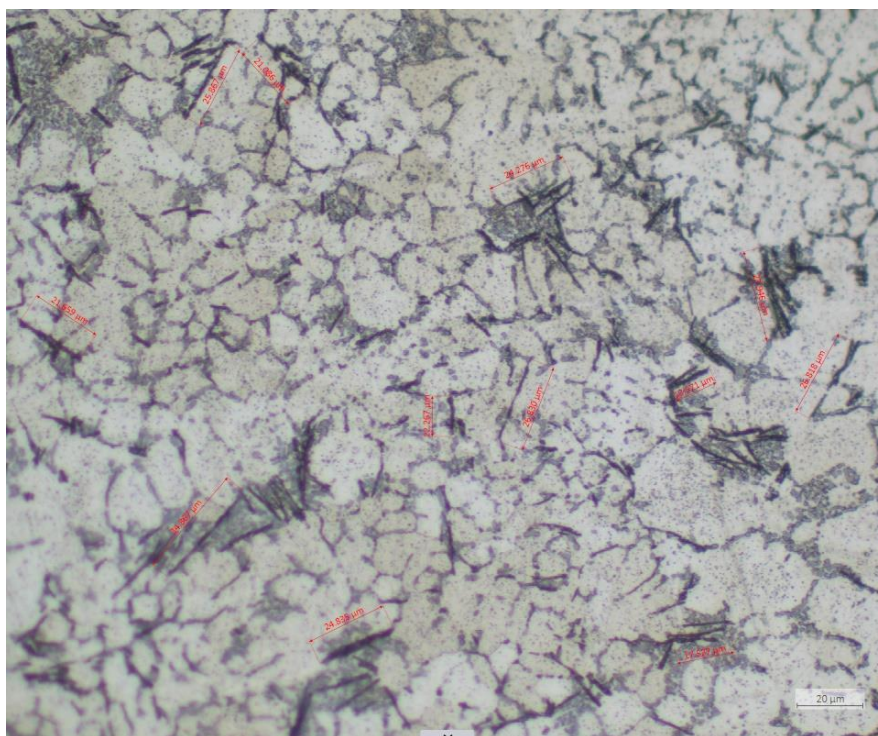


Figure 41: Optical sample of Alloy #5 at 4 hour solution time (500X)

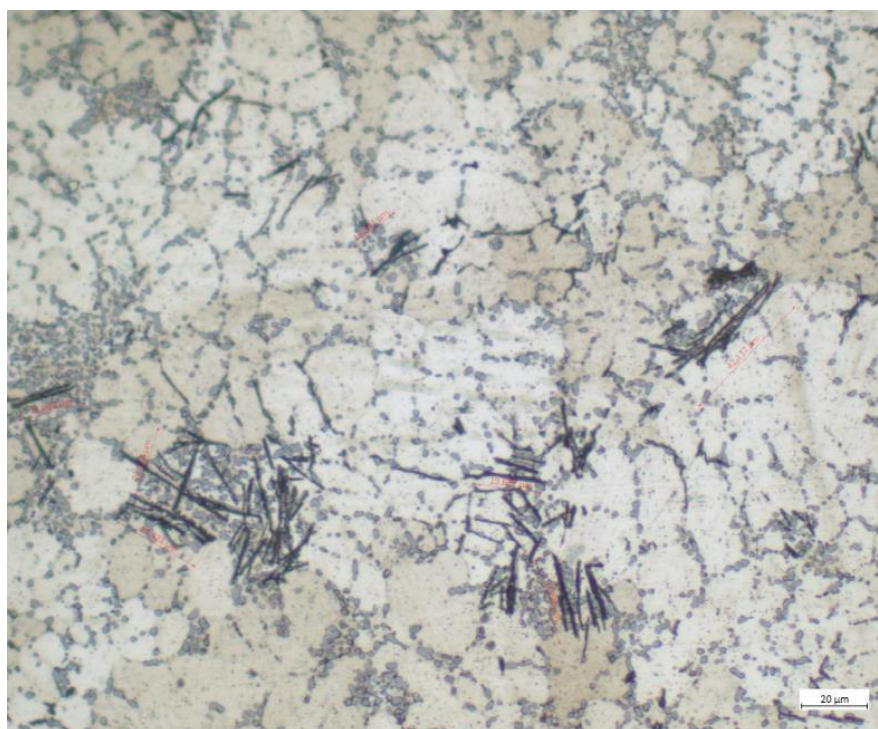


Figure 42: Optical sample of Alloy #5 at 8 hour solution time (500X)

The increase of elongation properties with heat treatment time for up to 8 hours can be attributed to the decrease of the β -AlFeSi length. However, it was also apparent in the microscopic observation that the coral-like and lamellar eutectic silicon structure in as cast samples, as depicted in Figure 45 decomposed and transformed into rounded granular structure with modification provided by the heat treatment time as can be seen in Figure 46, 47 and 48. The diameter of the granular silicon increased with the solution heat treatment time. The eutectic Silicon were observed with SEM and the average diameter of the eutectic silicon with solution time was recorded as in Table 30.

The observation provides reasoning behinds the decrease of elongation property of the alloy for heat treatment time above 8 hours. Despite the shorter β -AlFeSi length, the increase of heat treatment time resulted in larger size of granular silicon and more uniform dispersion, hence a more dominant resistance towards dislocation, therefore resulting in decrease in ductility. For Alloy #5, 8 hours is the optimal solution heat treatment time that yields the highest elongation property.

Table 30: Granular eutectic silicon diameter at different solution time

Solution time (hour)	Granular silicon diameter (μm)
1	1.24
2	1.50
4	1.73
8	2.03
16	2.64
32	3.17

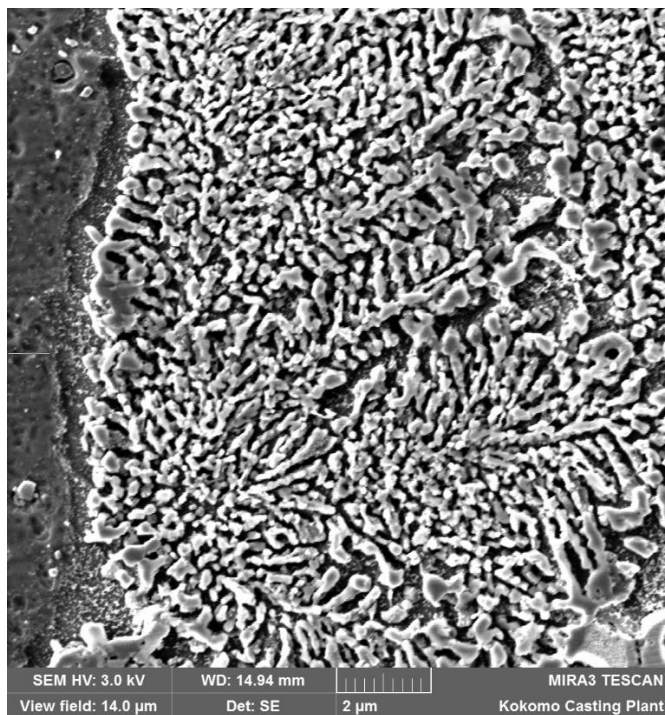


Figure 45: The lamellar eutectic silicon for as cast sample (20000X)

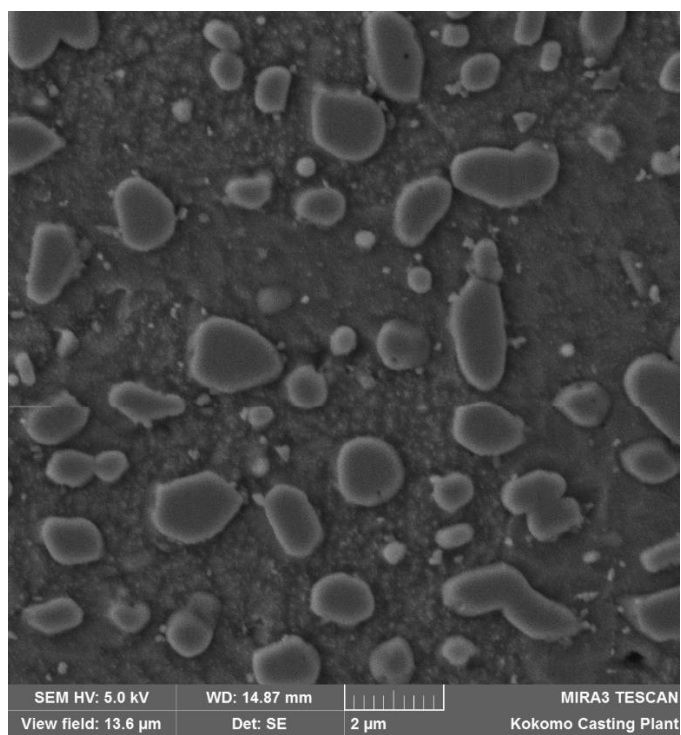


Figure 46: The granulated eutectic silicon at 1 hour solution time (20000X)

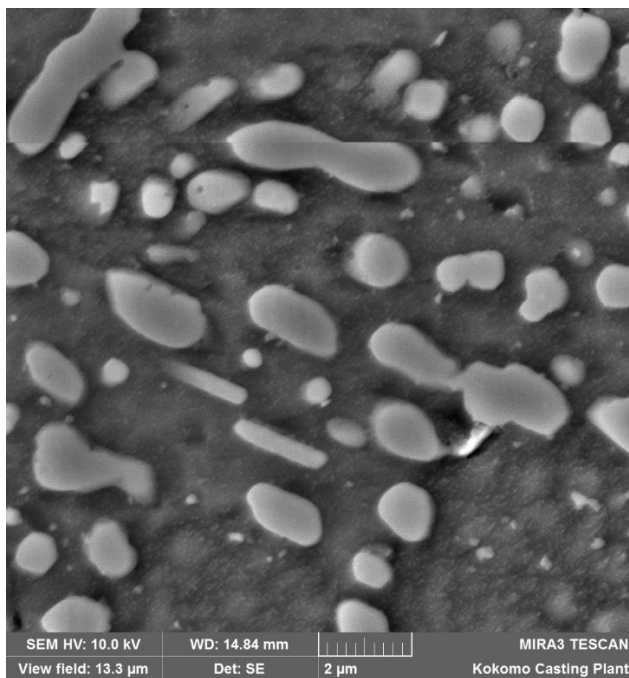


Figure 47: The granulated eutectic silicon at 8 hour solution time (20000X)

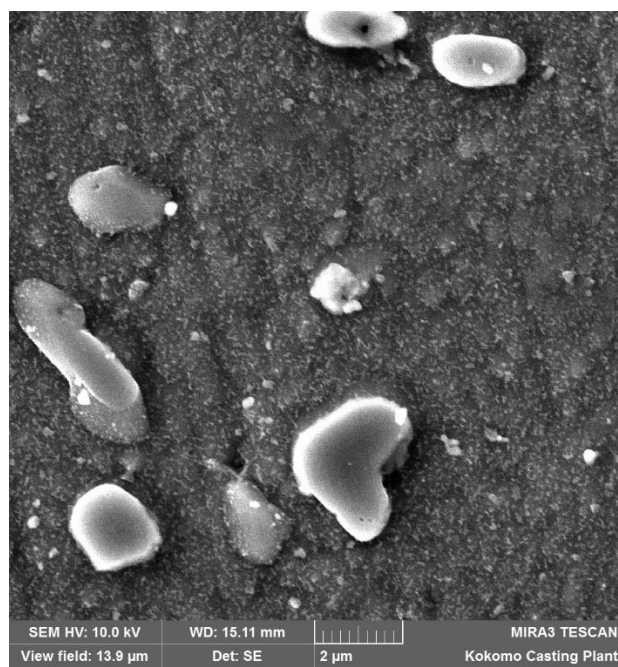


Figure 48: The granulated eutectic silicon at 16 hour solution time (20000X)

5.5 Chapter 5 Summary

The experimental work has successfully verified the finding from the thermodynamic simulation. From the result of mechanical testing, the elongation is significantly affected by the amount of Fe, Mn and Si. The addition of Fe decreases the elongation value. The mechanical tests also discovered that alloy strength is significantly affected by the amount of Fe and Mn rather than Si. The addition of Fe increases UTS value of the alloy, while addition of Mn negatively affects the UTS.

From the microstructure analysis, it can be concluded that the increase in β -AlFeSi length negatively affect the elongation. The drop in β -AlFeSi length significantly increase the elongation property when the length is below 23 μ m.

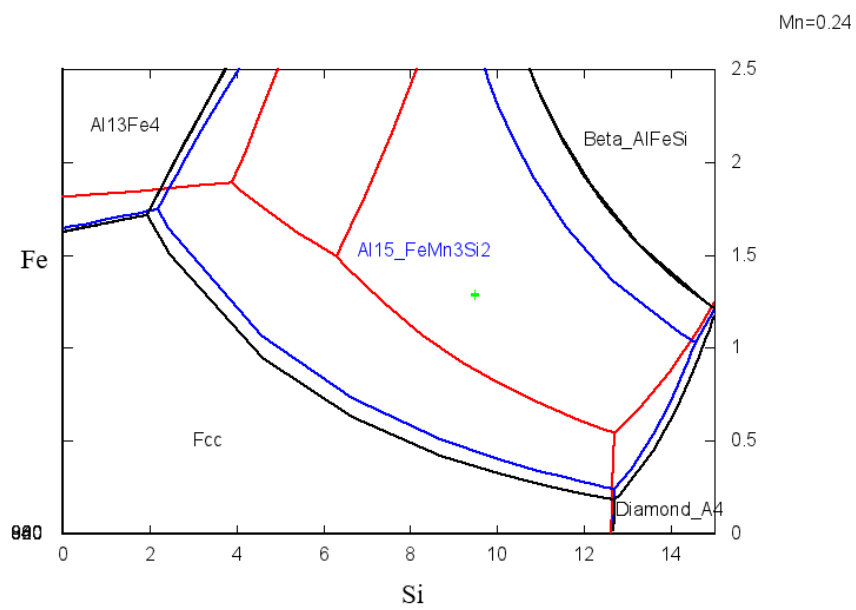
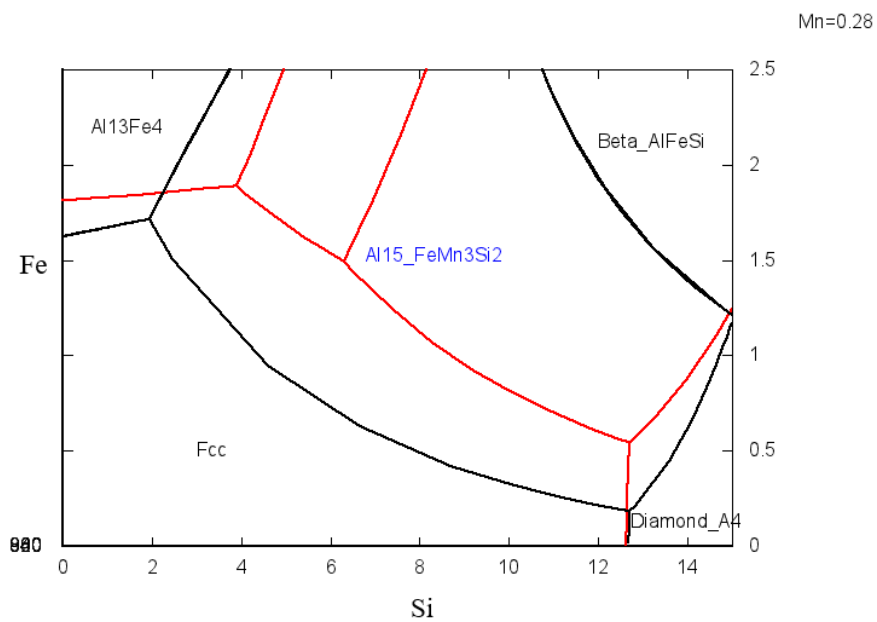
The heat treatment was proven to be a viable method of improving the elongation property of the designed alloys. Modified T4 heat treatment with solution temperature 30°C below the solidus temperature significantly improved the elongation of the die casting alloys for up to 90%. The elongation increment of each alloy is dependent on the solution time. However, with heat treatment, the improvement in elongation also negatively affect the strength of the alloy. From microstructure observation, increasing solution heat treatment decreases the length of the β -AlFeSi and breaks the lamellar eutectic silicon into granulated form.

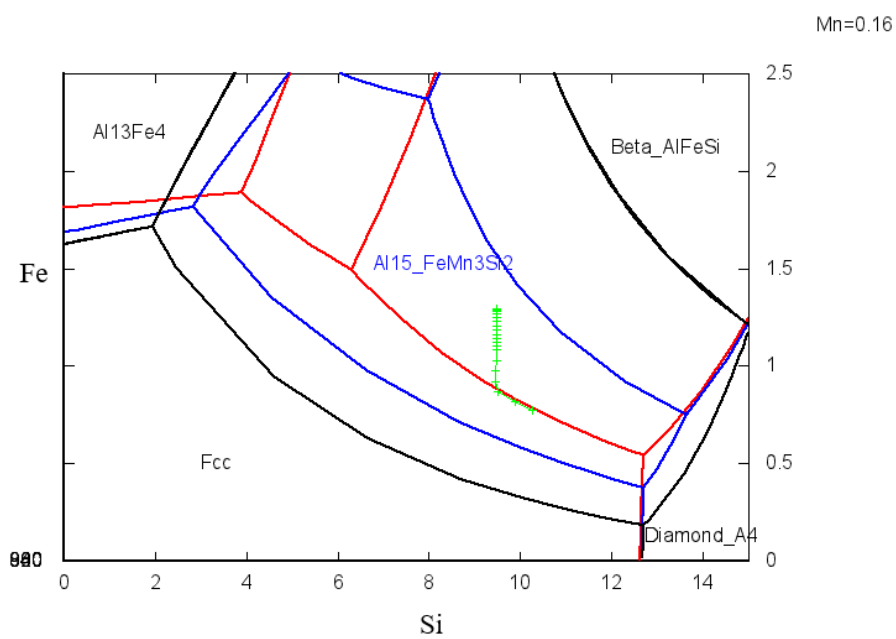
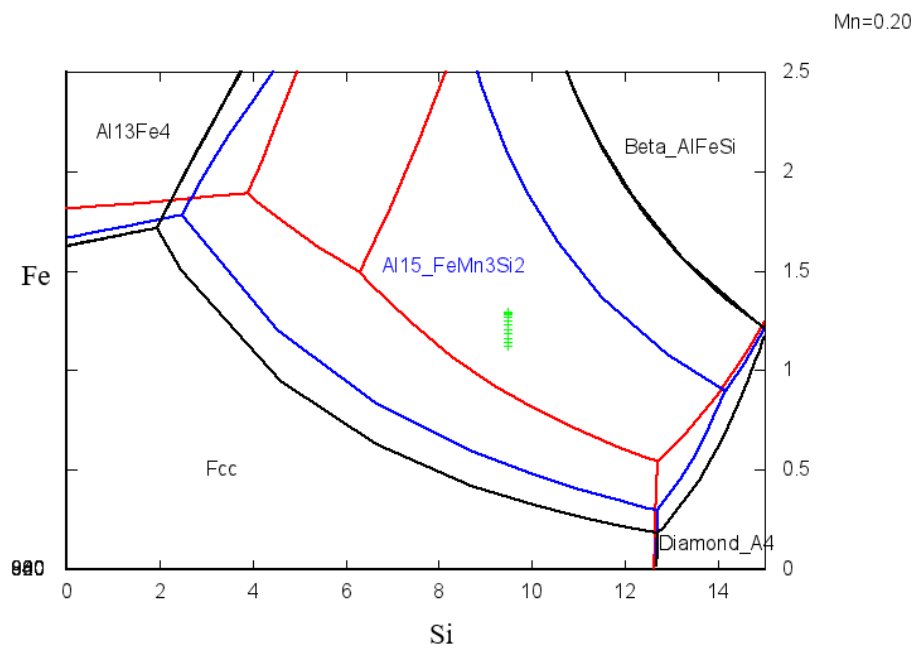
CHAPTER 6. CONCLUSIONS

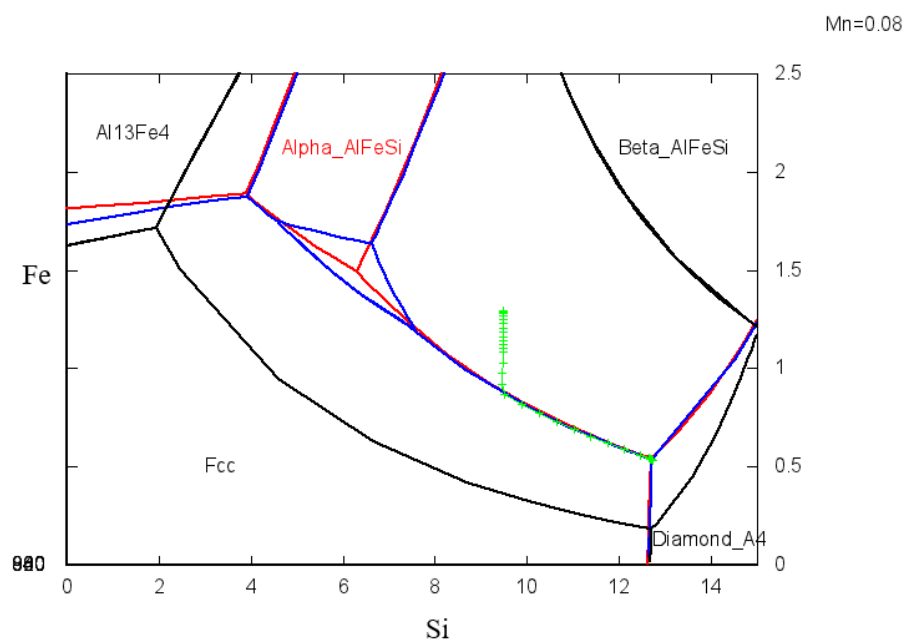
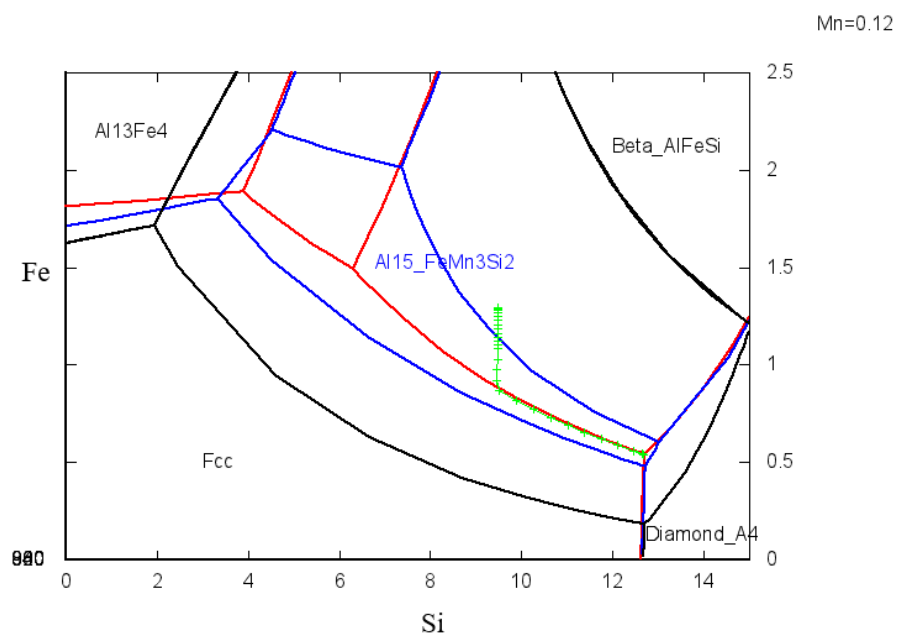
This chapter reviews the entire research work and draws conclusions from the findings in this research. The conclusions, listed in the order of sequence in this dissertation, are as follows:

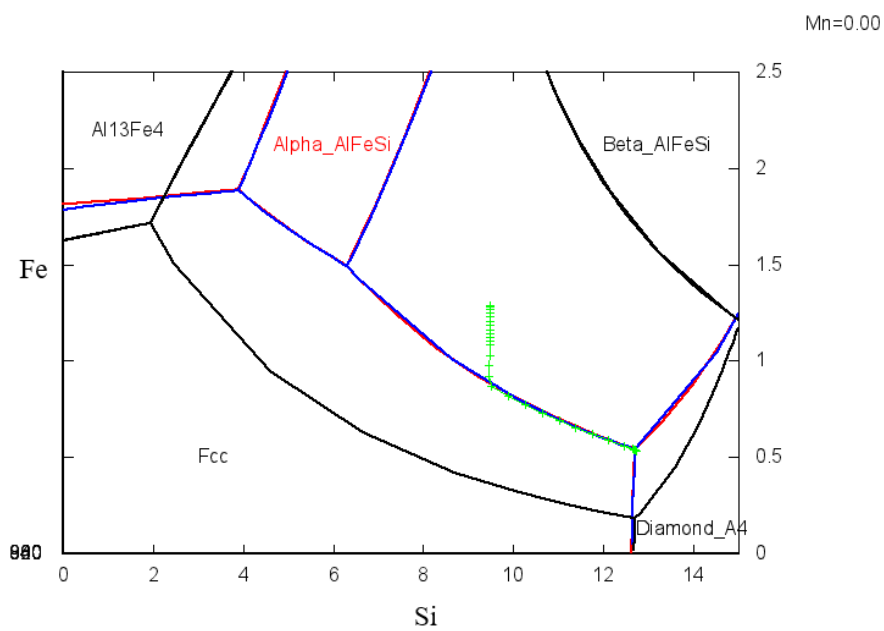
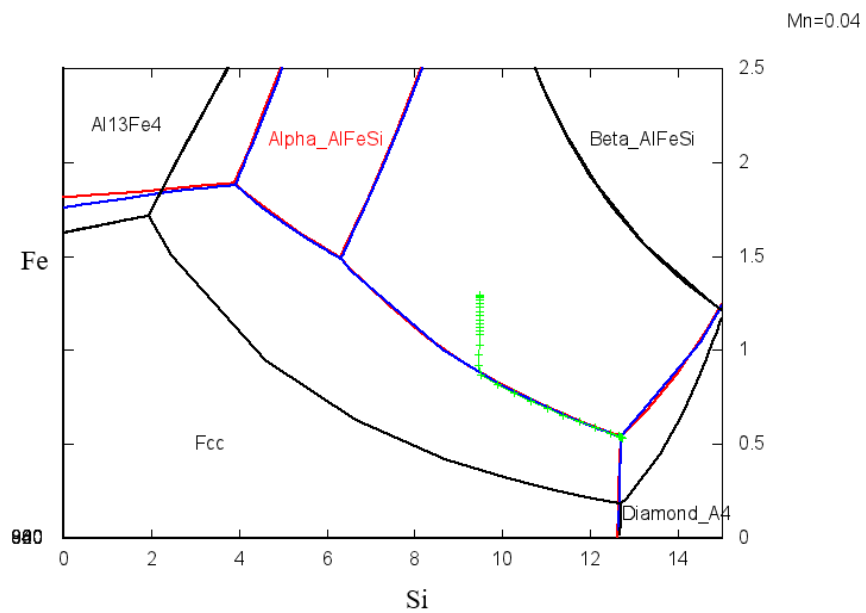
1. The thermodynamic simulation results show that Si, Fe and Mn are the elements that actively affect the formation of the intermetallic α -AlMnFeSi and β -AlFeSi phases. The change in the composition of these elements will change the phase nucleation sequence, subsequently affecting the mechanical properties of the alloy.
2. The addition of Fe in the composition of the alloy favors the formation of the β -AlFeSi phase.
3. The solidification path analysis shows that fraction of β -AlFeSi formation is dictated by whether the composition is above or below the α -AlFeSi and β -AlFeSi boundary line. If the Fe level is above the boundary line, the β -AlFeSi phase is larger due to it being formed at the starting of the solidification.
4. The longer the solidification path through the the α -AlFeSi and β -AlFeSi boundary line, the higher the fraction of β -AlFeSi phase formation.
5. The elongation is negatively affected by the amount of Fe, Mn and Si. The addition of Si, Fe and Mn decreases the elongation value.
6. Alloy strength is significantly affected by the amount of Fe and Mn rather than Si. Addition of Fe increases UTS value of the alloy, while addition of Mn negatively affects the UTS.

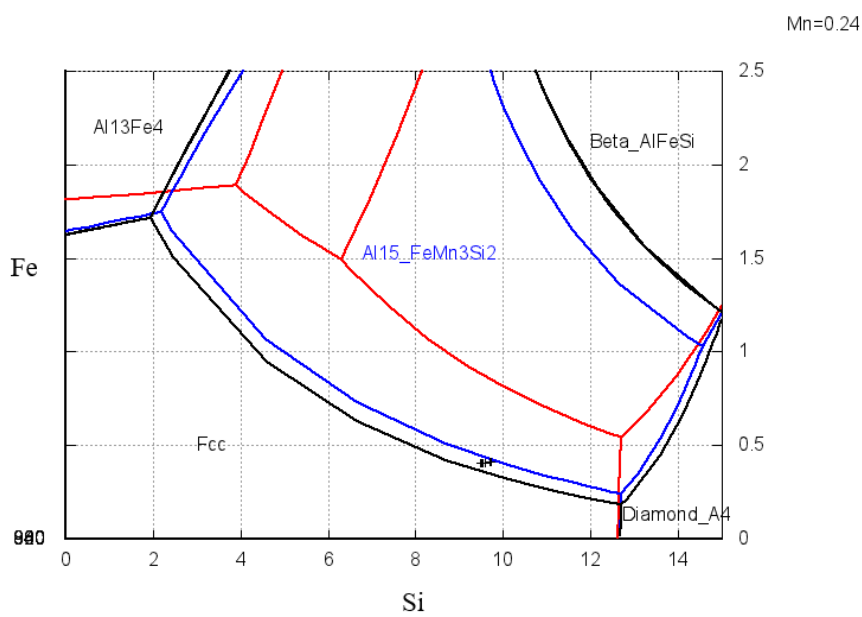
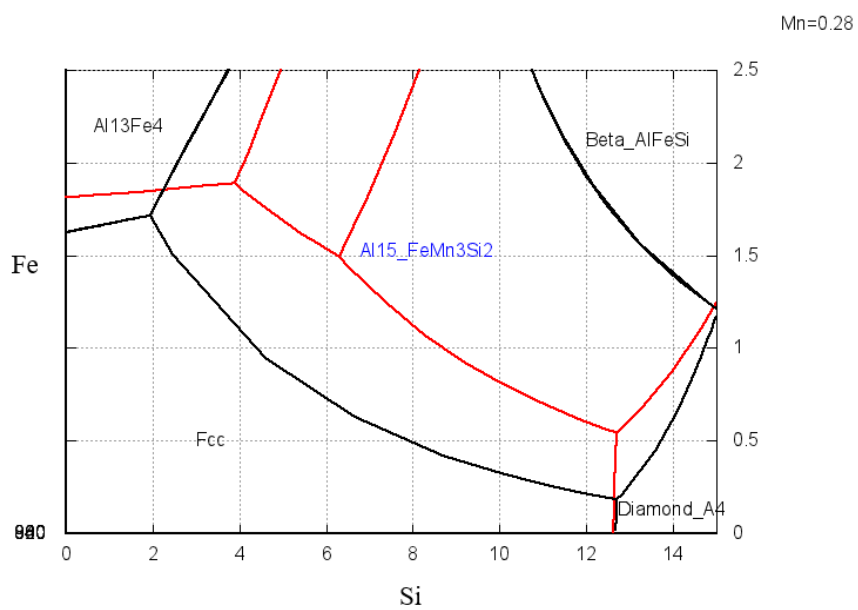
7. Generally, the increase in β -AlFeSi length negatively affect the elongation. The drop in β -AlFeSi length significantly increase the elongation property when the length is below 23 μ m.
8. Modified T4 heat treatment with solution temperature is 30°C below the solidus temperature significantly improves the elongation of the die casting alloys for up to 90%. While the elongation is improved with heat treatment, the strength of the alloy is reduced at the same time.
9. Solution heat treatment breaks the needle-like β -AlFeSi phase into shorter length, resulting in improvement of the elongation.
10. Solution heat treatment also decomposes lamellar eutectic silicon structure into larger and more dispersed granulated form of eutectic silicon, resulting in decrease of the elongation property beyond the optimal heat treatment time.

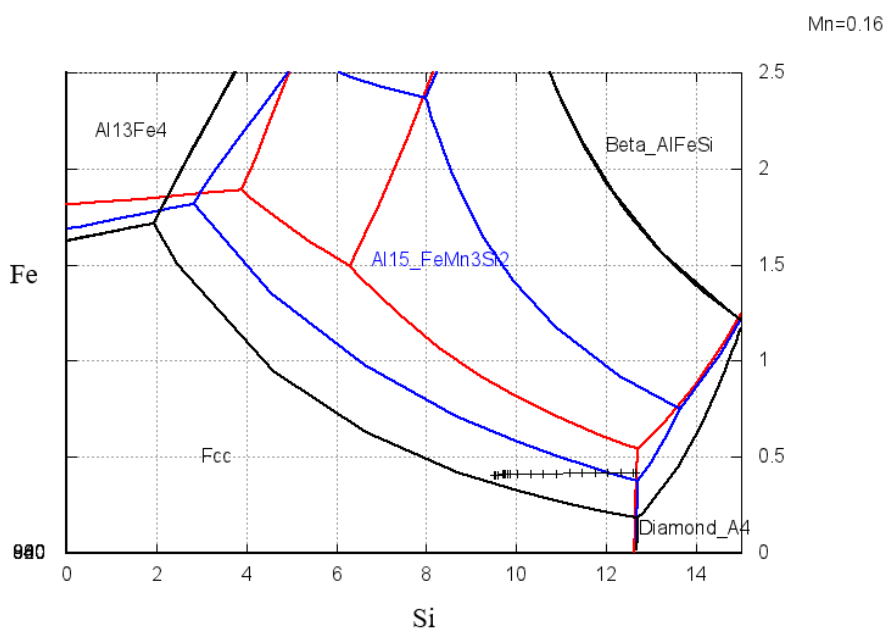
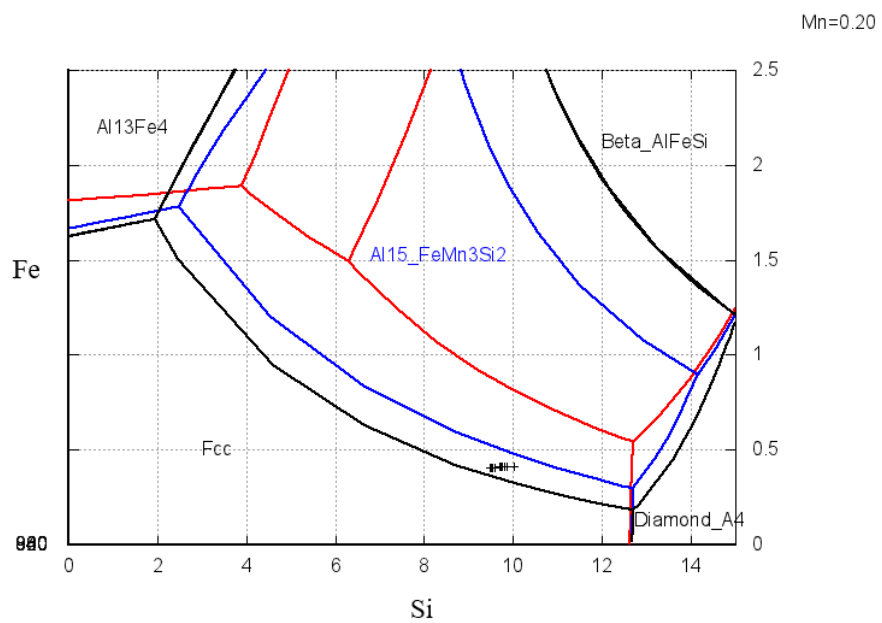
APPENDIX A: SOLIDIFICATION PATH OF A360

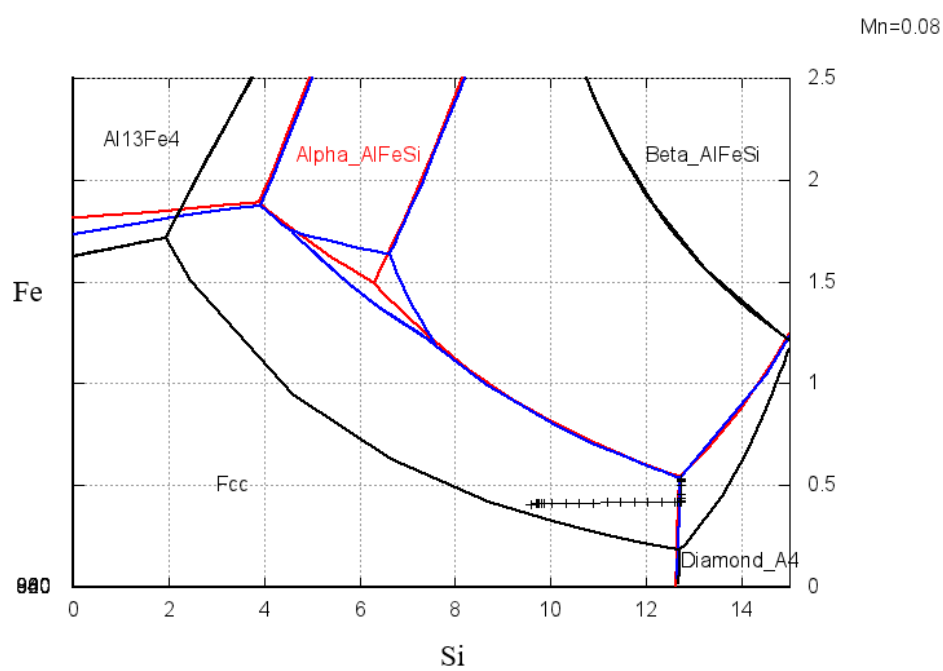
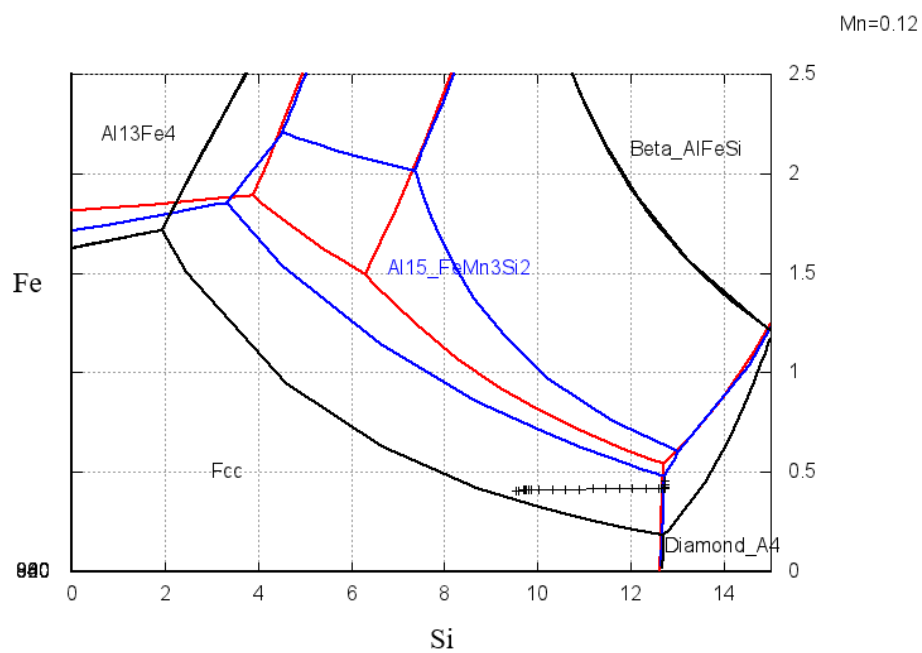


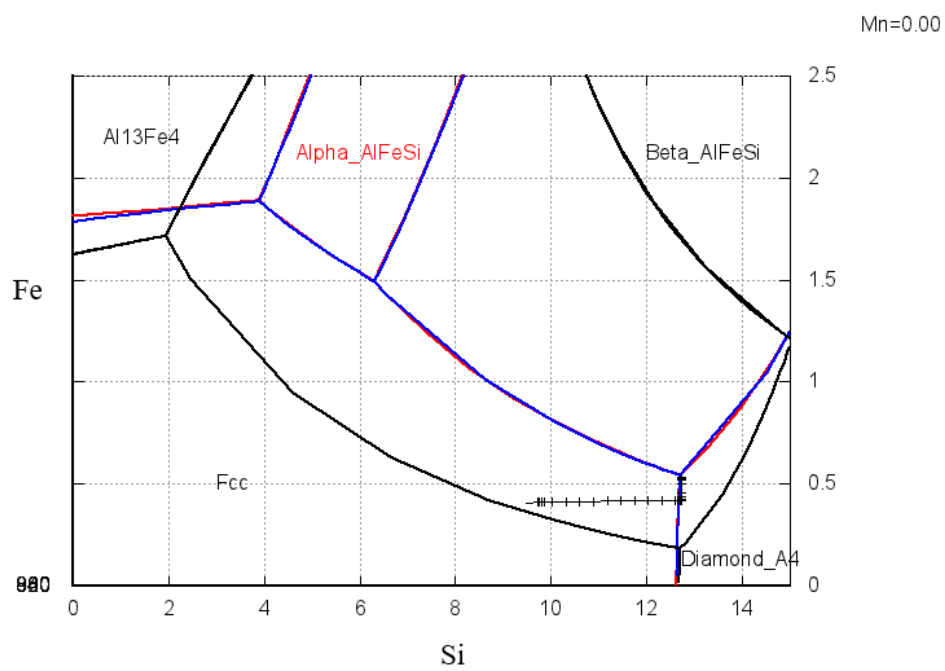
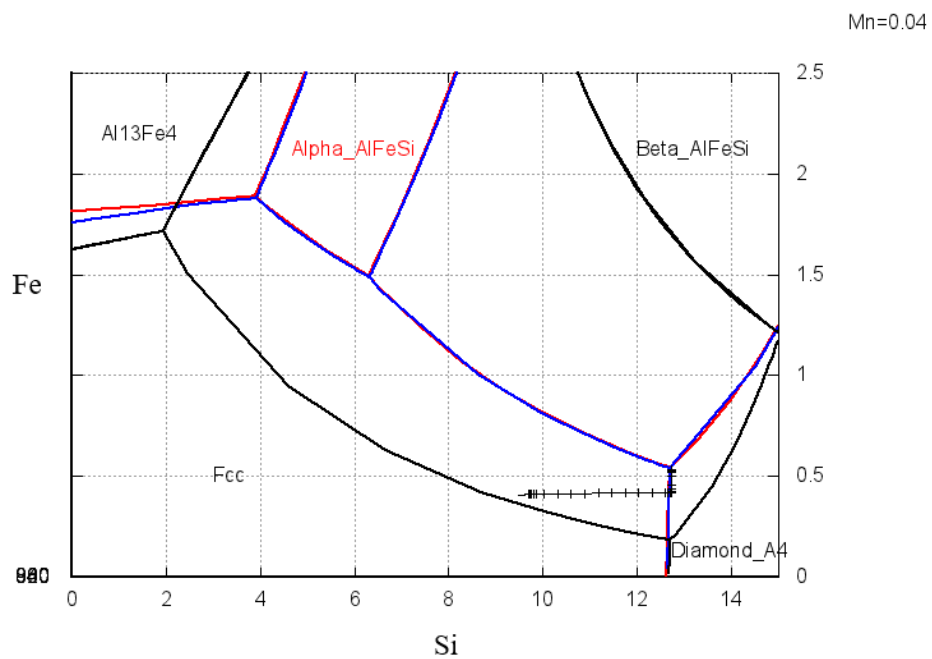




APPENDIX B: SOLIDIFICATION PATH OF B360







LIST OF REFERENCES

- Anderson, J. C. (1970). *Materials Science*. New York: Wiley.
- Ashtari, P., Tezuka, H., & Sato, T. (2003). Influence of Sr and Mn additions on intermetallic compound morphologies in Al-Si-Cu-Fe cast alloys. *Materials Transactions*, 44(12), 2611-2616.
- Backerud, L., Chai, G., & Tamminen, J. (1990). *Solidification of Characteristics of Aluminum Alloys (Vol 2)*. AFS Skanaluminum.
- Campbell, J. (1991). *Casting*. Oxford, United Kingdom: Butterworth-Heinemann.
- Cáceres, C., & Taylor, H. (2006). Enhanced ductility in Al-Si-Cu-Mg foundry alloys with high Si content. *Metallurgical and Materials Transactions B*, 37(6), 897-903.
- Cao, X., & Campbell, J. (2004). Effect of Sr on primary α -Fe phase in liquid Al-11.5 Si-0.4 Mg cast alloy. *Materials Science and Technology*, 20(4), 514-520.
- Castro-Román, M., Aguilera-Luna, I., Gaona-Coronado, A., Herrera-Trejo, M. & Torres-Torres, J. (2015). Role of Fe/Mn Ratio and Cooling Rate on Precipitation of Iron Intermetallics α -AlFeMnSi and β -AlFeSi in a 356 Alloy. *Transactions of the Indian Institute of Metals*, 68(6), 1193-1197.
- Cho, Y. H., Lee, H. C., Oh, K. H., & Dahle, A. K. (2008). Effect of Strontium and Phosphorus on Eutectic Al-Si Nucleation and Formation of β -Al₅FeSi in Hypoeutectic Al-Si Foundry Alloys. *Metallurgical and Materials Transactions A*, 39(10), 2435-2448.
- Closset, B., Paray, F., Gruzleski, J., & Mulazimoglu, H. (1996). Microstructures and properties of strontium treated aluminium electrical conductor alloys. *Light Metals*, 737-744.
- Crepeau, P. N. (1995). Effect of iron in Al-Si casting alloys: A critical review. *Transactions of the American Foundrymen's Society*, 103, 361-366.
- DeGarmo, E. (2003). *Materials and processes in manufacturing (9th ed.)*. New York: Wiley.

- Doehler, H. H. (1951). *Die Casting*. New York: McGraw-Hill.
- Donahue, R. H. (2011). Proposed environmentally green high pressure die casting alloys with low Iron for improved mechanical properties and Strontium for die soldering resistance. *NADCA*
- Donahue, R. H. (2016). *Designing Better Structural Al DC Alloys*. Presented at 2016 Chrysler Casting Symposium, Kokomo IN.
- Donahue, R. H., Cleary, T. M., & Anderson, K. R. (2010). U.S. Patent No. US 6923935 B1. Washington, DC: *U.S. Patent and Trademark Office*.
- Dumont, Deschamps, & Brechet. (2003). On the relationship between microstructure, strength and toughness in AA7050 aluminum alloy. *Materials Science & Engineering A*, 356(1-2), 326-336.
- Espinoza-Cuadra, Gallegos-Acevedo, Mancha-Molinar, & Picado. (2010). Effect of Sr and solidification conditions on characteristics of intermetallic in Al–Si 319 industrial alloys. *Materials and Design*, 31(1), 343-356.
- Green, J. (2007). *Aluminum Recycling and Processing for Energy Conservation and Sustainability*. Materials Park: A S M International.
- Groover, M. P. (2010). *Fundamentals of modern manufacturing: materials processes, and systems*. John Wiley & Sons.
- Hartlieb, M. (2013). Aluminum Alloys for Structural Die Casting. *Die Casting Engineer*, 57(3), 40-43.
- Hwang, Banerjee, Doty, & Kaufman. (2009). The effect of Mg on the structure and properties of Type 319 aluminum casting alloys. *Acta Materialia*, 57(4), 1308-1317
- Karamouz, M., Azarbarmas, M., Emany, M., & Alipour, M. (2013). Microstructure, hardness and tensile properties of A380 aluminum alloy with and without Li additions. *Materials Science and Engineering: A*, 582, 409-414.
- Kaufman, J., Rooy, E., & American Foundry Society. (2004). *Aluminum alloy castings: Properties, processes, and applications*. Materials Park, OH: ASM International.

- Khalifa, W., Samuel, F., & Gruzleski, H. (2003). Iron intermetallic phases in the Al corner of the Al-Si-Fe system. *Metallurgical and Materials Transactions A*, 34(13), 807-825.
- Kim, H. Y., Park, T. Y., Han, S. W., & Lee, H. M. (2006). Effects of Mn on the crystal structure of α -Al (Mn, Fe) Si particles in A356 alloys. *Journal of Crystal Growth*, 291(1), 207-211
- Kores, S., Vončina, M., Kosec, B. & Medved, J.(2012). Formation of AlFeSi phase in AlSi12 alloy with Ce addition. *Metallurgija*, 51(2), 216-220.
- Kral, M.V., McIntyre, H.R. & Smillie, M.J (2004). Identification of intermetallic phases in a eutectic Al–Si casting alloy using electron backscatter diffraction pattern analysis. *Scripta Materialia*, 51(3), 215-219.
- Lu, L., & Dahle, A. (2005). Iron-rich intermetallic phases and their role in casting defect formation in hypoeutectic Al–Si alloys. *Metallurgical and Materials Transactions A*,36(13), 819-835.
- Mahta, M., Emamy, M., Daman, A., Keyvani, A., & Campbell, J. (2005). Precipitation of Fe rich intermetallics in Cr- and Co-modified A413 alloy. *International Journal of Cast Metals Research*, 18, 73-79.
- Mbuya, T. O., Odera, B. O., & Ng'ang'a, S. P. (2003). Influence of iron on castability and properties of aluminium silicon alloys: literature review. *International Journal of Cast Metals Research*, 16(5), 451-465.
- Mondolfo, L. (1976). Aluminum alloys : Structure and properties. *Butterworth Group*.
- Mulazimoglu, M. H., Paray, F., Gruzleski, J. E., & Kulunk, B. (1994). Modification of intermetallic phases by strontium in aluminum wrought alloys. *Light Metals*, 27,1047–1056.
- Murali, S., Raman, K. S., & Murthy, K. S. S. (1994). Morphological studies on betaFeSiAl5 phase in Al- 7Si-0.3Mg alloy with trace additions of Be, Mn, Cr, and Co. *Materials Characterization*, 33, 99–112.

- Narayanan, L. A., Samuel, F. H., & Gruzleski, J. E. (1994). Crystallization behavior of iron-containing intermetallic compounds in 319 aluminum-alloy. *Metallurgical and Materials Transactions a-Physical Metallurgy and Materials Science*, 25, 1761-1773.
- Samuel, A, Samuel, F, & Ravindran, C. (2003). Factors Affecting Dissolution of CuAl₂ Phase in 319 Alloys. *Transactions of the American Foundry Society*, 111, 241-254
- Schulze, G. E. (1967). *Metallphysik*. Berlin: Akademie-Verlag.
- Shabestari, S. G. (2004). The effect of iron and manganese on the formation of intermetallic compounds in aluminum-silicon alloys. *Materials Science and Engineering A*, 383, 289–298.
- Taylor, J. A. (1995). Metal related castability effects in aluminium foundry alloy. *Cast Metals*, 8(4), 225-252.
- Verma, A., Sundaram, K., Grant, P & O'Reilly, K. (2013). Influence of cooling rate on the Fe intermetallic formation in an AA6063 Al alloy. *Journal of Alloys and Compounds*. 555. 274–282.
- Wang, M. (2014). Control of morphology al-fe-si phase in al-si-cu hypoeutectic alloy. *Dissertation Abstracts International 76-10B(E)*. Retrieved from <https://search-proquest-com.ezproxy.lib.purdue.edu/docview/1686824231?accountid=13360>
- Wang, M., Xu, W., & Han, Q. (2016). Effect of Heat Treatment on Controlling the Morphology of AlFeSi Phase in A380 Alloy. *International Journal of Metalcasting*, 10(4), 516-523.
- Yang, H., Ji, S., Yang, W., Wang, Y., & Fan, Z. (2015). Effect of Mg level on the microstructure and mechanical properties of die-cast Al–Si–Cu alloys. *Materials Science & Engineering A*, 642, 340-350.
- Yie, S. N., Lee, S. L., Lin, Y. H., & Lin, J. C. (1999). Mechanical properties of Al-11% Si casting alloys containing trace Be and Sr. *Materials Transactions, JIM*, 40, 294–300

- Young, & Clyne. (1981). An AlFe intermetallic phase formed during controlled solidification. *Scripta Metallurgica*, 15(11), 1211-1216.
- Zhang, L., Gao, J., Damoha, L., & Robertson, D. G. (2012). Removal of iron from aluminum: a review. *Mineral Processing and Extractive Metallurgy Review*, 39, 99-157.
- Zheng, J., Vincent, R., & Steeds, J. (2000). Crystal structure of an orthorhombic phase in β -(Al-Fe-Si) precipitates determined by convergent-beam electron diffraction. *Philosophical Magazine A*, 80(2), 493-500.
- Zhu, Schwam, Wallace, & Birceanu. (2004). Evaluation of soldering, washout and thermal fatigue resistance of advanced metal materials for aluminum die-casting dies. *Materials Science & Engineering A*, 379(1), 420-431.

VITA

Mohamad Rusydi Mohamad Yasin earned his Bachelor of Engineering (Mechanical) degree from University of Auckland, New Zealand in 2010. He later pursued Master of Engineering (Mechanical) from the same university and graduated in 2012. He has worked at Texas Instruments Malaysia and involved in development of copper wire bonding process. He later worked as a lecturer at Universiti Malaysia Pahang and involved in research on processing of metals. In 2015, he pursued Ph.D. in Technology in Purdue University, USA and working on the development of high ductility aluminum alloy for die casting under the supervision of Dr Qingyou Han (2015-2018) and Dr Xiaoming Wang (2018-2019).